Emulation of Ankle Function for Different Gaits through Active Foot Prosthesis: *Actuation Concepts, Control and Experiments*

Vom Fachbereich Maschinenbau
Technischen Universität Darmstadt
zur Erlangung des Grades eines
Doktor-Ingenieurs (Dr.-Ing.)
genehmigte

Dissertation

von

M.Sc. Mahdy Eslamy
aus Iran, Sari

Berichterstatter:	Prof. Dr. Andre Seyfarth
Mitberichterstatter:	Prof. Dr. Ing. Stephan Rinderknecht
Tag der Einreichung:	26.06.2014
Tag der mündlichen Prüfung:	09.09.2014

TECHNISCHE
UNIVERSITÄT
DARMSTADT

Darmstadt 2014
D17

Declaration of Authorship

I, Mahdy Eslamy, declare that this thesis titled,

'Emulation of Ankle Function for Different Gaits through Active Foot Prosthesis:

Actuation Concepts, Control and Experiments'

and the work presented in it are my own. I confirm that:

- This work was done wholly or mainly while in candidature for a research degree at this University.
- Where any part of this thesis has previously been submitted for a degree or any other qualification at this University or any other institution, this has been clearly stated.
- Where I have consulted the published work of others, this is always clearly attributed.
- Where I have quoted from the work of others, the source is always given. With the exception of such quotations, this thesis is entirely my own work.
- I have acknowledged all main sources of help.
- Where the thesis is based on work done by myself jointly with others, I have made clear exactly what was done by others and what I have contributed myself.

Signed: _____

Date: _____

TECHNICAL UNIVERSITY OF DARMSTADT

Abstract

Institute for Mechatronic Systems in Mechanical Engineering (IMS)
Technical University of Darmstadt, Germany

Doctor of Engineering (Dr.-Ing.)

Emulation of Ankle Function for Different Gaits through Active Foot Prosthesis:

Actuation Concepts, Control and Experiments

by Mahdy Eslamy

A main effort has been devoted in this thesis to consider the effects of the actuator *components* (i.e. springs, dampers and motors) and their *configuration* (i.e. the way they are assembled) in power and energy requirement of powered foot prostheses. It has been investigated which actuation mechanism would have the least requirements to perform a certain human gait (e.g. walking, running, ascending or descending the stairs). This thesis shows that the components of the robotic foot and their configurations are important design factors. This information is fundamental for building mechanical prototypes of active foot prostheses.

In addition, the human body is equipped with muscle assemblies to actuate a joint. In robotics this phenomenon is called *over-actuation*. In this thesis, it was investigated if and how this fact could be used to reduce power-energy requirements in active foot prosthesis.

Furthermore, the control structures of the active foot prostheses are investigated and discussed and the results of the first laboratory experiments with the Powered Ankle Knee Ortho-prosthesis (*the PAKO platform*) are explained. In continuation to this topic, some master controller schemes were introduced for gait identification. A video of experiments with PAKO platform can be seen here:

https://www.youtube.com/watch?v=i7N3L6RsNNU

Abstrakt auf Deutsch

Emulation of Ankle Function for Different Gaits through Active Foot Prosthesis:
Actuation Concepts, Control and Experiments

Der Schwerpunkt dieser Dissertation liegt in der Untersuchung der Auswirkungen der Bestandteile (z.B. Sprungfedern, Dämpfern und Motoren) und Konfigurationen (z.B. die Art deren Zusammensetzung) auf den Leistungs- und Energiebedarf in aktuierten Fußprothesen. Es wird untersucht, welcher Antrieb die geringsten Anforderungen an die Ausführung der menschlichen Gehbewegung stellt. In dieser Dissertation wird gezeigt, dass die Bestandteile des Roboter-Mechanismusses und die Konfiguration des Systems wichtige Konstruktionsfaktoren sind. Dieses Wissen ist grundlegend für den Herstellungsprozess von mechanischen Prototypen von aktiven Füßen.

Darüber hinaus ist der menschliche Körper mit Muskelgruppen ausgestattet, welche ein Gelenk aktuieren. In der Robotik wird dieses Phänomen "Überaktuation" genannt. Im Rahmen dieser Dissertation wird untersucht, ob und wie diese Tatsache genutzt werden kann, um den Leistungsenergiebedarf in aktiven Fußprothesen zu senken.

Weiterhin werden die Kontrollstrukturen der aktiven Fußprothesen untersucht und diskutiert und die Ergebnisse der ersten Laborexperimente mit dem Powered Ankle Knee Orthoprothesis (die PAKO-Plattform) erklärt. Als Weiterführung dieser Thematik werden einige Stellgrößenschemata für die Gangbildidentifizierung eingeführt. Ein Video der Experimente mit der PAKO-Plattform können unter folgendem Link angesehen werden:

https://www.youtube.com/watch?v=i7N3L6RsNNU

Acknowledgements

I would like, firstly, to thank my supervisors at Lauflabor (LL) Prof. Seyfarth and at IMS institute Prof. Rinderknecht. They were both very kind and patient in case of discussions and challenging situations. Indeed I learned a lot from them. In addition, I would like to express my sincere thanks to my colleagues at LL Laboratory. We had great times at work.

Working with TwinCAT software was not possible for me in case I did not get familiar with Joan Murt Lluma′, the R&D and IT manager at TAMAutomation, Spain. I am grateful to him for helping me get familiar with programming in this industrial control software.

I would like to express my eternal gratitude for the heart-warming support, encouragement and love from my wife, family and friends back in Iran. I am always grateful to them.

And last but not least, I would like to thank all passionate people who have taught me during the course of my life up to now. In addition, I would like to appreciate the original authors of this Latex template (Gunn and Patel) for their outstanding work which was a great help for me.

I wish them all happy times.

Contents

List of Figures

List of Tables

Abbreviations

AAFO	**A**ctive **A**nkle **F**oot **O**rthosis
AE	**A**ctive **E**lement
CAD	**C**omputer **A**ided **D**esign
CE	**C**ontractile **E**lement
CoT	**C**ost **o**f **T**ransport
CW	**C**lock-**W**ise
CCW	**C**ounter **C**lock-**W**ise
DC	**D**irect **C**urrent
DD	**D**irect **D**rive
DOF	**D**egrees **O**f **F**reedom
EMG	**E**lectro-**M**yo**G**raphy **S**ignal
ER	**E**nergy
GA	**G**enetic **A**lgorithm
GAS	**G**astrocnemius
GRF	**G**round **R**eaction **F**orces
∞	**I**nfinity
LEA	**L**ower **E**xtremity **A**mputations
LL	**L**auf**L**abor
MTJ	**M**odified **T**ranspose **J**acobian

MTU	**M**uscle **T**endon **U**nit
PAKO	**P**owered **A**nkle **K**nee **O**rtho-prosthesis
PD	**P**roportional **D**erivative
PE	**P**assive **E**lement
PEDA	**P**arallel **E**lastic **D**amping **A**ctuator
PEE	**P**arallel **E**lastic **E**lement
PLC	**P**rogrammable **L**ogic **C**ontroller
PP	**P**eak **P**ower
PS	**P**arallel **S**pring
R	**R**unning
ROM	**R**ange **O**f **M**otion
SACH	**S**olid **A**nkle **C**ushion **H**eel
SE	**S**eries **E**lement
SEA	**S**eries **E**lastic **A**ctuator
SEDA	**S**eries **E**lastic **D**amping **A**ctuator
SMA	**S**hape **M**emory **A**lloys
SOL	**S**oleus
SSSC	**S**ound **S**ide **S**ensory **C**ontrol
ST	**S**trucrured **T**ext
TwinCAT	**T**he **Win**dows **C**ontrol and **A**utomation **T**echnology
UPS	**U**ni-directional **P**arallel **S**pring
W	**W**alking

Symbols

C_d	damping coefficient	Ns/m
D	diameter of the spring coil	m
d	diameter of the spring wire	m
ER/W	work or energy	J
η_{scr}	efficiency of ball screw	[%]
F_{ank}	ankle force	N
F_g	GAS force	N
F_m	motor force	N
F_s	spring force	N
G	shear modulus	Pa
I_m	motor current	Amp
J_m	rotor (motor) inertia	kg.m^2
K_p	position gain (in PD control)	Nm/rad
K_t	torque constant (of motor)	Nm/Amp
K_s	stiffness of series spring	N/m
K_{ups}	stiffness of parallel or uni-directional parallel spring	N/m
K_v	velocity constant (of motor)	V/(rad/s)
K_v	velocity gain (in PD control)	Nm/(rad/s)

L	lead of ball screw	m
L_g	length of lever arm (for GAS force w.r.t. ankle joint)	m
L_m	motor inductance	H
L_s	length of lever arm (for SOL force w.r.t. ankle joint)	m
l_{0g}	free length of GAS spring	m
l_{0s}	free length of series spring in SEA	m
l_{0p}	free length of parallel spring e.g. in SEA+PS	m
μ	friction coefficient of ball screw	—
N_a	number of active coils (for spring)	—
PP	peak power	W (J/s)
P_{me}	required electrical power of motor	W
r	radius of ball screw	m
R_m	motor resistance	Ω
T_{ank}	ankle torque	Nm
T_g	torque produced by GAS on the ankle joint	Nm
T_m	motor torque	Nm
T_s	torque produced by SOL on the ankle joint	Nm
θ_{ank}	ankle angle	deg
θ_k	knee angle	deg
θ_m	motor angular position	rad
θ_{sh}	shank angle	deg
$\dot{\theta}_{sh}$	shank angular velocity	deg/sec
V_m	motor voltage	V
x_g	actuation length	m
$\dot{x}_g$	derivative of actuation length	m/s

x_n	nut position	m
$\dot{x}_n$	nut velocity	m/s
x_s	spring actual length	m

To my love and my beloved family

Chapter 1

Introduction, Motivation and Fundamentals: From Biological to Mechanical Foot

1.1 Introduction

Daily activities like walking, running, jumping, negotiating slopes and stairs that are mainly performed by human lower extremities, unlike what may seem, happen through a complicated process. Those activities are the result of complex cooperation between a number of organs in the human body in a procedure that involves brain, spinal cord, peripheral nerves, muscles, bones and joints [1].

From a robotic point of view, the *leg*, which is responsible for human locomotion, involves three joints: hip, knee and ankle. The muscles are the *biological actuators* which are responsible for the *motions* of the limbs (or equivalently *links* in robotics). In a way, humans are advanced complex articulated robotic systems.

In general, the human leg can be thought of as a 7-DOF[1] structure, with three rotational DOFs at the hip, one at the knee, and three at the ankle joint [2]. The leg muscles are attached to different bones (or from a robotics point of view limbs, links) at their two ends and cross over either one joint (monarticular muscle) or two joints (biarticular muscle)[2].

For the ankle joint, the main mono-articular muscle to plantarflex the foot is the Soleus muscle (SOL). One end of SOL is attached to the shank and the other end is connected to Achilles tendon and hindfoot. The main bi-articular muscle related to this joint is the Gastrocnemius muscle (GAS).

[1] Degrees Of Freedom
[2] The muscles that pass through several joints are called polyarticular muscles [3].

One end of GAS is attached to the thigh and the other end with SOL ends up to Achilles tendon and finally gets connected to the hindfoot (Fig. 1.1). The SOL and GAS together are called the triceps surae [1].

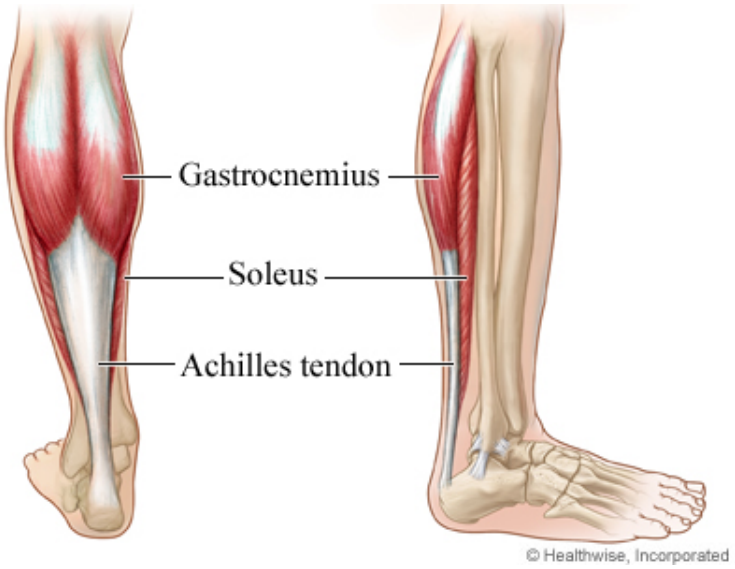

FIGURE 1.1: The mono- and bi-articular plantar-flexor muscles related to the human ankle joint: Soleus and Gastrocnemius muscles [4].

The ankle joint, could move with respect to three different anatomical planes (a 3-DOF motion). These planes are shown in Fig. 1.2. However, the human gaits (walking, running, etc.) are mostly defined with respect to the saggital plane. The reason is that the largest movements occur in this plane during locomotion. Normal human walking and running can be defined as a method of locomotion involving the use of the two legs, alternately, to provide both support and propulsion [1].

As in this thesis, a main concentration would be devoted to the active prosthetics for the lower limbs, understanding the biomechanics of human locomotion is crucial for the design of active prostheses, orthoses or exoskeletons related to the lower extremities. In the following paragraphs, I will briefly describe some of the terminologies used for explaining the human locomotion.

In human biomechanics, the *gait cycle* is defined as the interval between two successive occurrences of one of the repetitive events of walking, running etc. [1]. Although any event could be chosen to define the gait cycle, it is generally convenient to use the instant at which one foot contacts the ground (initial contact). Consequently, a gait cycle starts with the heel contact and ends with the next contact of the same foot. The foot complex itself is divided into the hindfoot, midfoot and forefoot.

The walking and running gaits are usually divided into two main sections: *stance* and *swing* phases. They are expressed as a percentage of a gait cycle. In stance phase the foot is in contact with the ground, and in swing phase (for the same leg) it is off the ground. In a normal walking gait, stance phase is approximately from 0-60% of the gait cycle and swing phase is nearly from 60-100% [5].

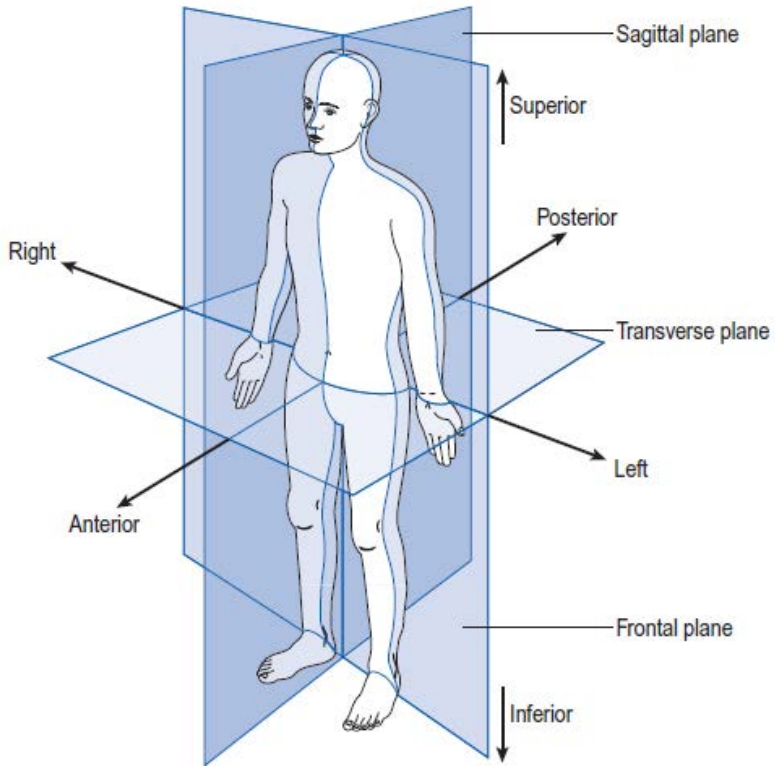

FIGURE 1.2: The three anatomical planes related to the human body [1].

The stance phase (which is also called the support phase or contact phase) lasts from initial contact to toe off [1]. It is subdivided into [1] (see also Fig. 1.3):

1. Loading response
2. Mid-stance
3. Terminal stance
4. Pre-swing.

The swing phase lasts from toe off to the next initial contact (of the same foot). It is subdivided into [1]:

1. Initial swing
2. Mid-swing
3. Terminal swing.

Most of the power during walking is generated by the calf muscles in terminal stance and pre-swing. This burst of positive power that is generated around the ankle is referred to as *the ankle push-off*

[6]. The duration of a complete gait cycle is known as the *cycle time*, which is divided into stance time and swing time. The shape and duration of the gait cycle varies from step to step and it strongly depends on the gait speed, subject morphology, subject weight, terrain conditions etc. [7].

In Fig. 1.3 different parts of a gait cycle are shown.

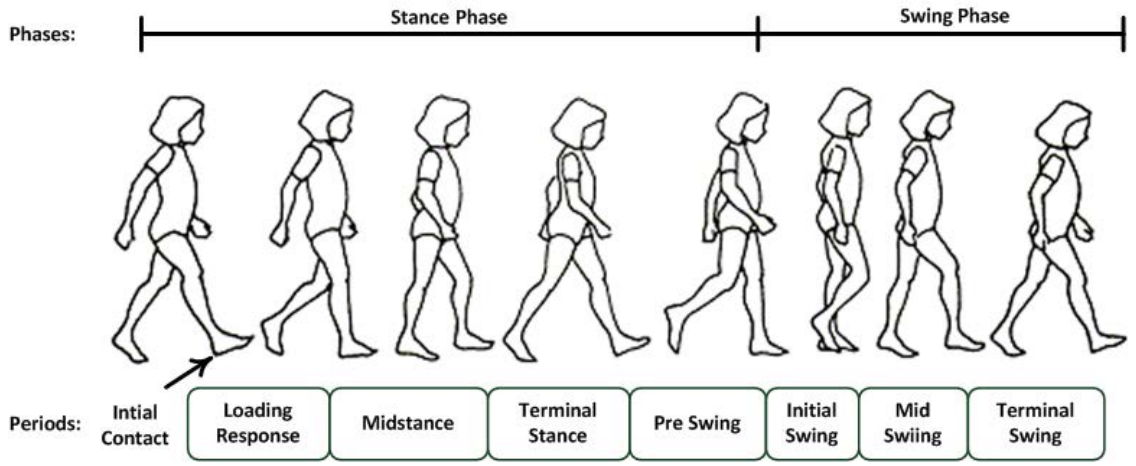

FIGURE 1.3: Division of a gait cycle [8].

Details of the experimental methods used to obtain kinematics (e.g. angle, velocity, acceleration of the joint) and kinetics (e.g. joint torques, ground reaction forces) data in human walking and running can be found in [5]. Although in some other studies we might see differences in their kinematics and kinetics data, the general trends of the graphs of the biomechanical parameters (e.g. joint angles and torques) seem more or less similar. In Fig. 1.4 the ankle angles and torques for normal walking (1.6 m/s) and running (2.6 m/s) are shown.

The ankle torque T_{ank} is normalized to body mass. It is obtained based on inverse dynamics procedures [9]. In Tab. 1.1 the cycle times for a wide range of speeds in walking and running gaits are shown.

TABLE 1.1: The cycle time for different speeds in walking and running gaits [5].

Gait	Walking					Running				
Speed [m/s]	0.5	1.0	1.6	2.1	2.6	0.5	1.0	1.6	2.1	2.6
cycle time [sec]	1.37	1.14	0.98	0.86	0.75	0.84	0.83	0.81	0.78	0.75

Although it might seem that there is symmetry between the two legs' motion during locomotion, detailed studies show that the motions of the leg joints are slightly asymmetric during locomotion [10]. Another point is the term *normal*. In the previous lines the word *normal gait* was used. We should note that in this thesis, normal applies to the young healthy subjects that participated in

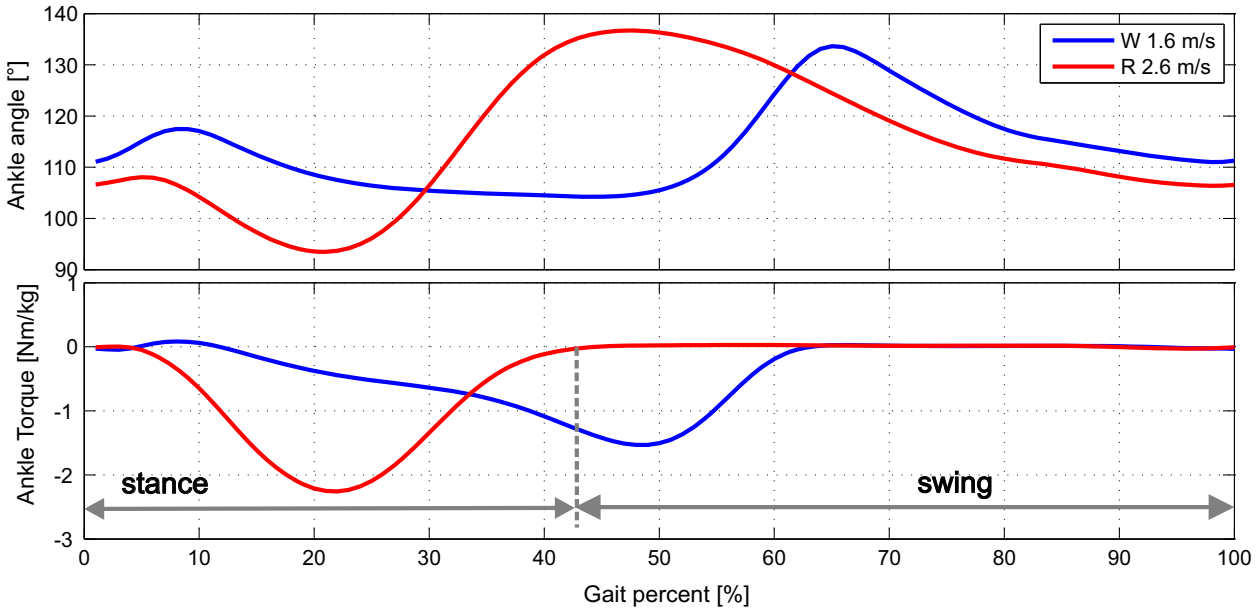

FIGURE 1.4: The ankle torques (T_{ank}) and angles for normal walking (1.6 m/s) and running (2.6 m/s). Stance and swing phases are indicated for the running gait [5]. The ankle angle is defined as the angle between shank and foot, see [5] for more details.

laboratory experiments to collect the gait data. The characteristics of the subjects used to obtain gait kinematics and kinetics are shown in Tab. 1.2.

TABLE 1.2: Subject characteristics used for obtaining kinematics and kinetics data [5] (mean ± std)

number of subj.	age [yrs]	body height [m]	body mass [kg]	speeds [m/s]
21	25.4 ± 2.7	1.73 ± 0.09	70.9 ± 11.7	0.52, 1.04 1.6, 2.07, 2.6

Consequently, these data cannot be used for comparisons with the people whose ages are very different from those seen in Tab. 1.2. We may note that every person has its own individual gait pattern, and even for a single subject the kinematics and kinetics are not exactly the same for all steps during locomotion. This doesn't mean that his/her gait is abnormal.

For a full understanding of normal gait, it is also important to know which muscles are moving a specific limb and the level of the activity for that specific muscle during the gait cycle. The muscle activity could be measured by EMG (*elctromyography*) signals. The role of the muscles was studied firstly by Scherb [11]. He reported a myokinesiographic method of recording muscle action during gait. The subjects walked on a treadmill while the examiner palpated the onset and duration of muscle contractions. Foot switches detected weight-bearing on three areas of the foot, printing the results on a kymograph [11].

1.2 Motivation of research in the field of ankle-foot prosthesis

Human gait (walking, running, ascending/descending stairs or slopes etc.) is the outcome of a complex and fascinating interaction between leg joints, brain, spinal cord, peripheral nerves, muscles and bones. Humans elaborately exploit and take advantage of their unique musculo-skeletal structure together with the neural system to perform their desired locomotion. They are able to change their gaits (e.g. from walking to running) quickly or adapt themselves to different terrain surfaces (e.g. level ground to stairs) in a fast and robust manner. Nevertheless, the underlying procedure that makes them capable for such high flexibilities is still hidden and under investigation by the research community.

Unfortunately, there are many people who cannot benefit from this fascinating structure because of limb loss (i.e. amputation due to diseases, accidents etc.). This undesired situation is not only very strenuous for the patients but also for the people with close contact to them.

According to some statistics in Germany about 220,000 persons live with leg amputations [12]. Every year there are about 28,000 amputations in Germany. 88% have one leg amputated and 12% have two missing legs. Amputations are due to accidents or diseases.

There are also other statistics presented in Tab. 1.3 which give different information for leg and foot amputations for several years in Germany [13].

According to medical statistics, just in the US, the number of diabetes-related Lower Extremity Amputations (LEAs) increased from 33,000 in 1980 to 84,000 in 1997, dropping to 75,000 in 2003 [14]. From 1988 to 2009, the number of the LEA discharges from hospitals increased by 24% (in 2001 it even increased by 58%) [15].

TABLE 1.3: Number of LEAs done in Germany (Lower Extremity Amputation, in thousands [13])

years	2004	2005	2006	2007	2008	2009	2010	2011	2012
Lower Extremity Amputation	67	69	68	67	68	67	69	63	62

Furthermore, the huge number of stroke survivors and senior citizens should also be added to these values. Such disabilities drastically change the lifestyle of these people. To overcome the walking problems (either amputation of weakness) of those amputees the first attempts started with the development of passive prosthetic (orthotic) feet. In addition the foot has a key role for human locomotion and providing push-off [5], therefore, returning back its function to the amputees is a vital target in prosthetics design.

1.2.1 Passive prosthetic feet

Commercially available ankle-foot prostheses (Fig. 1.5) are mostly completely passive during stance (BioM iWalk [16] is a newly introduced active foot), and unfortunately, cannot provide net positive work that is required for push-off and propulsion of the body (Fig. 1.6). In passive prosthetic feet, some positive work is generated only by releasing the previously stored elastic energy during the contact phase with the ground. As a result, it cannot add required power to the human gait [17]. The Proprio foot (Fig. 1.5C) could provide active adjustment of foot during swing phase (e.g. to adapt the foot angle in stairs, slopes), however it does not contribute to active push-off during locomotion.

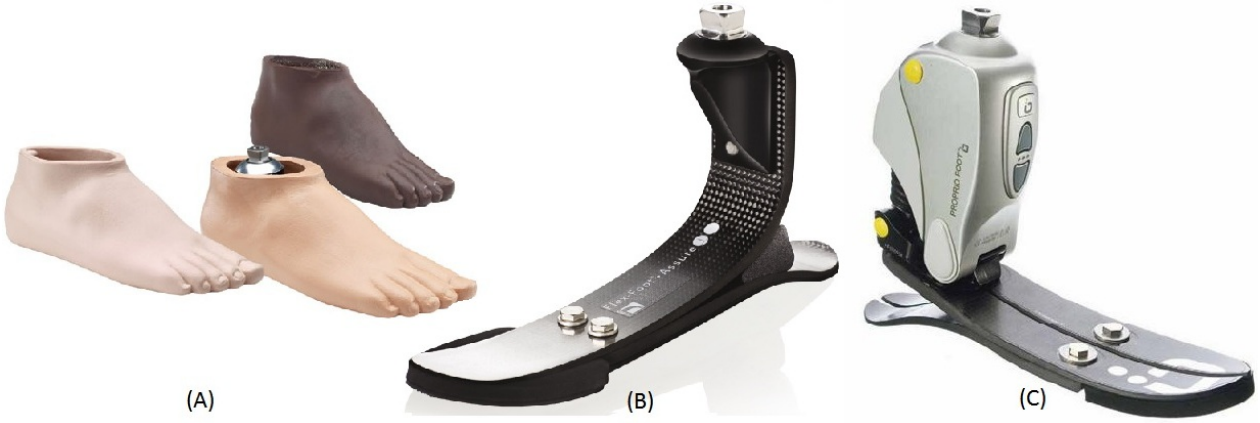

FIGURE 1.5: Examples of conventional ankle-foot prostheses, A: SACH foot (**S**olid **A**nkle **C**ushion **H**eel), B: Flex-foot (Ossur), C: Proprio (Ossur).

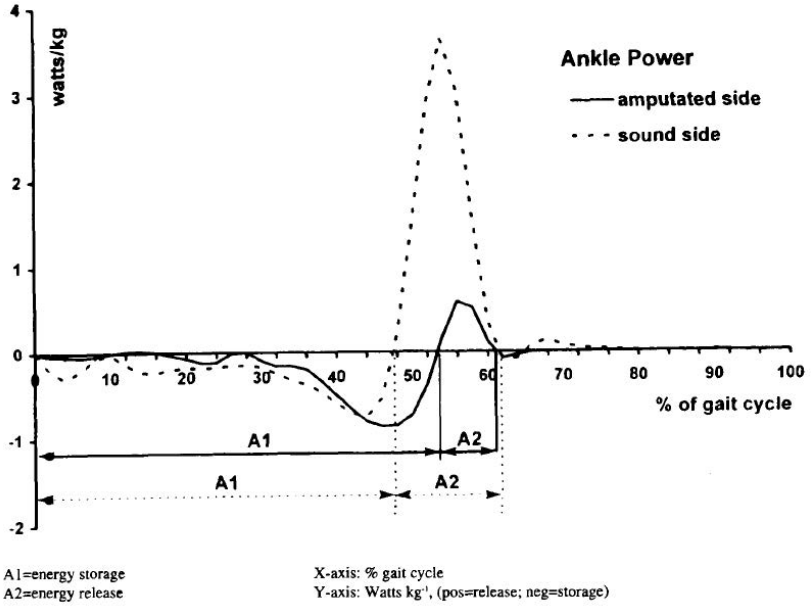

FIGURE 1.6: Ankle power comparison: able-bodied and amputated [17] (power vs. gait percent).

As shown in Fig. 1.7, the human ankle provides a significant amount of net positive work during the stance period of walking or running gaits (especially at moderate to fast speeds) [5].

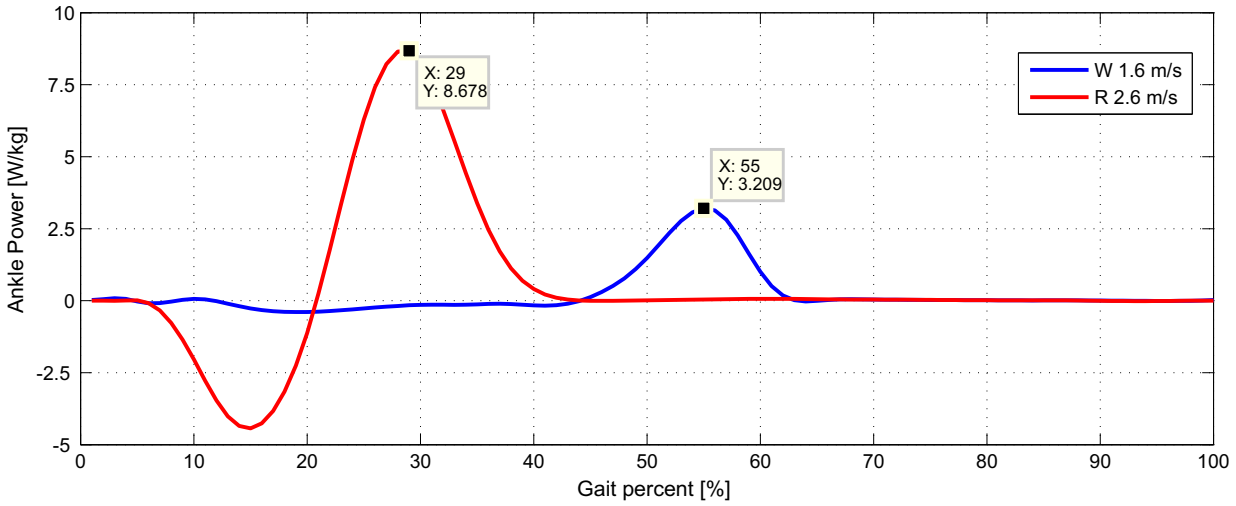

FIGURE 1.7: The human ankle provides a noticeable amount of positive power during locomotion, graphs for normal level walking (1.6 m/s) and running (2.6 m/s) [5].

Lower extremity amputees using these conventional passive prostheses experience many problems during locomotion. It is shown in the literature that the deterioration from normal kinematics and kinetics is dependent on the level of amputation or even the cause of it [18]. Studies show that transtibial amputees have lower speeds than normal (able-bodied) subjects e.g. their average speed is 45% (for vascular amputation) and 13% (for traumatic amputation) less than normal people [18]. In the absence of net power generation at the ankle joint, amputees with passive prostheses have been shown to expend more metabolic energy (20% more oxygen consumption than normal subjects [19]). It is also reported that the ankle kinematics deviates noticeably from that of able-bodied people denoting a lack of ankle plantar-flexion to produce push-off during late stance [20]. In addition the intact and prosthetic sides exhibit an asymmetrical gait pattern [20]. The knee joint torque has been reported to change noticeably from able-bodied data during stance phase, however little difference was found during swing phase [21]. Furthermore, the hip joint kinetics also show changes with respect to able-bodied people however the changes were less severe than that of the knee joint [20]. At the same time knee or hip kinematics had little differences with those of able-bodied control subjects [20]. In contrast, for running gait it has been shown that the hip or knee joint torque or power changes very noticeably (see e.g. [22]). As seen in Fig. 1.6, there is a significant ankle power difference between the affected and unaffected sides during powered plantarflexion in walking. Furthermore, the results of the research in this field are also dependent on the type of the passive prosthetic foot [23].

To overcome some of the problems regarding the passive feet and returning back the normal function of the ankle joint, in recent years, researchers have begun to develop active (powered) foot prostheses for the amputees. In the next subsection, some of theses efforts are mentioned.

1.2.2 Powered ankle prostheses

To improve the amputees' locomotion ability, research has been done for the application of powered prosthetics for the lower extremities. In an early attempt [24] an artificial pneumatic muscle called *McKibben actuator* was used to develop a powered ankle-foot prosthesis. So far, however, its capacity to improve amputee gait compared to conventional passive-elastic prostheses has not been demonstrated.

To enhance the gait characteristics of the lower extremity amputees, different active (powered) prosthetic devices are currently under development to increase the mobility of the amputees [25–27]. With these prostheses/orthoses that are designed to mimic the behavior of human leg joint (e.g. ankle and/or knee), a more natural, symmetric, and consequently, less energy consuming gait for the amputees is envisioned.

Different research groups around the world (the pioneers are located in the US) are active in this field. New generations of powered prosthetic devices together with lightweight, energy storing elastic elements and efficient mechanisms have been designed and built [25–27]. At MIT, researchers developed the *iWalk PowerFoot One* series that uses a DC motor together with springs [25]. A prototype of this active foot is shown in Fig. 1.8.

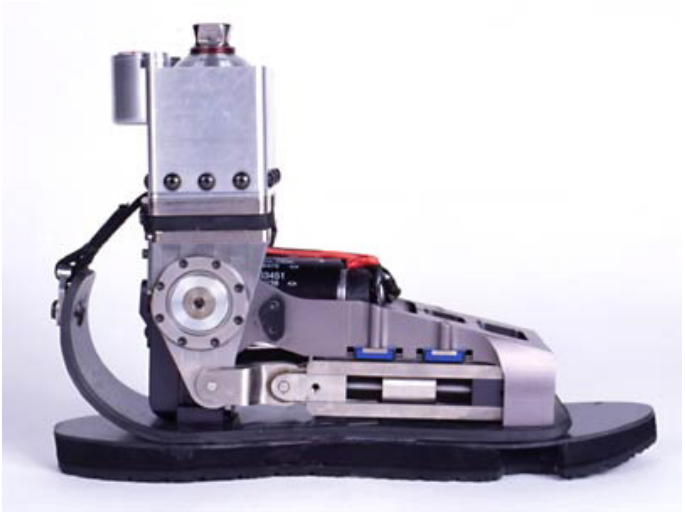

FIGURE 1.8: The active foot iWalk developed by MIT researchers (early version).

The MIT researchers used the CoT (cost of transport) to show the effectiveness of their robotic prosthesis in comparison to passive ones. They measured the oxygen consumption and carbon dioxide production to prove the improvements.

At Arizona State University, the Sparky series was developed which uses the *robotic tendon* and is equipped with a DC motor and a spring to provide the required ankle power and torque during locomotion. The Sparky prototype is shown in Fig. 1.9. In comparison to MIT foot it uses a less stiff spring.

FIGURE 1.9: The SPARKy (Spring Ankle with Regenerative Kinetics) robot. This design uses a DC motor with a spring [28].

Researchers at Vanderbilt University, have developed a powered ankle and knee prosthesis for transfemoral amputees as shown in Fig. 1.10. They have also produced a commercial version of it which is called *self contained* powered ankle and knee prosthesis. This device operates with the onboard battery. It is shown in Fig. 1.10A. Other than using a DC motor to actuate the joints, they developed also another version of the active prosthesis that uses pneumatic actuators (Fig. 1.10C). Goldfarb (Vanderbilt University) has also developed an ankle prosthesis with a different type of power source. This powered ankle is called "Rocket Powered Prosthetic Ankle". A figure of which is shown in Fig. 1.11.

The rocket powered prosthesis uses monopropellants as an energy medium to power the prosthetic device. Monopropellants are so-called because they do not need to be mixed with other gases to be used as fuel, only requiring a bit of catalyst to decompose. The second major development in this new prosthetic foot is the sleeve muscle actuator (Fig. 1.11). This actuator, powered by the monopropellant, is smaller, more powerful, and weighs less than a comparable electric motor [29]. No further information was published up to now for the experiments with an amputee.

In the fields of orthotics and exoskeletons, some prototypes are also developed by different groups. Examples of knee-ankle orthoses and ankle orthoses with artificial hydraulic or pneumatic muscles are shown in Figs. 1.12 and 1.13.

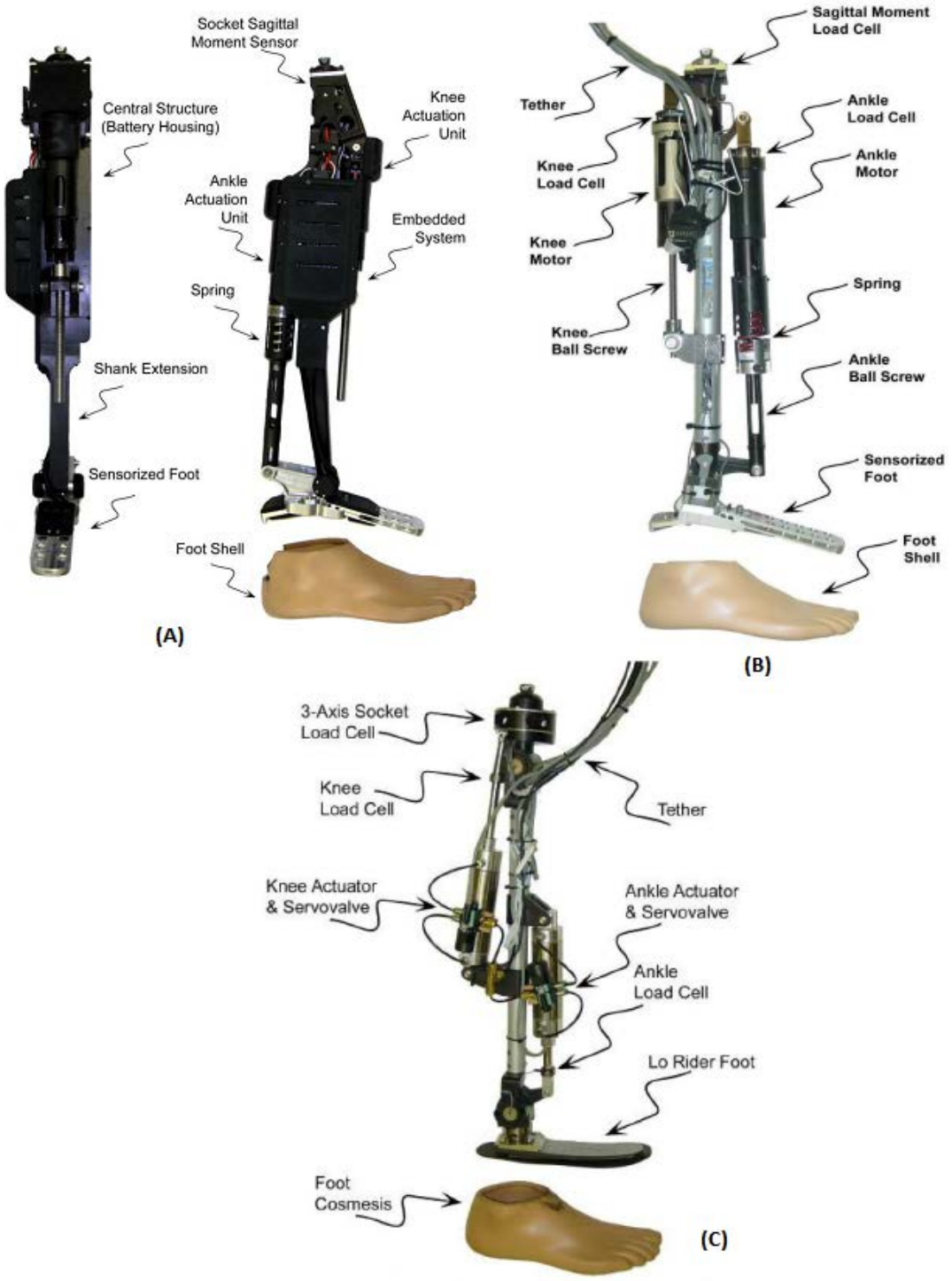

FIGURE 1.10: The self contained (A, untethered), tethered (B) and pneumatic (C) powered ankle and knee prosthesis developed by researchers at Vanderbilt University (US) [27].

FIGURE 1.11: The Rocket powered prosthetic foot developed by Goldfarb from Vanderbilt University (US) [29].

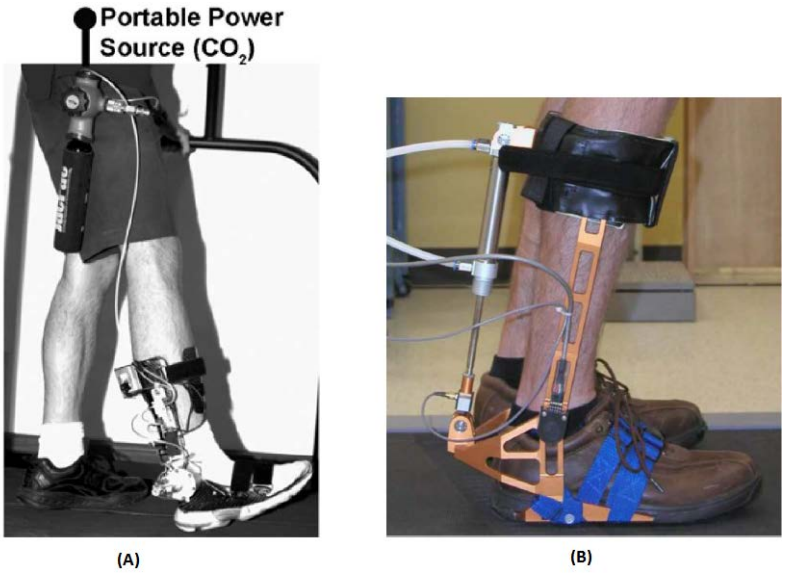

FIGURE 1.12: (A): Portable powered ankle-foot orthosis. Rotary actuator is powered with a compressed carbon dioxide (CO2) bottle worn by subject on waist [30], (B) photograph of the electro-hydraulic anklefoot orthosis [31].

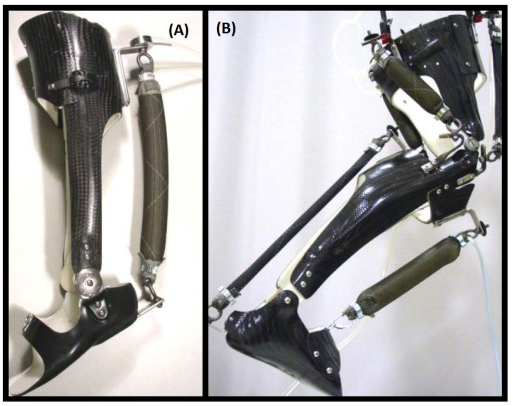

FIGURE 1.13: (A) An ankle-foot orthosis with an artificial pneumatic plantar flexor muscle. (B) A knee-ankle-foot orthosis with artificial pneumatic muscles providing flexion and extension torque at each joint. Plastic tubes provide compressed air to the artificial muscles from an external air source [32].

1.3 The aims of this study

There exist two main questions related to the currently developed powered ankle prostheses. The first is the *actuation scheme* (parts and the assembly) and the second is the *control structure* (the way they recognize different locomotion types and finally perform a desired motion).

1.3.1 The actuation scheme

1.3.1.1 The components used in current powered ankle prostheses and their configurations

Most of the powered ankle prostheses developed so far in different groups use a spring arranged in series (e.g. Figs. 1.9,1.10) to a DC motor. When a spring is in series to the motor this actuation arrangement is called *SEA (series elastic actuation)* concept. This concept is shown in Fig. 1.14.

A main *question* arises here as *why* a spring and motor and *why* SEA configuration? In order to investigate on this question a main effort in this thesis is devoted for this purpose.

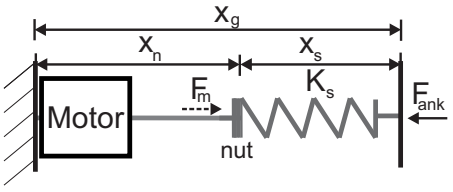

FIGURE 1.14: Scheme of the series elastic actuator (SEA), the dashed line shows the internal force.

1.3.1.2 Alternative actuation schemes

One of the main questions of this thesis is how we can reproduce human-like locomotion by means of a mechanical device i.e. a robotic ankle that could emulate the function of the lost biological foot. To construct such a robotic prototype, a model of the biological system (i.e. the musculo-skeletal structure) is required and next, we need to know the requirements of that robotic system.

As for the muscle structure, most muscle models are based on the early works of Hill [33]. In his studies, Hill concludes that muscle has elasticity, damping and activation characteristics. In a mechanical system that would be translated into an arrangement of spring, damper and motor (as a power source).

The models that inspired the work of this thesis are based on the muscle models that Durfee et al. [34] and Günther et al. [35] used in their studies. Those muscle models are shown in Figs. 1.15 and 1.16 respectively. Similar models are used also in other studies. A main difference between Fig. 1.15

and 1.16 is that in Fig. 1.16 a series damping element (D_{SE}) is also included. The authors claim that this would reduce high frequency oscillations [35].

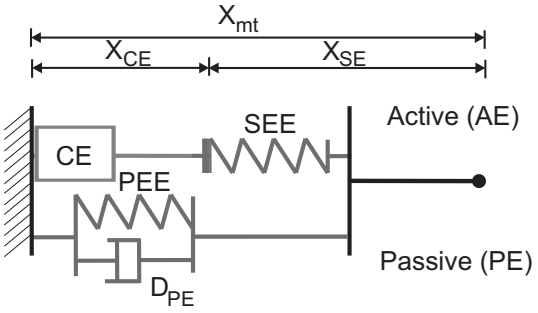

FIGURE 1.15: Muscle Model from Durfee et al. [34], X_{mt}: length of muscle-tendon unit, CE= Contractile Element, AE= Active Element, PE= Passive Element, SE= Series Element, SEE= Series Elastic Element, PEE= Passive Elastic Element.

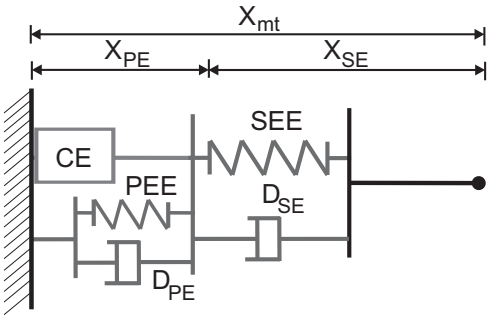

FIGURE 1.16: Muscle Model from Günther et al. [35], CE= Contractile Element, SEE= Series Elastic Element, PEE= Passive Elastic Element, SE= Series Element, PE= Parallel Element, D_{PE}= Parallel Damping Element, D_{SE}= Series Damping Element.

Comparing Fig. 1.15 and Fig. 1.14, we see that the SEA concept is a simplified configuration of the more comprehensive model presented in Fig. 1.15. Figs. 1.15 and 1.16, show that more detailed muscle models could be used in powered ankle prostheses. In the following chapters, we will investigate *whether or not* being more detailed would bring more benefits in comparison to SEA concept.

What does *more benefit* mean here? A desirable feature of a powered prosthetic foot is the low energy consumption and also low power requirement. Lower power and energy requirement would lead to smaller motor and battery. Hence, making it possible to increase the performance capacity of the active device with a lower weight.

It will be investigated in this thesis to consider the effects of the actuator *components* (i.e. springs, dampers and motors) and their *configurations* (i.e. the way they are arranged) on power and energy requirement in powered ankle prostheses. It is of interest to know which actuation mechanism would have the least requirements. This thesis shows the components of the robotic mechanism and the configuration of the parts are important design factors. This information is fundamental for designing novel prosthetic systems.

From mechanism point of view, another desirable feature of a powered ankle prosthesis could be the variability and adaptivity of its components (spring and damping) for different tasks and objectives. It would be of interest to have a compact mechanism that could change the stiffness or damping characteristics (such as biological muscle) for different locomotion types. Some groups have suggested mechanisms for changing the spring stiffness [36, 37], however, integrating such mechanisms in a compact prosthetic system requires more considerations. It depends on the designer to decide for the complexity and versatility of the device.

In the next section, I will describe some other desirable characteristics of an actuator for application in powered prosthetics.

1.3.1.3 Actuator properties

As the robotic ankle (the mechanical prototype) should be similar in function to the biological ankle-foot complex, it is required to characterize the desired features of the biological actuators (i.e. muscles) and their important properties. In Tab. 1.4, some important actuator characteristics that should be considered for design of active ankle prostheses are summarized.

TABLE 1.4: Some important criteria for the selection of actuators in powered prosthetics

Performance Characteristics
Max. Force (Torque)
Max Velocity
Max. Power
Power-to-Mass (or even volume) ratio
Torque-to-Mass ratio
Efficiency
Components Variability

In this respect, some of the properties of the mammalian skeletal muscles are shown in Tab. 1.5.

TABLE 1.5: Some of the properties of the mammalian skeletal muscles [38]

Property	Typical	Maximum
Strain (%)	20	>40
Stress (MPa)	0.1	0.35
Work Density ($kJ.m^{-3}$)	8	40
Density ($kg.m^{-3}$)	1037	-
Specific Power ($W.kg^{-1}$)	50	284
Efficiency (%)	-	40

In Fig. 1.17 the skeletal muscle structure is shown. A skeletal muscle is a bundle of parallel muscle fibers held together by connective tissues [39]. Nerve fibers, blood and lymphatic vessels weave their

way throughout the whole muscle. The connective tissues at the ends of each muscle fiber join together to form the whole muscle tendon which in turn connects the muscle to the bone. The force generated by muscle fibers is transmitted via the tendon to the bone where it appears as a torque about a joint [39]. If the joint torque generated by a muscle is greater than opposing torques (which may result from external loads or from opposing (antagonist) muscles) then the limb will rotate about the joint. Thus contraction of muscles produces angular displacements of limbs about joints [38].

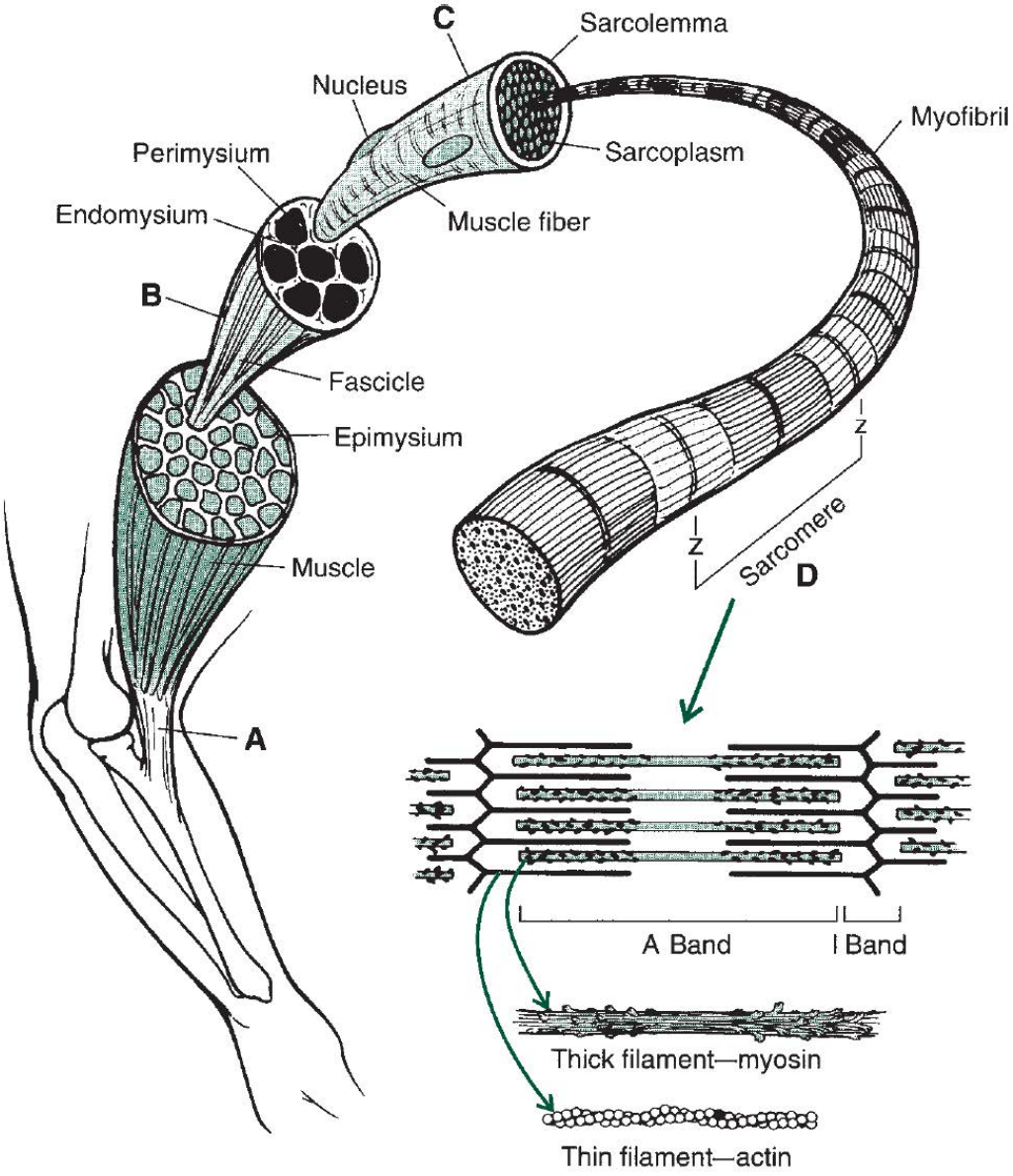

FIGURE 1.17: The skeletal muscle structure [39], **A**. Each muscle connects to the bone via a tendon or aponeurosis. **B**. Within the muscle, the fibers are bundled into fascicles. **C**. Each fiber contains myofibril strands that run the length of the fiber. **D**. The actual contractile unit is the sarcomere. Many sarcomeres are connected in series down the length of each myofibril. Muscle shortening occurs in the sarcomere as the myofilaments in the sarcomere, actin, and myosin slide toward each other.

Muscle does not surpass artificial actuators in any single aspect (for example continuous power to

mass is an order of magnitude lower than that of an internal combustion engine) [38]. However there are a number of attractive design features that could be utilized to great advantage [38].

For example, force can be regulated by controlling the number of the fibers that are activated in parallel (Fig. 1.17), a process known as *recruitment* [38]. This regulation of force, enables efficiency to be optimized over a wide range of loads and contraction velocities, in addition enabling control of acceleration and force. The control of force is made more effectively by the fact that inactive muscle fibers are relatively low in stiffness, and therefore do not require significant forces to strain. In current actuator technologies there is little ability for such structural adaptivity [38].

In addition, the ability to change stiffness is also important in control strategies. For example, in catching a ball, a too stiff arm will lead to a large (painful) impulse as the ball makes contact, and provides less time to grasp the ball before it bounces back. A very compliant arm will not be able to stop the ball. The optimum stiffness needs to be adapted to the ball mass and velocity. Such stiffness control can be emulated in artificial actuators by fast feedback control, but at the expense of added complexity and will only work if the actuator bandwidth is sufficient [38].

1.3.1.4 Power source for a powered ankle prosthesis

The power source in an active ankle prosthesis could be a DC motor (e.g. Figs. 1.8, 1.9, 1.10), pneumatics (e.g. Fig. 1.12A), hydraulics (e.g. Fig. 1.12B) or other sources (e.g. Fig. 1.11). In Tab. 1.6, the advantages and disadvantages of different actuation types used in robotic applications are compared.

TABLE 1.6: Advantages and disadvantages of robot actuators (hydraulic, DC motors and pneumatic)

Hydraulics	DC Motors	Pneumatics
• good for large robots	• usually for all sizes of robots	• usually for light applications
• high power-to-weight ratio	• good for high precision applications	• low pressure compared to hydraulics
• leaking is a problem	• does not leak. good for everyday applications	• no leaks, but noises
• require pump, reservoir, motor, hoses, etc	• reliable, low maintenance	• require air pressure, filter

Because of the desirable characteristics of DC motors mentioned in Tab. 1.6, in this thesis, I will replace CE (Figs. 1.15 and 1.16) with a DC motor for modelling purposes to represent the power source.

Other types of power sources can also be found in the literature like polymer gels [40], shape memory alloys (SMAs) [41, 42] or electroactive polymers [43]. Among the most successful polymer gels, is Polyvinyl Alcohol-Polyacrylic Acid (PVA-PAA), which when suitably treated, using water

(to produce dilation) and acetone (to produce contraction), replicates on a macroscopic scale the chemical-mechanical energy conversion cycle of organic muscle [40].

The SMA approach was used to develop an active ankle foot orthosis (AAFO) [41]. However, the relatively slow response rate of this kind of actuator ($\sim$ 0.25 Hz) and the mechanical inefficiencies that result from poor conversion of thermal energy into mechanical energy (approximately 2-3%) are significant disadvantages that limit the function of this kind of actuator for application in prosthetics and orthotics [41]. The electroactive polymer approach was used to build a swimming robot. However it is reported that this kind of actuation might not be agile enough [43].

1.3.1.5 Over-actuation

The main foot plantarflexors are Soleus (SOL) and Gastrocnemius (GAS). As shown in Fig. 1.1, in human lower extremity the two muscles (actuators) contribute to foot plantarflexion. This phenomenon that different leg muscles collaborate with each other to perform a certain motion is called *over-actuation*[3].

To the best of author's knowledge, no publication has been reported for bi-articular powered ankle prosthesis. A main question for the bi-articular device is the method for force distribution between the actuators.

In this thesis, this topic will be addressed by considering a powered SOL and passive GAS. The target, as previously mentioned, is to investigate the effects of mono- and bi-articulation on the power and energy requirement in an active foot prosthesis.

1.3.2 Control structure

The human lower extremity, its function and the way different parts are cooperating together is still in question. From control perspective the important questions related to the active foot prostheses are (1) the *gait recognition* and (2) the *gait transition* strategies. In addition, other control issues such as *motor position control* could be also important[4].

We may note that those afore-mentioned control objectives are not the only requirements. They were mentioned, because at first, the robotic system must perform acceptably for certain conditions like locomotion on level ground or stairs. However, for outdoor locomotion, it is required that the robotic foot reacts in addition, very well to the obstacles or terrain uncertainties. The balance and stability of the amputee user is a key objective in powered foot prostheses.

[3] Over-actuation is the situation in which two or more actuators are controlling a joint.

[4] However, for the case that a DC motor is used it might not be a severe problem. For the case of a pneumatic actuator this could be a problem because of the compressability of the gas.

The control target in an active ankle prosthesis is to create ankle motions that follow the kinetics and kinematics of an able-bodied person, improving the amputee's locomotion in a safe and robust manner.

By gait recognition, it is meant to develop methods to identify the type of the user's gait. Whether he/she is running, walking, jumping, etc. Then, we should know the speed and the gait percent (or gait phase) of that specific locomotion, so that a desired motion for the drive (e.g. a DC motor) is provided based on that gait, speed and gait percent.

Unfortunately, an algorithm that could predict all of the humans' motions correctly has not yet been developed. Currently developed methods mostly rely on the kinematics and kinetics of human gait. One of the main drawbacks is the existence of *overlap* in kinematics and kinetics of human locomotion in different types of locomotions. Overlap means that there are gaits and speeds whose kinetics or kinematics pattern are quite similar to each other. Hence making it hard to distinguish between different motions easily and accurately. Different groups active in this field have used some algorithms to classify human locomotion. However, all of them are designed for some types of locomotions (e.g. [44]) and still not really in real world applications completely foolproof and robust even for those specific applications ([45] reports chattering and delays in gaits and gait transitions).

The authors in [46] mention a gait detection procedure based on phase plane invariants. They use the shank angular velocity and angle to identify the speed and the gait percent. However in practice, there are some limitations. For example this method could not be used for different people with a single reference data. Each individual requires its own set of references. In addition it works for some speeds and is not a universal method. However for normal walking and running speeds it operates acceptably.

Establishing reference data from different kinematics and kinetics variables (ankle angle, knee angle, GRF (Ground Reaction Forces), angular velocity and accelerations of the joints) and comparing it with real time sensor data is another method [47]. This algorithm uses the minimum difference between the measured data and the reference data to identify in which mode the user is moving. However chattering between different modes of locomotion is also reported [47]. In another attempt impedance control was used to control the active ankle prosthesis [44]. They used finite state machines to determine the mode of the locomotion and then based on force control algorithms or impedance control sent the necessary commands to the motor.

Other intent recognition methods could be also used in powered foot prostheses. One method is to use EMG (elctoymyography) signals [48]. Surface EMG signals, for example, are used to extract command signals from the muscles in residual limbs. Then signal processing is started to send meaningful commands to the actuator. In [49] the authors use a biomimetic EMG-controller that worked based on muscle modelling. They used a bi-linear muscle model that had elasticity and damping characteristics. Given EMG signals and the corresponding desired ankle-foot trajectory,

they estimated the values (e.g. damping, stiffness) using optimization procedures. In the same study the authors used neural networks to produce desirable ankle angles. The inputs and output of the network were pre-processed EMG signals from the residual muscles and the estimated ankle position respectively. These methods were used for swing phase control (position control mode). No further information was provided for a real time experiment with an active ankle prosthesis.

In addition, some methods used the state of the sound leg and provided control command for the impaired one. This is called echo control approach [50]. For example, Ossur's PowerKnee uses a similar approach called sound side sensory control (SSSC) [51]. In this method the affected leg always has the commands that are one step behind. This might cause problems for real world applications.

In [52] the authors used a trajectory tracking controller for an active orthosis actuated by an SEA. The gait pattern was generated by a polynomial fit of a normal-gait pattern and was a function of the stride time. The system measured the duration between two heel strikes and fed it into the polynomial function accordingly.

Muscle reflexes could also be used for closed-loop feedback control of ankle dynamics that could potentially adapt to different speeds. Models controlled with only local reflexive feedback loops are able to produce walking simulations that qualitatively agree with human gait dynamics and muscle activations [53, 54]. This purely feedback-based approach has been applied to a powered anklefoot prosthesis to control it as if it were driven by a human muscle with a local force feedback reflex [55]. This system exhibited slope-adaptive behaviour but the use of a force-feedback reflex alone, without parameter interventions, did not result in the biological trend of increasing net ankle work across speed [53, 56].

In general, the control structure for active foot prostheses could be divided to two main categories: the *master* and *the slave* controller (Fig. 1.18). The master controller is in charge of recognizing the gait and the transition between the gaits. The slave controller is used to send appropriate corresponding signals to the drive. The slave controller in this work could be a proportional-derivative (PD) controller. Other methods like Jacobian control, impedance control, force control and hybrid position-force control could also be used. In Fig. 1.18 a schematic view for the control structure is shown.

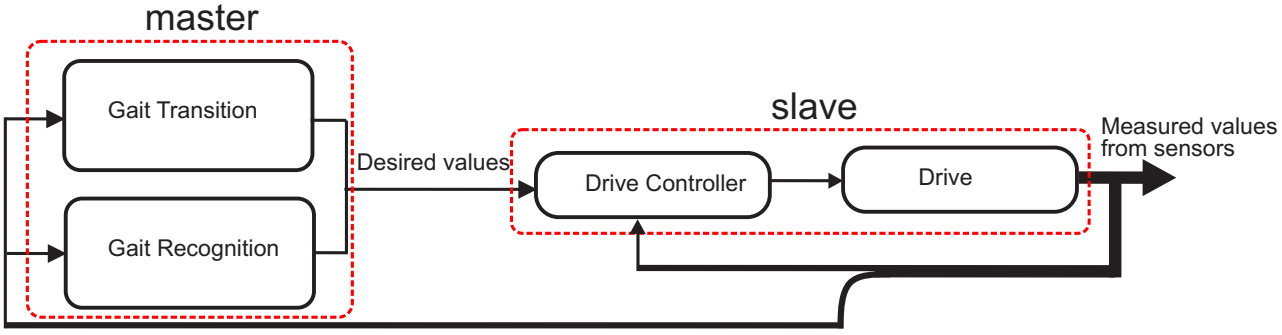

FIGURE 1.18: A proposed control structure for a powered ankle-foot prosthesis.

In this thesis, novel approaches will be suggested for the gait recognition. To do that, the method presented in [46] will be improved and in addition, another method will be suggested for the gait recognition based on the nearest neighborhood concept (distance between the sensor data and the reference data).

In the next section, the robotic foot prosthesis *PAKO* that is developed in Lauflabor Locomotion Laboratory will be described. Research and laboratory tests are currently being done on this robot.

1.4 PAKO: the Powered Ankle Knee Ortho-prosthesis

In order to investigate more on the actuation mechanism for a powered foot prosthesis and locomotion control, the *PAKO* platform is developed in Lauflabor (LL) locomotion laboratory. PAKO stands for **P**owered **A**nkle **K**nee **O**rtho-prosthesis.

1.4.1 Key mechanical features

The PAKO platform is shown in Fig. 1.19. The word *Ortho* is used because the user would *wear* the robotic foot and it surrounds his/her shank and foot. The word *prosthesis* is used since it has a prosthetic foot which is used to emulate the function of the biological foot of an able-bodied person. The robotic prosthesis is designed in a way that it can be used by an able bodied person. This eliminates the need for doing the experiments with a real amputee. In order to achieve this goal, a whole shank case is used to fix the shank and the foot of the subject to the robot structure. Also, the thigh of the subject is fixed to the thigh case (Fig. 1.19).

With the help of the thigh case, it is intended to improve the overall control of the robot by the user. Also, at this part, a second actuator could be installed in the future for doing experiments on bi-articular actuators to investigate the function of knee joint and GAS in walking and running. With this type of design it is not necessary to do gait experiments with a real amputee. In order to get symmetric gait with the system, two PAKO systems for the two legs are used.

PAKO is built on aluminum frame and the thigh and shank case are made out of carbon fiber. The dimensions of the structure are shown in Fig. 1.19A. To transfer the motor rotation to the spring, the motor is coupled to a ball screw. In addition, security dampers are used at the upper/lower limits of the ball screw nut in order to guarantee the safety of the robot. No gears are used as they reduce the system efficiency. The foot is a commercial OttoBock 1H38 prosthetic foot.

As shown in Fig. 1.20, by rotating CW/CCW (clockwise, counter-clockwise) the disc-like parts (enclosed by the red rectangle) one can move them upward/downward and hence manipulate the stiffness of the spring by changing the number of the active (engaged) coils. Note that the stiffness

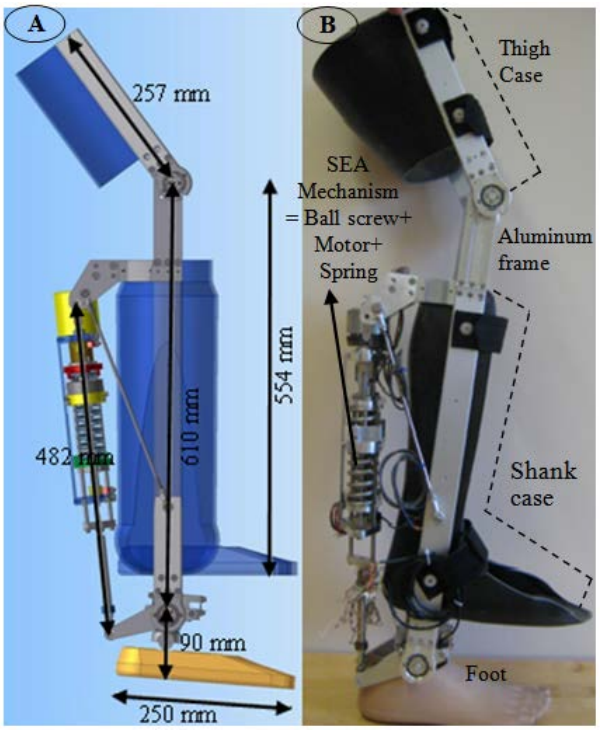

FIGURE 1.19: A) The CAD view with dimensions B) The constructed robotic prosthesis PAKO I.

and the number of the active coils of a spring are related to each other by

$$K = \frac{G\ d^4}{8\ N_a\ D^3} \tag{1.1}$$

in which K is the stiffness of the spring, G is the shear modulus, d is the diameter of the wire used to build the spring, N_a is the number of the active coils and D is the diameter of the spring coil.

The advantage of this mechanism is that it can be used in the same robotic system for different gaits analyses, without disassembling/assembling different springs. Also no sensor will be manipulated. In the current version, the spring stiffness is changed manually. It could be possible to change the stiffness automatically by an additional motor, which could be a continuation to this project. In chapter 2, it would be explained in detail why such a mechanism was used in PAKO.

1.4.2 Key sensor and electronics features

1.4.2.1 Sensors

The following sensors are implemented within each PAKO robot: (1) two sensors placed on the ball of the foot (near the joint), for measuring ground reaction forces (GRF) normal to the transverse and frontal planes (2) motor encoder (3) two proximity sensors for lower/upper end positions of the

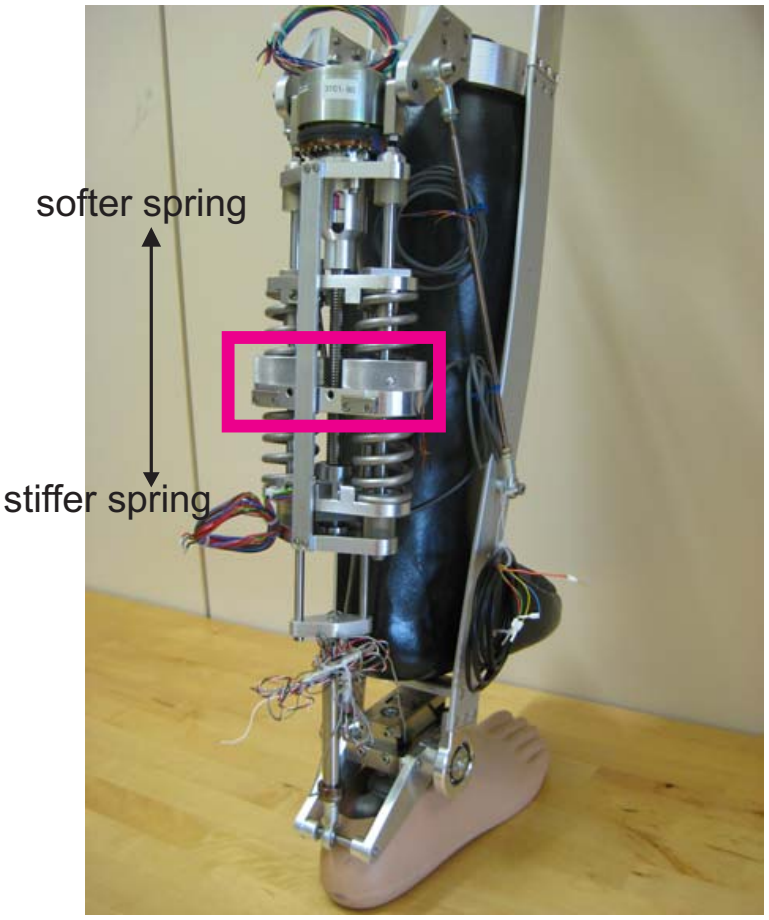

FIGURE 1.20: The number of the active coils and therefore the stiffness of the spring changes by rotating the two disk-like components enclosed by the red rectangle.

nut for the safety of the design and homing procedure (4) the SEA force sensor (5) gyro sensor and acceleration sensor for the shank angular motions (6) knee angle sensor and (7) ankle angle sensor.

1.4.2.2 Control software

The software used for control and programming of the PAKO robot is called TwinCAT (**T**he **Win**dows **C**ontrol and **A**utomation **T**echnology). This software is used in industry and works based on the principle of PLCs (programmable logic controllers). The language used for writing the program is ST (structured text). The communication of the electronics is via EtherCAT technology using RJ45 connection. The TwinCAT software is developed by Beckhoff company. The amplifiers are from ELMO Motion Control. The power supply supports the motors with 48 V and 32 A output.

1.5 Thesis outline

Chapter 2 describes the series elastic actuator (SEA) which is widely used in compliant actuators. I start from a biological perspective of muscle design and map that morphology into a mechanical system that governs an active ankle prosthesis. A main effort would be given to determine the required motor power and energy to perform human-like walking and running. Then the focus will be on the actuator inefficiencies, and the ideal power and energy requirement will be compared with that of the more realistic power calculations.

In chapter 3, the search for alternatives of the SEA concept will be continued. Like before, the inspirations are based on biology. The parallel elastic elements will be focused on to see if those structures could be used in active ankle prosthesis to reduce power and energy requirements in comparison to SEA concept.

In chapter 4, a new perspective for design of active ankle prostheses is opened up by considering the application of a damper in such systems. Gaits like walking, negotiating up and down the stairs will be in concentration since they are encountered frequently in daily life. It will be investigated whether it is useful to have a damper in active ankle prostheses and if so, what kind of configuration is suggested for such a design.

In chapter 5, the muscle assembly in human lower extremity is taken into account. There are two main muscles in charge of human foot motion which are Soleus and Gastrocnemius. It will be investigated how this configuration in biology could be copied into a mechanical system (i.e. an active ankle prosthesis) to reduce its power and energy in comparison to the case when just a mono-articular system (like Soleus) is used.

In chapter 6, results of the experiments with the mechanical prototype PAKO are shown and discussed. The experiments are done on a treadmill in our lab. Different controllers will be implemented and their results will be compared. In addition different methods for gait recognition strategies are discussed.

In chapter 7, final conclusions about a compromise design for active foot prostheses are made. In addition the control concepts that could be further developed are discussed and new ideas are suggested for more adaptive and human-like robotic prosthetic ankle. In addition, suggestions are made to improve the current design of PAKO platform (also in chapter 6).

Chapter 2

Series Elastic Actuation (SEA): Inspiration from Biology Pays

2.1 Introduction

The muscle models shown in Figs. 1.15 and 1.16 are quite comprehensive, and from a technical point of view, relatively difficult to implement in an active foot prosthesis (due to the high number of components that would be required for the final prototype, the system could not be compact and light weight). In this chapter, it will be investigate how those models could be simplified while still be effective for application in active foot prostheses.

2.2 Biological basis

Muscle models in Figs. 1.15 and 1.16 could be highly simplified to just a motor unit (or CE contractile element). Such a structure is called a *direct drive* (DD) system. In another approach, we could allow one spring in series with CE. This structure is known as *series elastic actuator* (SEA) [57]. Apparently, having a spring in series with motor unit is not too complex, however the benefits of such structure is extensively discussed in the robotics literature. These actuation concepts (DD and SEA) are schematically shown in Fig. 2.1.

2.3 Compliance

For an SEA structure (Fig. 2.1), the equivalent stiffness K_{eq} is obtained by

$$\frac{1}{K_m} + \frac{1}{K_{se}} = \frac{1}{K_{eq}} \tag{2.1}$$

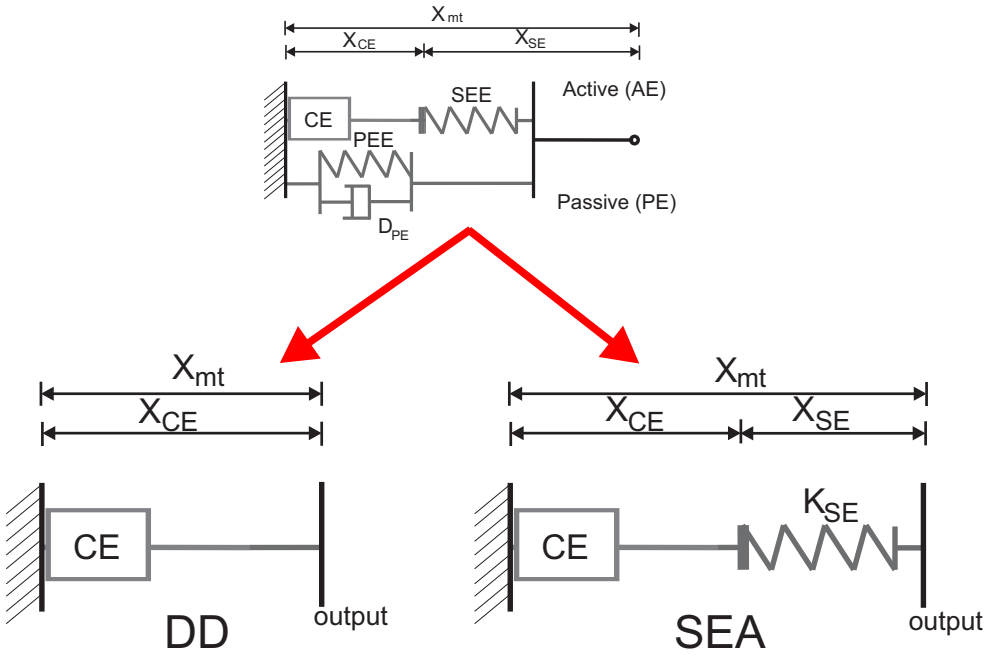

FIGURE 2.1: The concepts of direct drive (DD) and series elastic actuator (SEA). These models are simplified versions of the muscle models presented in Chapter 1, X_{mt}: length of muscle-tendon unit, CE= Contractile Element (resembling a motor unit), AE= Active Element, PE= Passive Element, SE= Series Element, SEE= Series Elastic Element, PEE= Passive Elastic Element, D_{PE}= Parallel Damping Element.

(where K_m is the stiffness of motor), consequently an immediate conclusion is that

$$\frac{1}{K_{eq}} > \frac{1}{K_m} \quad \Longrightarrow \quad K_{eq} < K_m \tag{2.2}$$

or the SEA system is more compliant (softer) than DD. This feature has many advantages in robotic systems. First, it increases the robotic system's capabilities for interacting with the environments. As an active ankle prosthesis has contact with the surface of the ground, the performance of the system on different surfaces would be better than the case of a stiff actuator (DD) is used. Second, its influence on the actuator's power density (power/mass [W/kg]) is noticeable. This feature will be talked more in the following sections. The spring has the capability to store energy slowly, and to release it quickly. This catapult effect could be used in active ankle prosthesis. This could remove some of the workload from the motor side.

2.4 Application of DD and SEA concepts in active foot prosthesis

In design of active ankle prostheses, different issues could be taken into account. These issues vary from mechanical to control aspects. From the construction point of view, these robotic systems should be compact with as low as possible requirements. To achieve this goal, a main interest would go toward power and energy considerations. As said before, other objectives could also be taken into

account, however finding a way to reduce power-energy requirements in such systems is a desirable approach. Therefore, In this section we will investigate the required power and energy of DD and SEA actuation mechanisms in active ankle prosthesis.

A mechanical prototype could be designed by putting a motor (e.g. a DC motor) in place of CE (compare Fig. 2.1 vs 2.2b) and using a transmission mechanism to convert the rotary motion of motor into linear motion (e.g. a ball screw [58]). In Fig. 2.2a schematic view of the active ankle prosthesis together with the model of SEA actuator is shown. For walking 1.6 m/s the ankle angle and torque are shown in Fig. 2.3. This graph is shown to give an overview of the kinetics and kinematics pattern of ankle joint for a normal walking speed [5]. The ankle torque T_{ank} is converted to ankle force

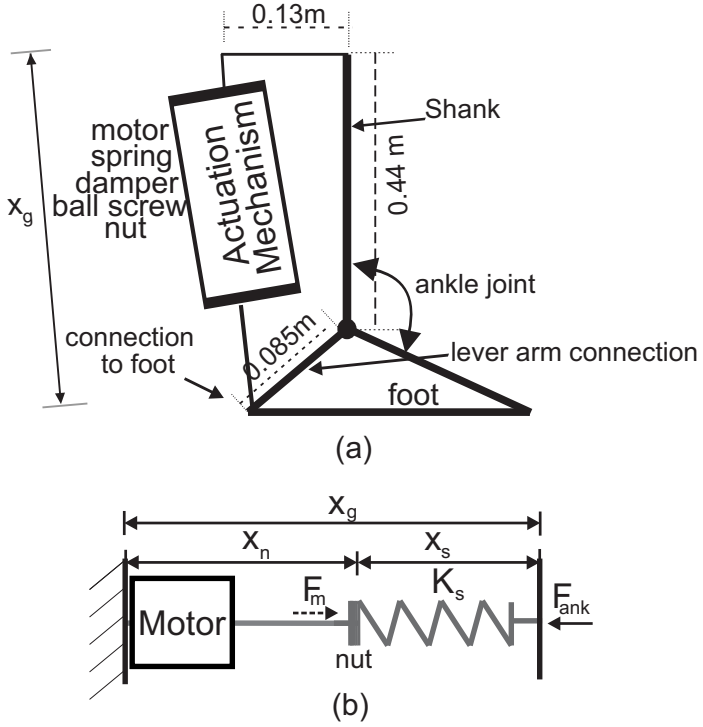

FIGURE 2.2: Schematic view of (a) the powered ankle with dimensions used for calculations and (b) model of series elastic actuator [26]. For calculation purposes, the ankle angle is the angle between shank and foot [5].

F_{ank} using lever arm and system geometry (Fig. 2.2a). The length x_g (Fig. 2.2) is calculated based on ankle angle [5] and geometrical dimensions shown in Fig. 2.2a.

The transmission used in powered ankle prostheses is mainly ball screw [25, 59, 60]. Therefore the following calculations are related to this type of mechanism. The required motor power P_m for SEA is obtained by the multiplication of the motor force F_m (or equivalently ankle force F_{ank}) and (ball screw) nut velocity $\dot{x}_n$ [58]

$$P_m = F_m \cdot \dot{x}_n \tag{2.3}$$

according to Fig. 2.2b

$$x_g = x_s + x_n \tag{2.4}$$

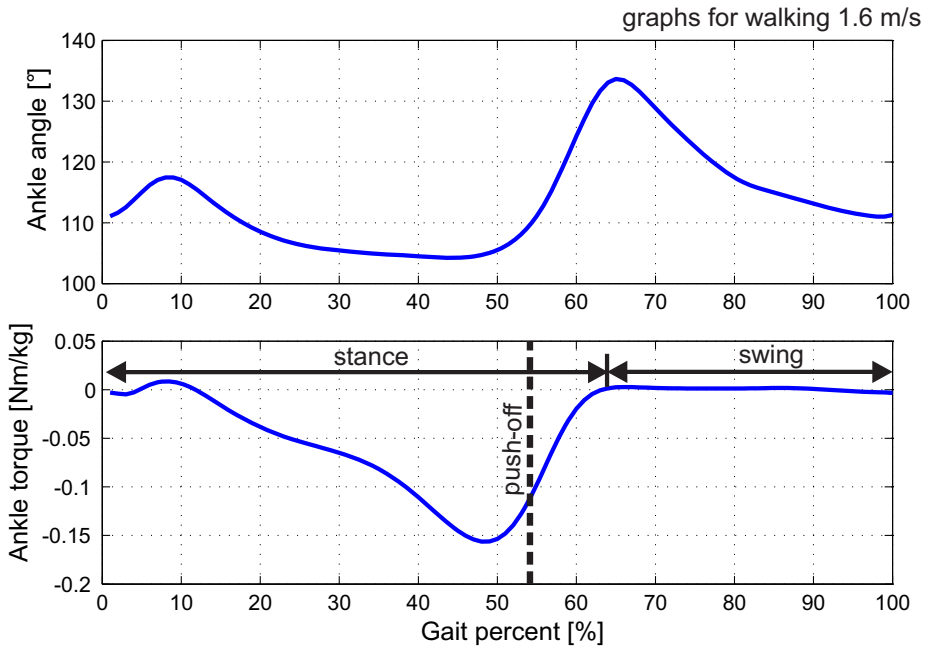

FIGURE 2.3: Ankle torque (T_{ank}) and angle graphs for walking 1.6 m/s [5].

where x_s is the actual length of the series spring. On the other side,

$$F_m = K_s \Delta x_s \tag{2.5}$$

$$\Delta x_s = l_{0s} - x_s \tag{2.6}$$

where K_s and l_{0s} are the stiffness of series spring and its free length respectively. Using Eqs. 2.4-2.6 the nut velocity $\dot{x}_n$ is obtained as

$$x_n = x_g + \frac{F_m}{K_s} - l_{0s} \Longrightarrow \dot{x}_n = \dot{x}_g + \frac{\dot{F}_m}{K_s} \tag{2.7}$$

according to Eq. 2.3, the motor power P_m is

$$P_m = F_m \ (\dot{x}_g + \frac{\dot{F}_m}{K_s}) \tag{2.8}$$

note that as the spring is in series with motor, F_m and F_{ank} are similar (from value point of view).

Human ankle power can be both negative and positive [5] (the required motor power with that of biological ankle will be compared later in this chapter). When it is negative, a resistance motion is applied to the ankle, and when it is positive, a propelling motion is applied [5, 59]. A motor unit cannot typically provide negative power [58, 59], as a result it must provide power to both resist and propel human motion [58, 59]. Therefore, the absolute value of power requirement is considered. Consequently, the required energy is

$$E_m = \int |P_m| \ dt \tag{2.9}$$

the integration is over a gait cycle (Tab. 2.1, [5]).

TABLE 2.1: Main features of ankle kinematics and kinetics for normal level walking [5]

gait type	max. biological power [W/kg]	max. torque [Nm/kg]	range of motion (ROM) [°]	stance until [%]	speed [m/s]	cycle time [sec]
Level walking	3.2	-1.53	105-133	65	1.6 m/s	0.98

In Eq. 2.8, the required motor power P_m is dependent on spring stiffness K_s. Values of F_m and x_g are obtained by human ankle data [5] and geometrical dimensions of the actuator (Fig. 2.2). Thus, stiffness K_s becomes the only parameter that would influence the required motor power. In simulation, for spring stiffness a range of 1kN/m to 500 kN/m (1 kN/m step size) was considered.

As previously mentioned, it is desirable to minimize power and/or energy requirements in an active ankle prosthesis. For each value of K_s, the required motor (peak) power was obtained based on Eq. 2.8. Then the results were compared and then the K_s value that resulted in minimum peak power (PP) or energy (ER) requirement was selected. A same method and range was used to determine minimum ER requirement.

2.5 Power and energy requirements in DD and SEA actuators

To compare the motor peak power and energy requirements between different active ankle actuation concepts shown in Fig. 2.1, the biomechanics data of human ankle are required. Experiments on human walking and running (each at 5 different speeds) were performed with 21 healthy subjects (Tab. 2.2) on an instrumented treadmill equipped with 3D force sensors (Kistler, 1000Hz) [5]. Joint kinematics were recorded using high speed infra-red cameras (Qualisys, 240Hz). Joint torques were calculated by inverse dynamics [9].

TABLE 2.2: Experimental and subject characteristics (mean ± std) [5]

number of subj.	age [yrs]	body height [m]	body mass [kg]	speeds [m/s]
21	25.4 ± 2.7	1.73 ± 0.09	70.9 ± 11.7	0.52, 1.04 1.6, 2.07, 2.6

2.5.1 Approach for minimum PP requirement

In this approach, the results for the minimum required PP and their corresponding energy requirements are shown in Fig. 2.4 for a wide range of walking and running speeds and comparatively

for SEA and DD concepts. As it is seen, using a spring in series with motor obviously pays. The required motor PP in the SEA concept are less that of the corresponding DD concept for all speeds.

This result could be expected because SEA structure is an inspiration from biology and it is more analogous to the muscle structure than DD. That is a good reason to use such an actuation scheme for active ankle prostheses.

TABLE 2.3: The obtained optimal stiffness values to minimize motor peak power requirements at different walking and running speeds (see also [61])

Gait	Walking					Running				
Speed [m/s]	0.5	1.0	1.6	2.1	2.6	0.5	1.0	1.6	2.1	2.6
Stiffness [kN/m]	78	61	80	115	143	70	74	77	77	77

As seen in Fig. 2.4, noticeable reduction of power-energy requirement in an active ankle prosthesis is possible because of the series elasticity. In normal walking (1.6 m/s), for SEA concept, the minimum PP and its corresponding ER requirement reduced about 58% and 26%, respectively, in comparison to DD (Fig. 2.4).

The corresponding stiffness values that minimize PP requirement are shown in Tab. 2.3.

2.5.2 Approach for minimum ER requirement

The results for minimum ER requirements and their corresponding power requirements are shown in Fig. 2.5 for walking and running speeds. As seen in this figure, for the normal walking speed (1.6 m/s) the minimum ER requirement was reduced by 28% in comparison to DD. In comparison to minimum PP approach, it reduced 2% (compare Fig. 2.4 vs Fig. 2.5 for this speed). At the same time, the corresponding power requirement reduced 54% in comparison to DD and increased 4% in comparison to the minimum PP approach.

However, we may note that in minimum PP approach, for *all* speeds, the PP and ER requirements of SEA were less than DD concept. But, in minimum ER approach, for fast walking (2.6 m/s) such a trend is not observed (see Fig. 2.5).

The corresponding stiffness values that minimize ER requirement are brought in Tab. 2.4.

2.5.3 Minimum PP requirement versus minimum ER requirement

As shown in Figs. 2.4 and 2.5, the power requirement in minimum PP approach is less than minimum ER approach, however its corresponding energy requirement is slightly higher than the minimum ER approach. Therefore, selecting the stiffness based on minimum PP approach could be a logical

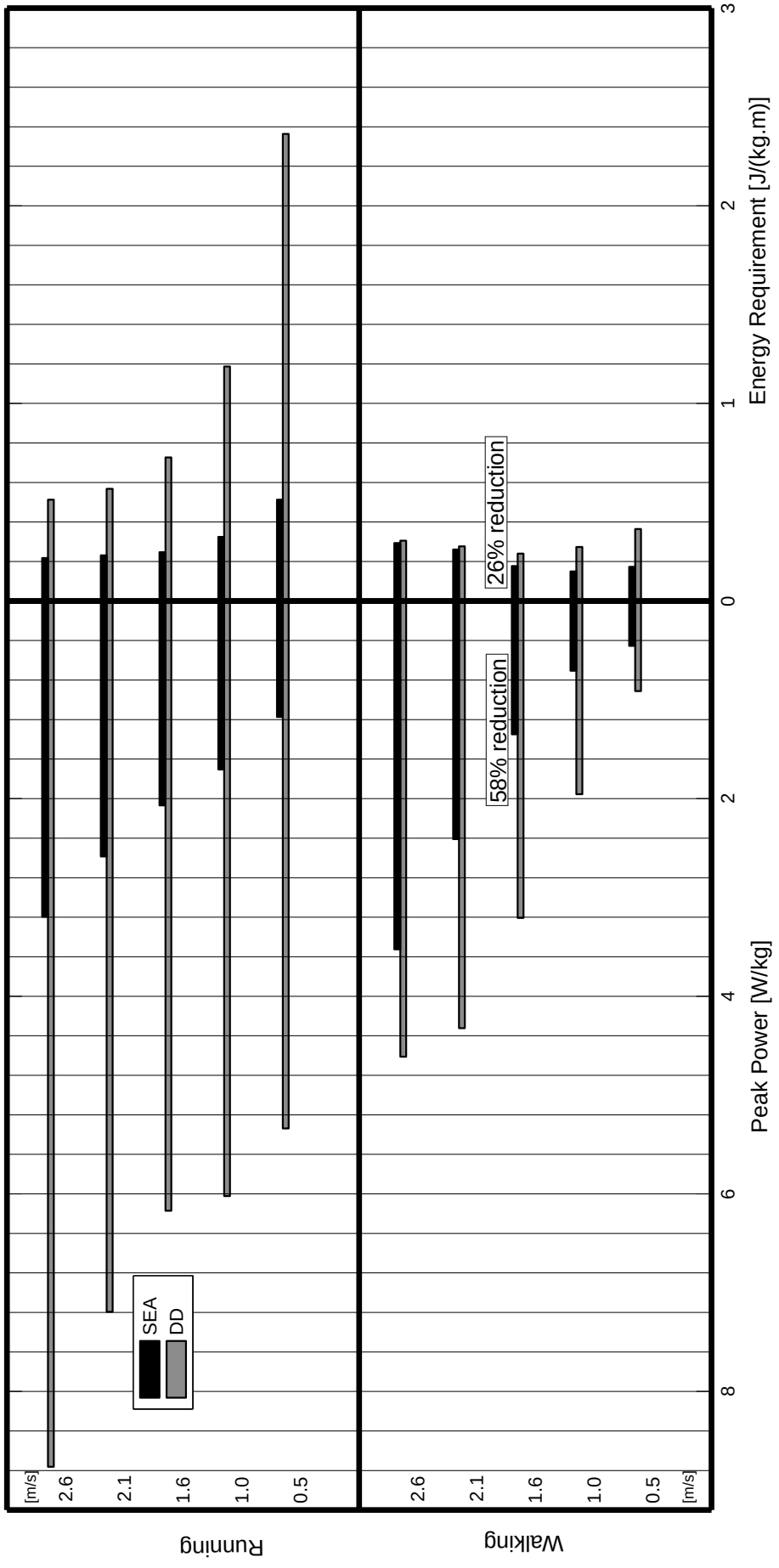

FIGURE 2.4: Comparison of calculated required motor power and energy in DD and SEA concepts, approach for the minimum required motor PP

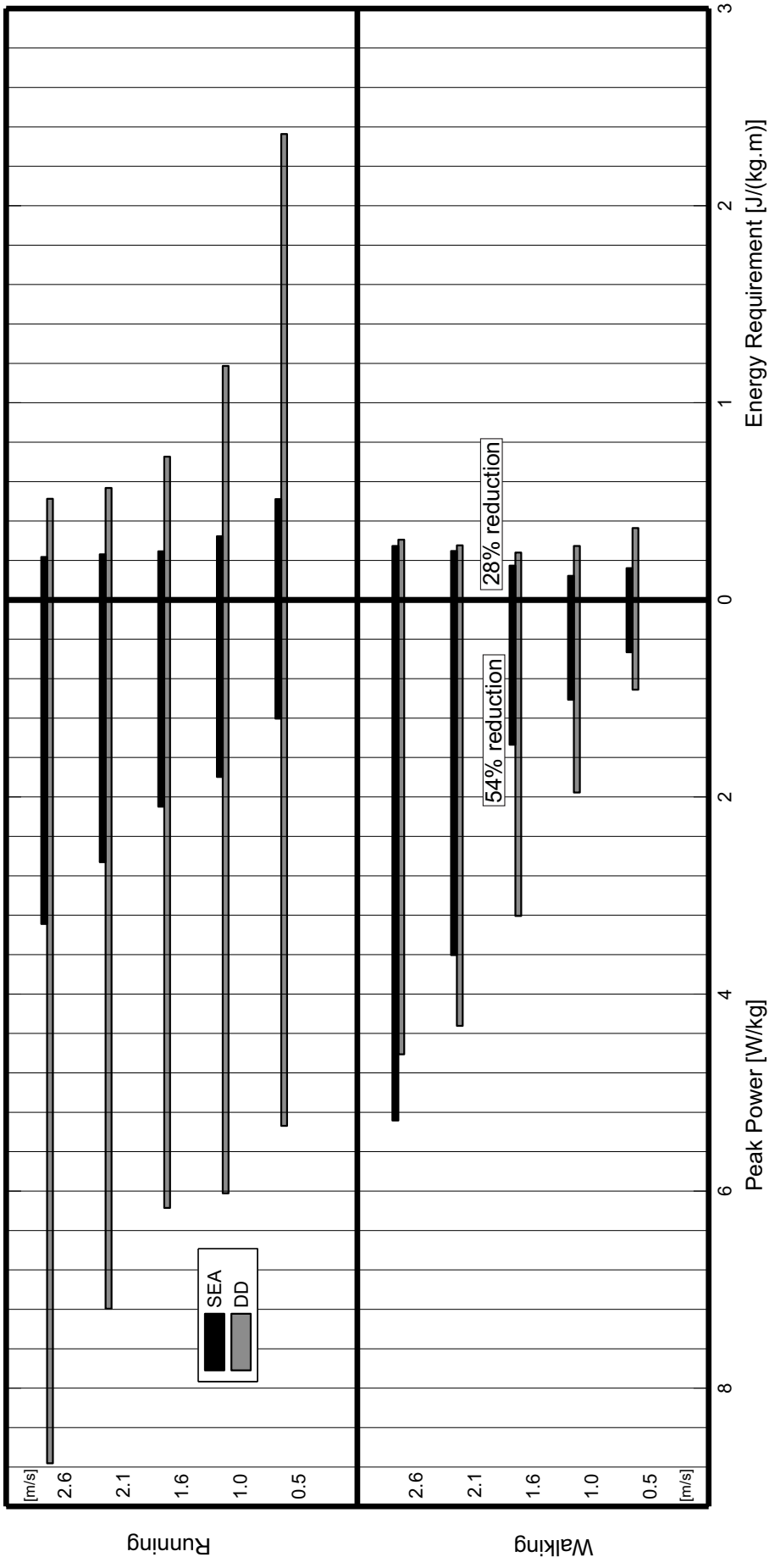

FIGURE 2.5: Comparison of calculated required motor power and energy in DD and SEA concepts, approach for the minimum required energy

TABLE 2.4: The obtained optimal stiffness values to minimize energy requirements at different walking and running speeds

Gait	Walking					Running				
Speed [m/s]	0.5	1.0	1.6	2.1	2.6	0.5	1.0	1.6	2.1	2.6
Stiffness [kN/m]	66	94	73	59	40	71	77	78	76	76

way for design of active foot prosthesis. Consequently, the results of this approach (i.e. minimum PP approach) will be given more attention from this section on.

2.6 Why series elasticity is effective?

2.6.1 Nut velocity

In the previous section we saw that the power requirement of an SEA is less than DD concept. As the name implies, series elasticity can not change the force pattern of motor in SEA concept in comparison to DD. According to Eq. 2.3, the only candidate that could have influence on motor power, would be the nut velocity (or equivalently motor velocity). During push-off period (e.g. 50-60% of the gait cycle) the nut velocity in SEA concept is less than DD to perform a same task (e.g. normal walking 1.6 m/s). This is shown on Fig. 2.6.

During push-off period ($\sim$ 50%-60%) the motor velocity in the SEA is less than DD concept. This is because the potential energy that is stored gradually in spring is released abruptly for push-off time. As a result, the motor could be in a more relieved condition. That is also seen from the velocity graphs in Fig. 2.6.

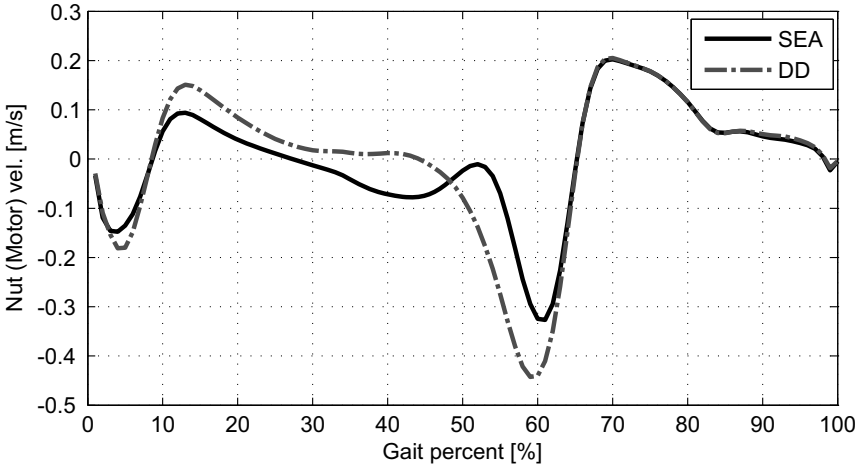

FIGURE 2.6: Comparison of calculated nut velocity (motor velocity) in DD and SEA concepts, approach for the minimum PP requirement (walking 1.6 m/s)

2.6.2 The catapult effect of spring

According to Fig. 2.7, spring stores nearly 13.4 J of potential energy during loading for walking 1.6 m/s (positive section of the spring power curve (green), the figure for changes of the spring length is not shown). The time span for this period is about 0.47 sec (0-48% of the gait, it is obtained based on the kinematics data [5]). The motor and spring graphs are for the minimum PP approach. Therefore, the average spring power for this period would be $\frac{\Delta W}{\Delta t}$= 28.5 W. In contrast, the average spring power for release section (negative section of the spring power curve (green), nearly 0.15 sec, 49-65%) is about 89.3 W. This result shows that the release of spring energy was faster than its storing. It shows the catapult behavior of spring.

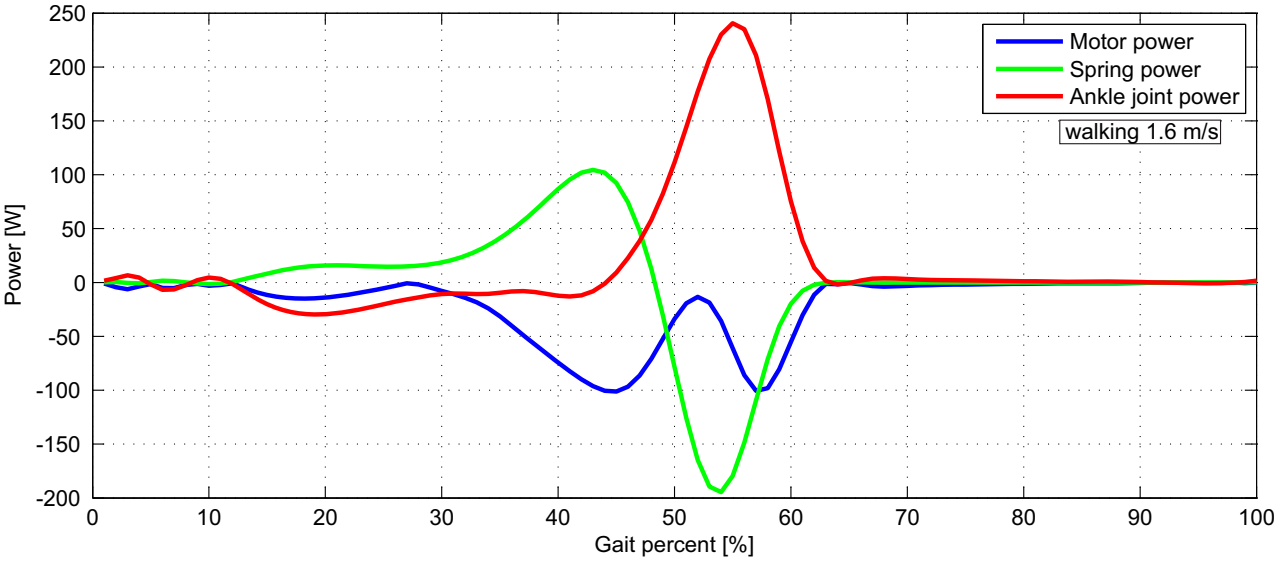

FIGURE 2.7: Comparison of motor (blue), spring (green) and ankle joint (red) power in SEA concept, minimum PP approach, walking 1.6 m/s.

Another point, is that the spring plays a key role in providing most of the required peak power in push-off period (during 52-56% of the gait cycle, Fig. 2.7, the total required power is the ankle joint power shown by the red curve). That is why the motor is required to contribute less to provide the rest of the required push-off power (compare motor power and ankle joint power for this period in Fig. 2.7).

2.7 Walking versus running

Looking at Fig. 2.4, in normal walking (1.6 m/s) the ratio of motor PP with respect to ankle joint power (the biological power) is nearly 0.42 (or equivalently 42%). In normal running (2.6 m/s) this ratio is 36%. The rest of the required power to produce biological ankle power is provided by *the series spring* (for both cases). In this manner, the role of series spring is larger in running (64%) than in walking gait (58%).

On the other hand, in Fig. 2.8 the ankle joint power for normal walking and running are shown. In Fig. 2.8, we see that the amount of negative work (stored energy) in the ankle joint for running is nearly 0.41% of the positive work ($\frac{21.68J}{52.58J}$). For this speed, the negative section is shown with light blue and the positive section with dark blue.

On the other side, for normal walking speed, this percentage is 0.25% (Fig. 2.8). The negative and positive sections are shown with light and dark green respectively.

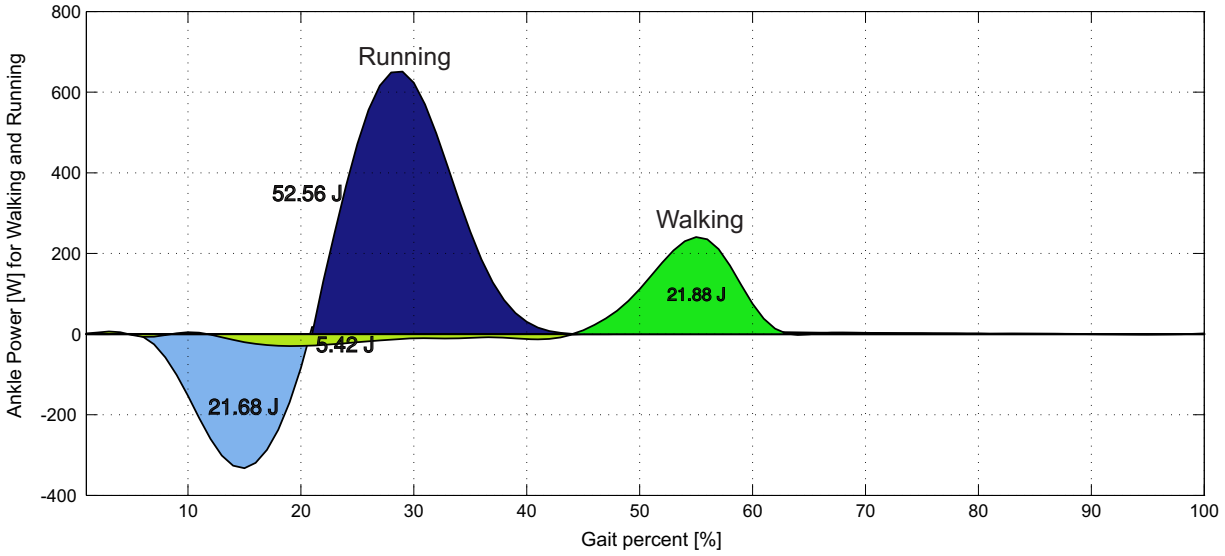

FIGURE 2.8: Comparison between negative and positive work in biological ankle joint in normal walking (1.6 m/s, light/dark green) and running (2.6 m/s, light/dark blue), graphs based on angle and torque data from [5] for a 75 kg person.

Here, we use the term *springy gait*. The more this percentage gets close to 100%, the more the gait could be springy meaning that the stored and released energy are close to each other. In this respect, that running speed could be considered more *springy* than walking.

In the next section, we consider the force-displacement curves of walking and running gaits. We will investigate the relation between the obtained stiffness values (K_s) and the slope of the force-displacement curves of the biological ankle joint.

2.8 The stiffness values

In this section, we study the relation between the stiffness values seen in Tab. 2.3 and the force-displacement curves for the corresponding speed. To do that, this curve is shown for running 2.6 m/s in Fig. 2.9. As seen, the slopes of the loading (red) and unloading (green) phases are different from the corresponding obtained value observed in Tab. 2.3. However, an average of them (the mean stiffness) is close to the value seen in Tab. 2.3.

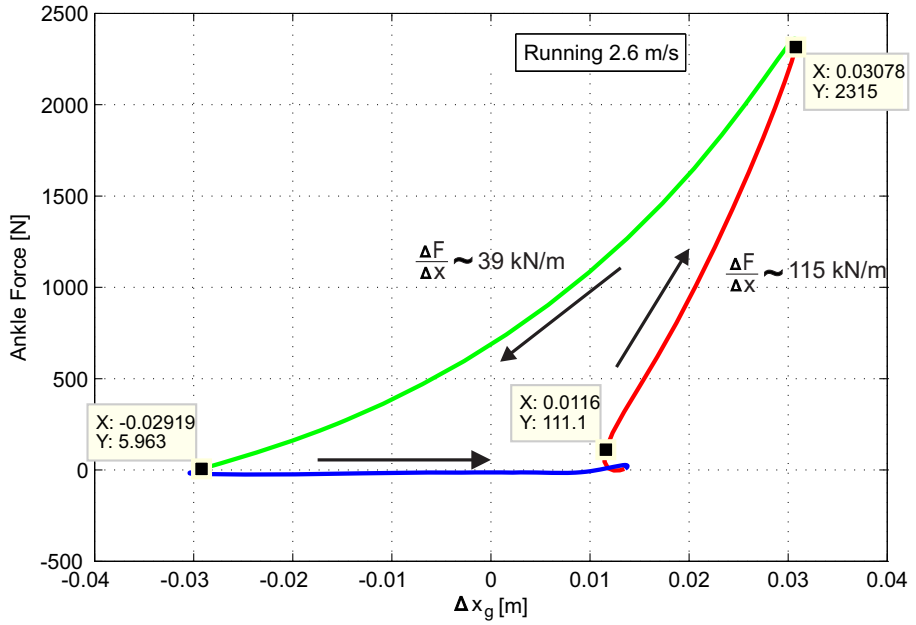

FIGURE 2.9: Comparison between the slopes of the ankle force-displacement curve in running 2.6 m/s during loading (red) and unloading (green). Note that $(39+115)/2 = 77$ and close to the stiffness value in Tab. 2.3 for this speed, (graph based on data from [5] for a 75 kg person).

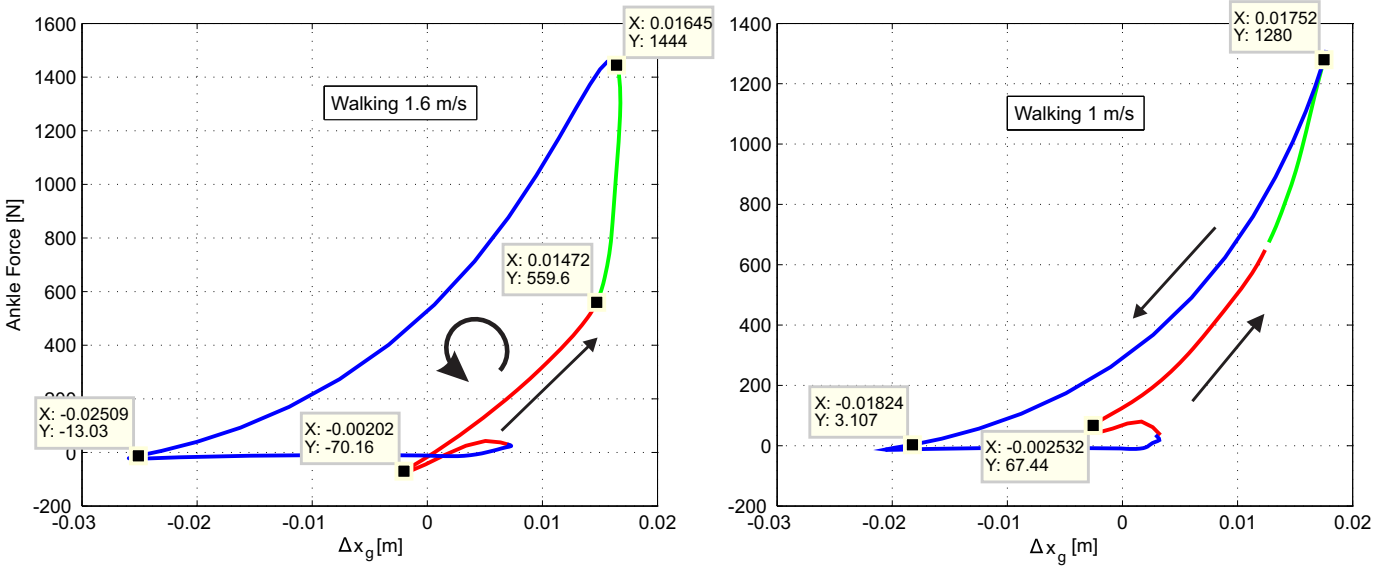

FIGURE 2.10: Comparison between the slopes of the ankle force-displacement curve in walking (graphs based on data from [5] and geometry Fig. 2.2 for a 75 kg person. Arrows show the direction of the gait cycle starting from red section.

This could show that for this speed the optimization found the best average value of the slopes (note that slope of a force-displacement curve represents stiffness).

The force-displacement curves for walking 1 m/s and 1.6 m/s are shown in Fig. 2.10. In these cases, the corresponding stiffness values in Tab. 2.3 are close to the slope of the loading section. For example looking at Fig. 2.10 for walking 1 m/s the slope of the curve is $\frac{\Delta F}{\Delta x} = \frac{(1280-67)}{(0.0175+0.0025)} \simeq 60$

kN/m which is close to the obtained value in Tab. 2.3. Furthermore, for walking 1.6 m/s the slope is nearly $\frac{(1444+70)}{(0.0164+0.0020)} \simeq 82$ kN/m which is again close to the value seen in Tab. 2.3.

2.9 From waking to running

In Tab. 2.5 the amount of negative, positive and net ankle joint work during a gait cycle is shown for different walking and running speeds.

As seen in Tab. 2.5, until 1.6 m/s, the net work W^{net} in walking is less than in running for each speed. However, for 2 m/s and 2.6 m/s, this paradigm changes and the net work W^{net} in walking is higher than that of the corresponding running speed. It could mean that at this speed, the person might change the gait from walking to running as it costs less energy for him/her.

TABLE 2.5: The negative W^-, positive W^+ and net work W^{net} in the *human ankle joint* for different speeds in walking and running, data for a 75-kg person, based on data from [5].

Gait	Walking			Running		
W [J]	W^-	W^+	W^{net}	W^-	W^+	W^{net}
0.5 [m/s]	-10.7602	8.8599	-1.9003	-35.9805	40.6595	4.6790
1 [m/s]	-9.5361	14.7168	5.1807	-31.8395	45.1267	13.2872
1.6 [m/s]	-5.2120	22.0956	16.8836	-23.3410	44.7223	21.3813
2 [m/s]*	-3.2407	33.7240	30.4833	-20.3062	47.6461	27.3399
2.6 [m/s]	-3.4312	40.8698	37.4386	-21.5873	52.6611	31.0738

2.10 Minimum PP and ER requirement in SEA

Eq. 2.8, shows that a spring stiffness could be found such that it minimizes the maximum required power (i.e. PP). Fig. 2.11 actually shows that such a stiffness value exists that would minimize PP or ER requirement (graphs are for normal walking 1.6 m/s).

The minimum PP and its corresponding ER together with minimum ER and its corresponding PP values are also shown in this figure (compare with Tab. 2.3 and 2.4, see also Figs. 2.4 and 2.5). Note that in case of very high stiffness values the required PP or ER will converge to that of the DD actuation concept.

In Fig. 2.12 the required power in SEA and DD concepts are shown for a gait cycle (walking 1.6 m/s). As it is seen to produce a push-off power of 3.20 W/kg, a peak power of 1.34 W/kg is required in SEA concept[1]. Thus, a power amplification of 2.38 is predicted.

[1]However, note that a biological peak power does not necessitate a motor peak power at the same gait percent, see the green dashed line (i.e. the push-off time) in Fig. 2.12.

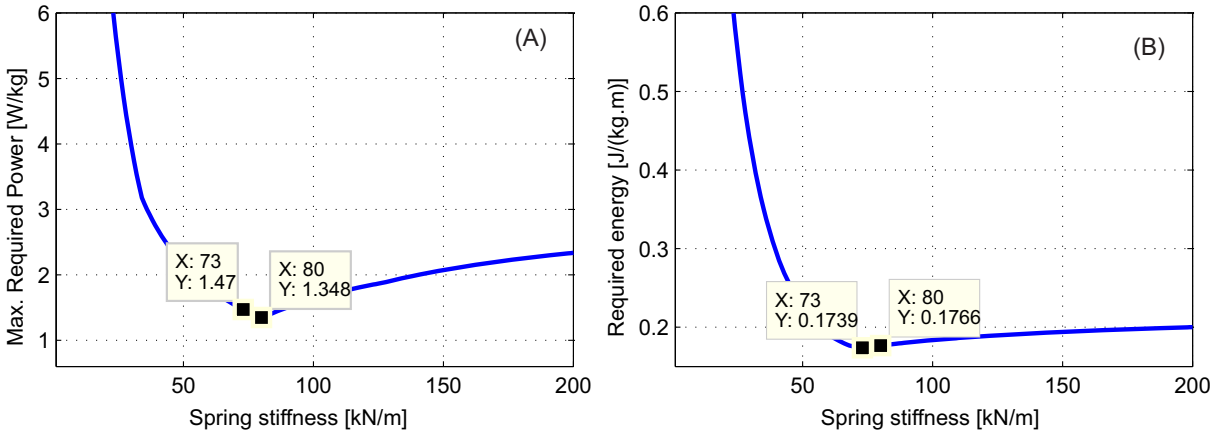

FIGURE 2.11: Required peak power (A) and the corresponding energy requirement (B) with respect to spring stiffness (graphs for walking 1.6 m/s).

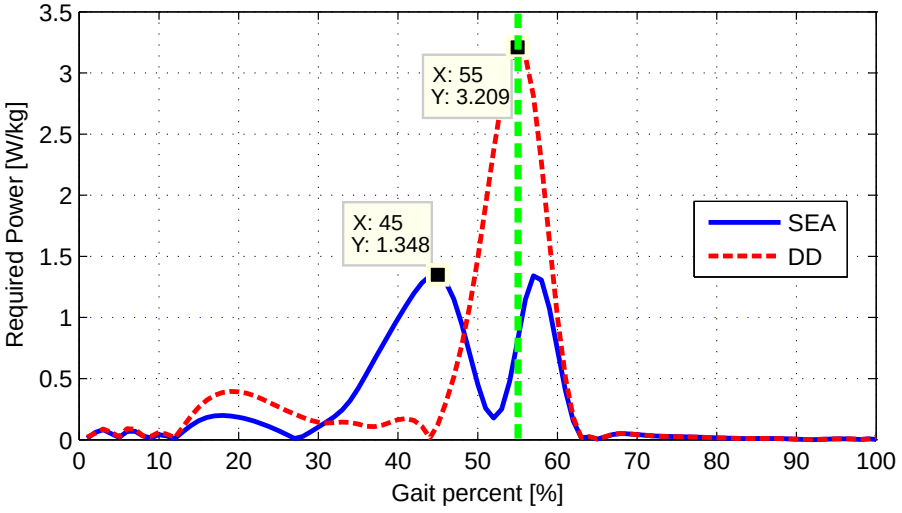

FIGURE 2.12: Required power in SEA and DD actuation concept (graphs for walking 1.6 m/s, the curve for SEA is for the minimum PP approach), the green dashed line shows the push-off time.

2.11 One stiffness for all gaits

According to Tab. 2.3 or Fig. 2.13 (shown by squares) the optimal stiffness value for each speed is different from other speeds. This might pose a problem when it is necessary to construct a prosthesis with constant stiffness. Because, not having an optimal stiffness value would result in the increase of power requirement as shown in Fig. 2.11. To solve this problem, one approach could be to find out which spring stiffness would result in a minimum sum of the peak power for all (walking and/or running) speeds. The sum of the minimum peak power of all walking speeds is 8.44 W/kg (Fig. 2.13).

The procedure to find the minimum sum was

$$min(\sum_{sp=1}^{5} P_{max,\ sp}^{K_s}) \quad for \quad K_s = 1\ ...\ 200\ kN/m \tag{2.10}$$

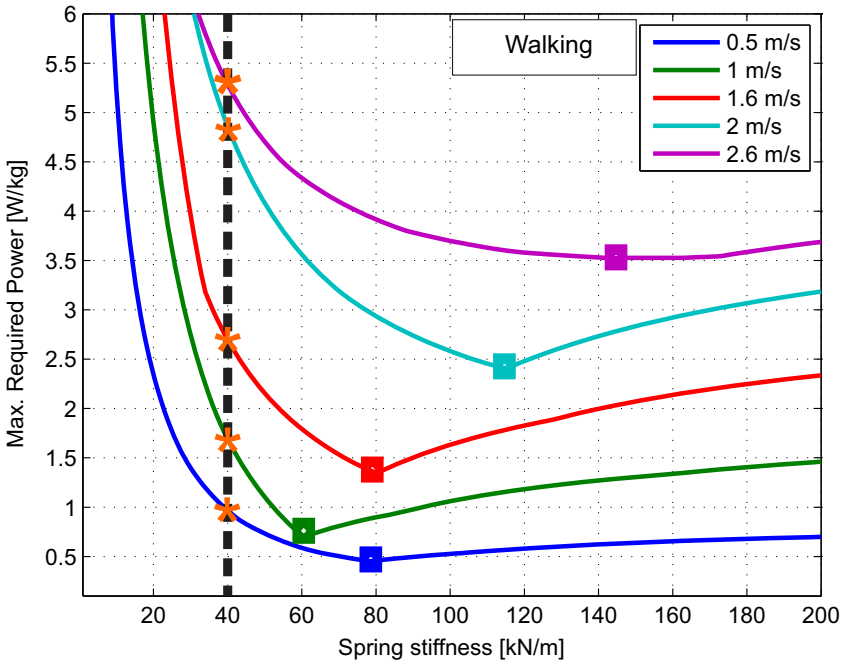

FIGURE 2.13: Required peak power in SEA actuation concept with respect to spring stiffness and walking speeds, see also Tab. 2.3. The sum of the minimum peak power of all walking speeds is 8.44 W/kg. For each stiffness value the five peak power values (e.g. as shown by the asterisks) corresponding to five speeds are processed by Eq. 2.10 to achieve Fig. 2.14.

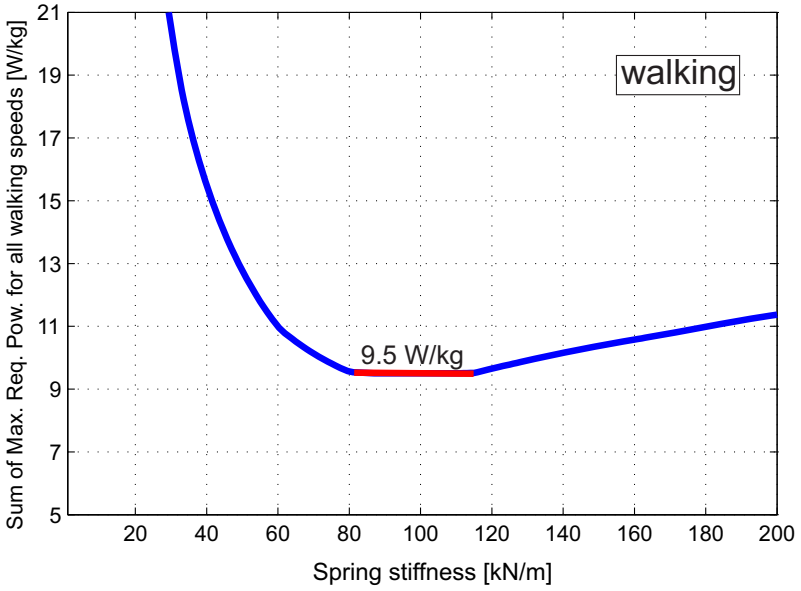

FIGURE 2.14: Sum of the required max. power for different walking speeds (in SEA actuation concept) with respect to spring stiffness (derived from Fig. 2.13).

For each stiffness in Fig. 2.13, there are five PP values. These values are summed up and then for a range of 1-200 kN/m, the stiffness with the minimum sum was found. The result is shown in Fig. 2.14.

The result of this approach is shown in Fig. 2.14 for walking. It was found out that there is a region in which the sum of peak power for all speeds (at each stiffness) is minimum. As shown in Fig. 2.14

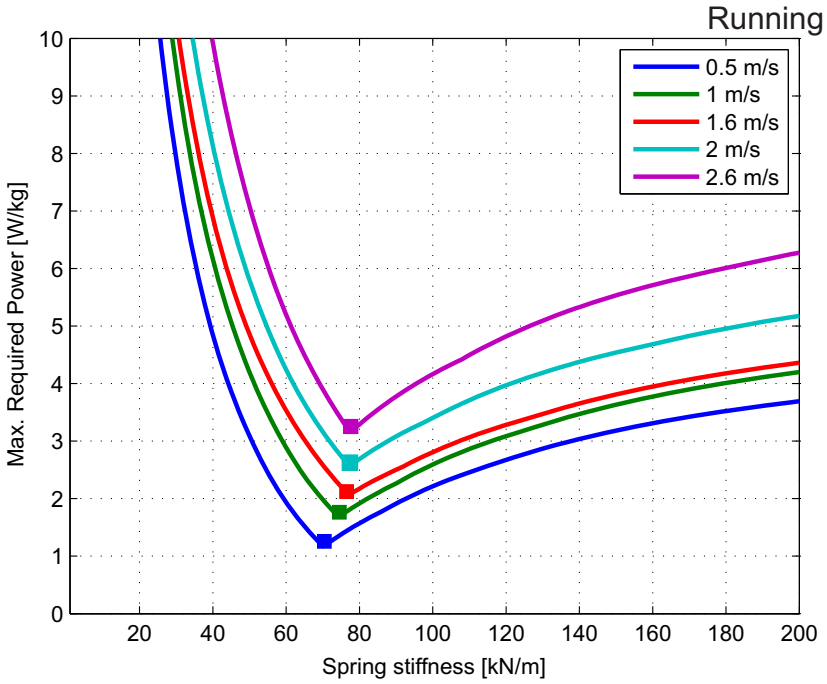

FIGURE 2.15: Required max. power in SEA actuation concept with respect to spring stiffness and different walking speeds, see also Tab. 2.3.

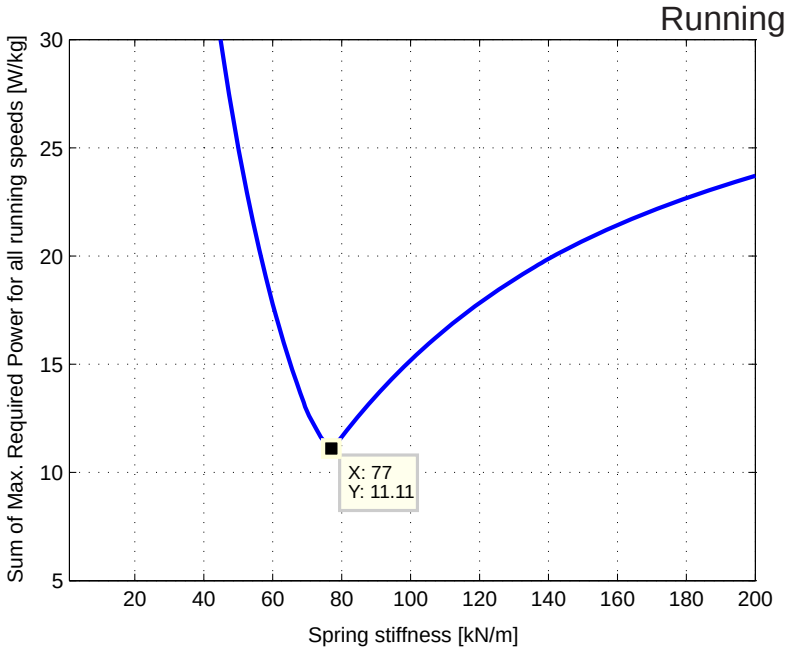

FIGURE 2.16: Sum of the required max. power for different walking speeds (in SEA actuation concept) with respect to spring stiffness (derived from Fig. 2.15).

this minimum is 9.50 W/kg and the stiffness range is nearly 82-115 kN/m (red line). However, as higher walking speeds are not common in human walking (see e.g. Tab. 2.5), a stiffness value of 82 kN/m is preferred which is in the vicinity of the stiffness value for normal walking speed of 1.6 m/s (see Tab. 2.3 and Fig. 2.13).

A same procedure was used for the running gait (Fig. 2.15). The result is shown in Fig. 2.16. As

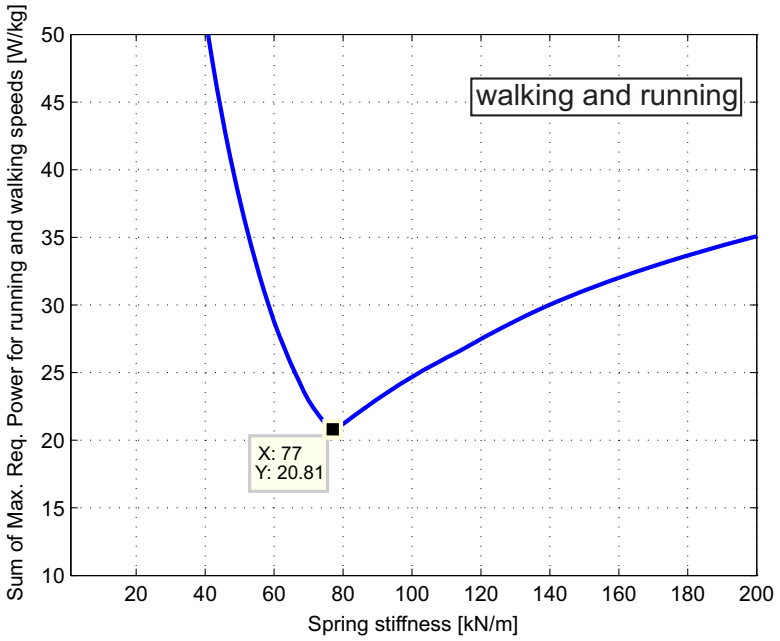

FIGURE 2.17: Sum of the required max. power for different walking and running speeds (in SEA actuation concept) with respect to spring stiffness (derived from Fig. 2.13 and 2.15).

seen for this gait, there is an optimal stiffness (77 kN/m) which minimizes the sum of the required peak power to 11.1 kN/m.

In continuation, by adding the curves for both walking and running gaits (Figs. 2.14 and 2.16) we can design a powered ankle that operates close to optimal condition for all walking and running speeds with a corresponding stiffness of 77 kN/m. The result is shown in Fig. 2.17.

2.12 Stiffness changes w.r.t. body mass (for PP approach)

In Tab. 2.6 the changes of the required spring stiffness with respect to body mass are shown (for PP approach). As seen the higher the body mass, the higher the spring stiffness.

TABLE 2.6: Changes of the required spring stiffness with respect to body mass (for minimum PP approach).

Gait		Walking					Running				
Speed [m/s]		0.5	1.0	1.6	2.1	2.6	0.5	1.0	1.6	2.1	2.6
Stiffness [kN/m]	75 kg	78	61	80	115	143	70	74	77	77	77
	100 kg	105	81	107	153	191	94	99	103	103	103
	125 kg	131	101	134	192	238	117	124	129	129	129
Stiffness/BodyMass [kN/(m.kg)]		1.05	0.81	1.07	1.54	1.90	0.94	0.99	1.03	1.03	1.03

In addition it is seen that for higher running speeds the spring stiffness are very close to each other. The reason is that the slope of the angle-torque curve is very similar for these speeds. Furthermore,

for a specific speed, the ratio of stiffness and body mass is approximately constant (last row in Tab. 2.6).

2.13 A more realistic model for power-energy requirements

The required motor power presented by Eq. 2.3 does not provide a realistic estimation for motor requirements. The inefficiencies of different parts in a robotic system increase the power-energy requirement in real world. In this section, we bring some of these factors into consideration and see their effects on the total power requirement. The required torque of a motor is dependent on its rotor inertia and external load (in brushless motors the friction is considered negligible). The motor torque is

$$T_m = \underbrace{\frac{F_m L}{2\pi\eta_{scr}}}_{external\ load} + \underbrace{J_m\ddot{\theta}_m}_{rotor\ inertia} \tag{2.11}$$

where L and η_{scr} are the screw lead and efficiency respectively [58] and J_m is the (motor) rotor inertia and $\ddot{\theta}_m$ is the motor angular acceleration. F_m is the motor force and is related to spring stiffness by Eq. 2.5. Motor angular velocity (or acceleration) could be obtained through [58]

$$\dot{\theta}_m = \frac{2\pi}{L}\dot{x}_n \tag{2.12}$$

The ball screw efficiency is usually high (nearly 80%-90%, different manufacturers' catalog). This efficiency could be used for calculations or in a more detailed approach one can use [58] (this efficiency is used when the load and motion are in opposite direction)

$$\eta_{scr} = \frac{L}{2\pi r}\frac{2\pi r - \mu L}{L + 2\mu\pi r} \tag{2.13}$$

where r and μ are the screw radius and coefficient of friction respectively [58]. The required electrical motor power P_{me} is

$$P_{me} = V_m\ I_m \tag{2.14}$$

where V_m and I_m are the motor voltage and current respectively. According to the motor model seen in Fig. 2.18,

$$V_m = L_m\dot{I}_m + R_m I_m + K_v\dot{\theta}_m \tag{2.15}$$

where L_m, R_m and K_v are the motor inductance, resistance and velocity constant factors. According to the different manufacturers, the inductance of their DC motors could be assumed to be negligible (see ThinGap or Maxon motors). Therefore, it can be neglected from Eq. 2.15.

Furthermore, motor current I_m is dependent on motor torque T_m by

$$T_m = K_t\ I_m \tag{2.16}$$

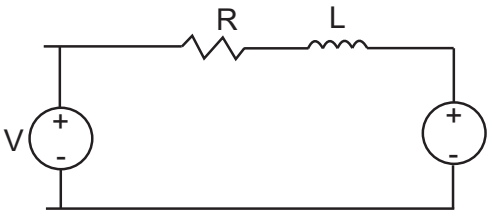

FIGURE 2.18: A model of DC motor, V relates to the power supply.

where K_t is the torque constant of the motor.

Based on Eqs. 2.14, 2.15, 2.16 the required electrical motor power is

$$P_{me} = (R_m \frac{T_m}{K_t} + K_v \dot{\theta}_m) \frac{T_m}{K_t} \tag{2.17}$$

This is a compressed form for expressing the motor power calculation. It should be noted that, considering Eq. 2.11 through Eq. 2.16, Eq. 2.17 includes the spring stiffness as an optimization variable as stated in Eq. 2.5. The procedure for finding the minimum value of P_{me} is similar to the ideal case without system inefficiencies and inertia which was discussed in previous sections.

In order to compare the more realistic calculated power P_{me} with the ideal one P_m, we compare the power requirements for three cases: (1) the case system is ideal (2) the case there is Maxon RE40 and (3) when there is ThinGap BL2320 as power source in the system. The power is calculated for normal walking (1.6 m/s). The motor properties are summarized in Tab. 2.7. The ThinGap motor is used for the PAKO platform. The Maxon motor was used in [25].

TABLE 2.7: Properties of Maxon RE40 and ThinGap TG2320 Motors together with ball screw parameters

type	[1]Maxon RE40	ThinGap BL2320
J_m [kg.m^2]	1.39e-5	1.64e-4
K_t [Nm/Amp]	0.060	0.035
R_m [Ω]	1.16	0.31
[2]K_v [V/(rad/s)]	0.060	0.036
L [mm] (ball screw)	2	2
η_{scr} [%] (ball screw)	80	80

[1] data for 48 V (in Maxon motor catalog)
[2] K_v and K_t values in DC motors are quite similar

The required motor PP and the corresponding ER requirement for the Maxon and ThinGap motors are shown in Tab. 2.8. The corresponding obtained optimal stiffness values are also seen in the same table.

TABLE 2.8: Required motor PP for Maxon and ThinGap motors (approach: minimum PP, walking 1.6 m/s)

Motor	[1]Ideal	Maxon RE40	ThinGap BL2320
PP [W/kg]	1.34	3.73	88.02
[2]ER [J/(kg.m)]	0.177	0.64	8.27
K_s [kN/m]	80	48	34

[1] see also Fig. 2.4
[2] the corresponding ER

TABLE 2.9: The effects of system parameters (for Maxon RE40) on required motor PP and optimal stiffness (approach: minimum PP, walking 1.6 m/s)

Case	required PP [W/kg]	change w.r.t previous PP [W/kg]	change w.r.t previous PP [%]	change w.r.t ideal PP [%]	corresp. Stiffness [kN/m]
[1]R_m=0 Ω, J_m=0 kg.m^2 η_{scr}	1.68	[2] 0.34	+25	+25	80
R_m=0 Ω J_m,η_{scr}	2.93	1.25	+74	+119	44
R_m,J_m,η_{scr}	3.73	0.8	+27	+178	48

[1] It means only screw deficiency η_{scr} is considered
[2] w.r.t ideal (1.34 W/kg), see also Tab. 2.8

In Tab. 2.9 the effects of different system inefficiencies on power increase are brought in order to show the individual effect of each parameter with respect to the ideal power. Tab. 2.9, shows that system parameters influence the peak power requirements.

As seen in Tab. 2.9, the rotor inertia has played a key role in determination of the spring stiffness. The optimization process has found a spring stiffness to reduce the effects of the rotor inertia. This is shown in Fig. 2.19. The required power to overcome inertia is $J_m\ddot{\theta}_m\dot{\theta}_m$ and $\dot{\theta}_m$ is related to $\dot{x}_n$ by Eq. 2.12 (accordingly the second derivative is also related).

2.14 Working region

Using Eq. 2.15 for constant voltage V_m operation

$$V_m = R_m I_m + K_v\dot{\theta}_m \Rightarrow \dot{\theta}_m = \frac{V_m}{K_v} - \frac{R_m.T_m}{K_v.K_t} \tag{2.18}$$

for the case that $T_m = T_{stall}$ it could be assumed that $\dot{\theta}_m = 0$ and hence $V_m = \frac{R_m.T_{stall}}{K_t}$. Therefore Eq. 2.18 could be re-written as

$$\dot{\theta}_m = \frac{R_m}{K_v.K_t}(T_{stall} - T_m) \tag{2.19}$$

$\frac{R_m.T_{stall}}{K_t.K_v}$ could be used as an estimation for motor no-load velocity (in Maxon motors). According to Eq. 2.19, motor velocity $\dot{\theta}_m$ is a function of motor torque T_m. The Eq. 2.19 is used to depict

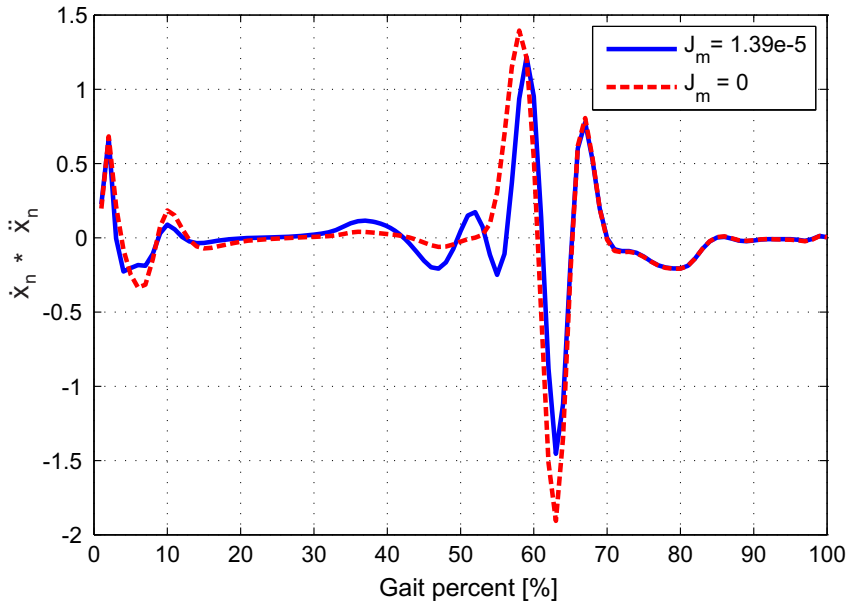

FIGURE 2.19: The result for $\dot{x}_n.\ddot{x}_n$ (or equivalently $\dot{\theta}_m.\ddot{\theta}_m$) between the case rotor inertia is taken into account (with K_s=48 kN/m) and the case it is not taken into account (with K_s=80 kN/m) (inertia for Maxon RE40, minimum PP approach, see also Tab. 2.8).

Fig. 2.20. In Fig. 2.20, the nominal working condition (nominal torque-velocity) of Maxon RE40 and the required working condition for this motor are shown.

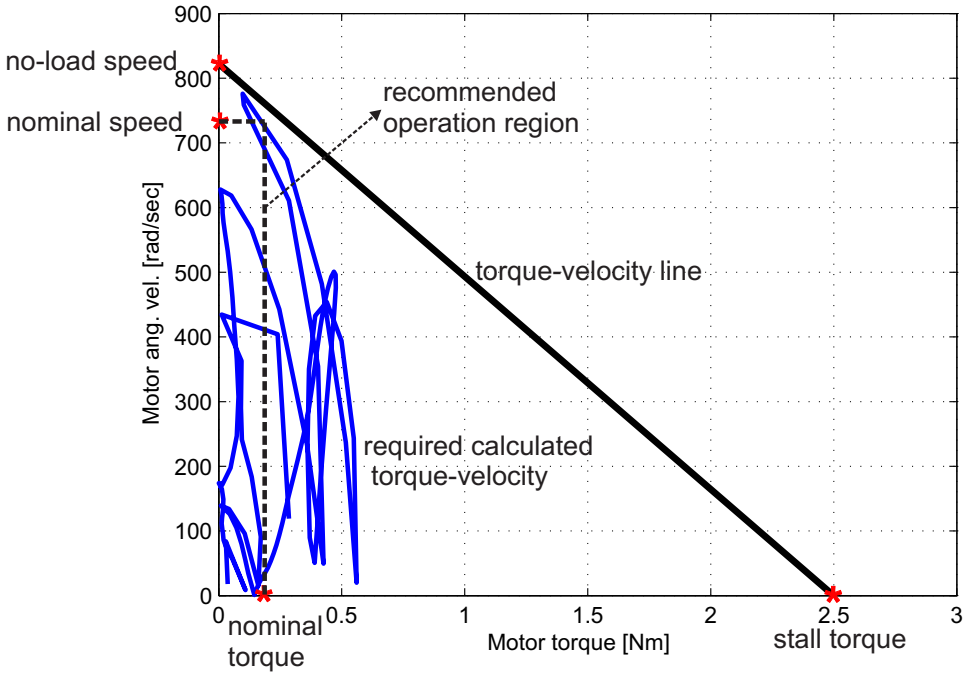

FIGURE 2.20: Recommended (dashed) and required (calculated) range of operation for Maxon RE40 (blue, minimum PP approach), together with torque-velocity line for this motor (according to Eq. 2.19).

As it is seen in Fig. 2.20 in some parts of the gait cycle the operation of the motor would be out of the nominal working conditions. However it is still under the extreme condition imposed by the

torque-velocity line. Nevertheless, we investigate the heating issue in the motor. In the next section, a thermal model of motor is presented and the effects of motor working in areas outside of the normal region will be investigated.

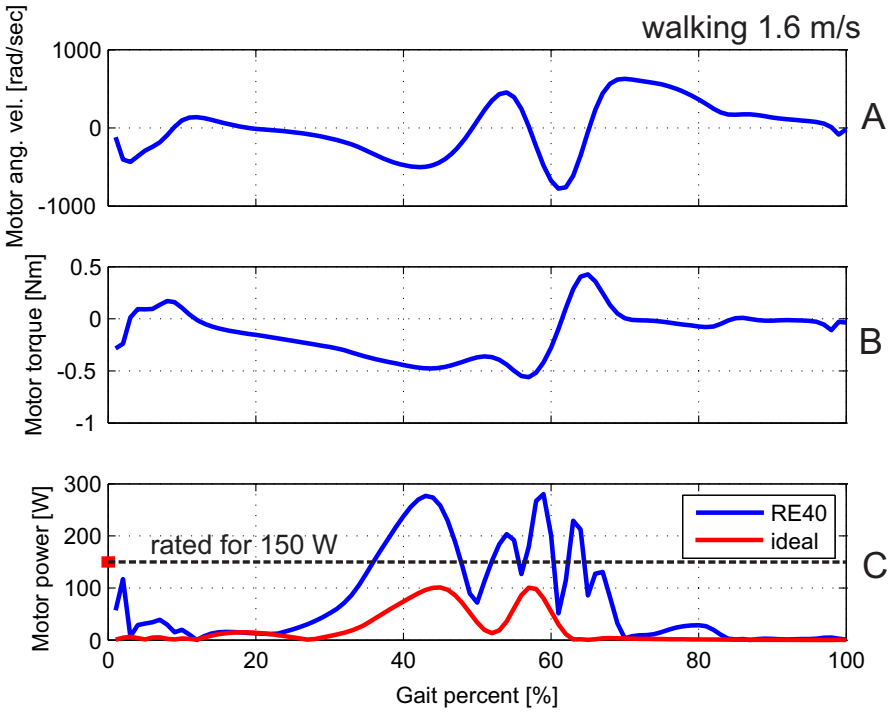

FIGURE 2.21: The required motor angular velocity and torque to perform walking 1.6 m/s, together with the curves for required motor power for RE 40 and the ideal required motor power (graphs for minimum PP approach).

In Fig. 2.21, the motor angular velocity and torque are shown for Maxon RE40 for walking at 1.6 m/s. In addition, the required motor power in this case is compared with that of the ideal motor. As observed, for the mid to late stance, the motor is working outside the rated power which is 150 W. Furthermore, after 60% (swing phase) there is high power demand, that is mainly due to the inertia of the rotor (in the swing phase the velocity of motor changes direction at high acceleration, due to this matter power loss due to inertia is noticeable).

2.15 Motor temperature

In this section we investigate the motor temperature changes in case the motor is working outside nominal conditions (w.r.t speed and torque). Based on first law of thermodynamics energy does not vanish it just gets converted to other forms. In this case the electric energy is converted into heat. The thermal energy that is produced by resistance for a time period Δt is

$$Q_R = R_m I_m^2 \Delta t \tag{2.20}$$

In heat transfer the phrase *thermal resistance* is usually used to create a connection between electrical and thermal science. Based on analogy between thermal and electrical circuits (see heat transfer textbooks for more information), similar to electrical circuits we can define a thermal resistance R_{th}. In electrical circuits the current flow I is related to the resistance R and electrical potential difference ΔV by $I = \frac{\Delta V}{R}$. Using this analogy, we could conclude that $q_{th} = \frac{\Delta T}{R_{th}}$ that relates the temperature difference, the thermal flow q_{th} and thermal resistance R_{th} to each other. This notion is used for the following discussion.

According to the first law of thermodynamics and using Fig. 2.22 the energy balance for the rotor is

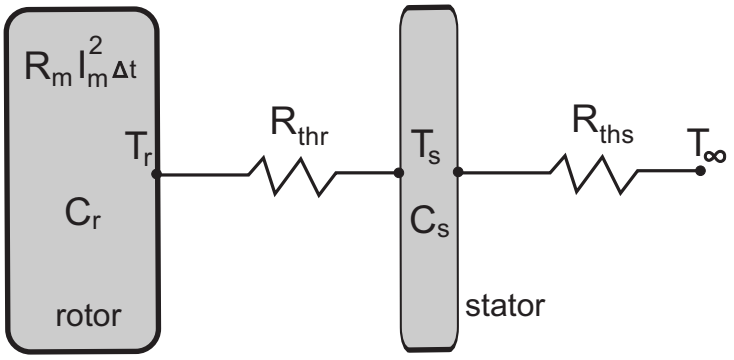

FIGURE 2.22: A thermal model for motor. T_r: rotor temperature, T_s: stator temperature, R_{thr}: rotor-stator thermal resistance, R_{ths}: stator-environment thermal resistance, T_∞: environment temperature, C_r: rotor thermal capacity, C_s: stator thermal capacity.

$$R_m I_m^2 \ \Delta t - \frac{T_r - T_s}{R_{thr}} \ \Delta t - C_r \ \Delta T_r = 0 \tag{2.21}$$

or in differential form

$$R_m I_m^2 - \frac{T_r - T_s}{R_{thr}} \ - C_r \ \frac{dT_r}{dt} = 0 \tag{2.22}$$

in which T_r and T_s are the rotor and stator temperatures respectively. C_r is the (thermal) heat capacity of the rotor.

according to Fig. 2.22, the energy balance for stator could be

$$\frac{T_r - T_s}{R_{thr}} \ \Delta t - \frac{T_s - T_\infty}{R_{ths}} \ \Delta t - C_s \ \Delta T_s = 0 \tag{2.23}$$

a differential equation could be also extracted from Eq. 2.23. The environment temperature T_∞ is taken 25°C.

the simulation was done in Matlab and Simulink. According to Fig. 2.21B, the highest motor torque (or equivalently current) would be nearly 0.6 Nm (walking 1.6 m/s). In this case, the highest power dissipation in the form of heat happens. Assuming that this maximum heat production is permanent (i.e. for a wide temporal interval this maximum amount of heat is produced), the worst scenario for the rotor temperature is simulated (estimated). The necessary parameters for calculations are obtained from Maxon catalog RE40 (see appendix A).

In Fig. 2.23, the simulation result for the changes of rotor temperature T_r with respect to time is presented (walking at 1.6 m/s). According to the Maxon catalog, the highest permissible temperature for rotor is 155°C. Fig. 2.23 indicates that under that afore-mentioned operation condition the rotor temperature would reach 155°C after 36 seconds.

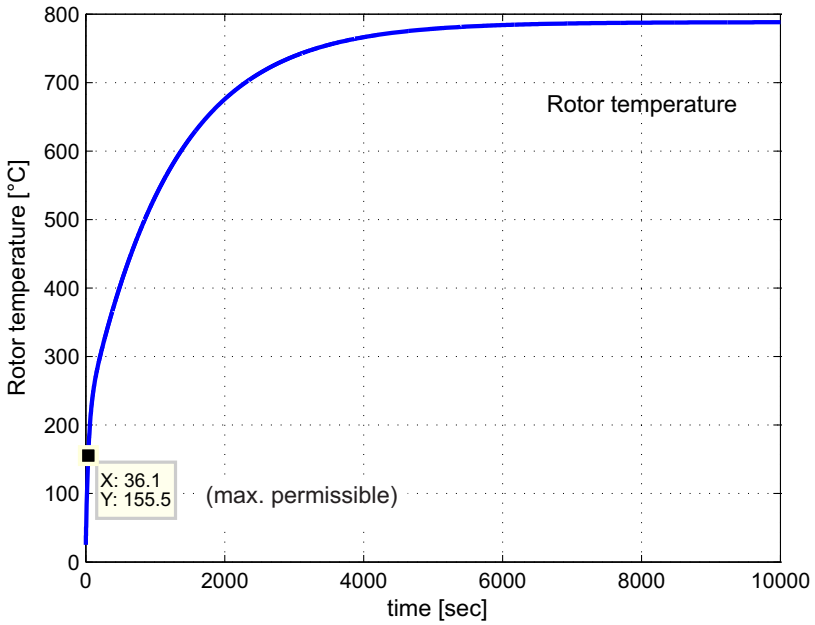

FIGURE 2.23: Change of rotor temperature with respect to time (graph for the worst case scenario, the necessary parameters for calculations are obtained from Maxon catalog RE40, see appendix A).

As seen in Fig. 2.21B, for the most part, the torque (or equivalently current) is not close to the maximum value for this walking speed (1.6 m/s). For this walking speed, when a mean value of motor torque was used for the simulation (0.2 Nm), the results showed that the rotor temperature does not reach the maximum permissible temperature of 155°C.

2.16 Motor control

To regulate motor position, a PD controller could be used. Eq. 2.7 gives a basis to obtain the desired values for motor position and velocity to be used for creating the command signal. This will be further discussed in chapter 6.

2.17 Other optimization approaches

2.17.1 Variables other than power-energy

It should be noted that other variables like motor velocity $\dot{\theta}_m$ or motor acceleration $\ddot{\theta}_m$ could be also considered as objective function for optimization. The procedure could be to minimize the

motor velocity and/or acceleration (e.g. to minimize $\dot{\theta}_m.\ddot{\theta}_m$). However minimizing power-energy requirements is a method that implicitly includes both of the variables.

2.17.2 Other optimization methods

In order to obtain the optimal stiffness values (e.g. Tab. 2.3), the required relations were programmed in Matlab. However other methods could be also available using the *Matlab's Optimization Toolbox*. For example, *Genetic Algorithm* (GA) was also used for searching the optimal stiffness values. For walking 1.6 m/s, for instance, the optimal stiffness predicted by GA was 80.233 kN/m. This is close to the one seen in Tab. 2.3.

2.18 Summary

In this chapter, the following issues were discussed and found:

1. Inspired from muscle-tendon unit (MTU), using spring in series with a motor is useful for reducing the power and energy requirement in active ankle prostheses.

2. The modelling shows for each speed and gait there is a unique spring stiffness that minimizes peak power (PP) or energy (ER) requirement.

3. Choosing a motor mostly depends on the working condition (gait, speed, age, sex). However, motor and mechanical parameters of the robotic prosthesis noticeably change the PP and ER requirement.

4. A thermal modelling of the rotor was used in order to analyze the temperature behavior of the motor for a severe case of continuous maximum load. It was shown, for the worst case scenario, the motor could not be under load for a wide temporal interval. However, for working in average condition, the motor could be used for a wide temporal interval.

Chapter 3

Alternative Actuation Approaches: Parallel Elastic Element (PEE)

3.1 Introduction

In Chap. 2, the effectiveness of SEA mechanism for reducing peak power (PP) and energy (ER) requirement was shown in comparison to direct drive (DD) approach. The idea was based on the biological muscle-tendon unit that benefits from series elastic element (SEE). Looking at Figs. 1.15 and 1.16, it is seen that the muscle model, has also elastic element in *parallel* with the contractile element (i.e. motor). This parallel elastic element (PEE) is the main concentration of this chapter. The focus would be what kind of advantages it might have for active ankle prosthesis especially in terms of PP-ER requirement.

SEA can reduce PP-ER requirement since the motor velocity can be reduced in comparison to direct drive (DD). Here, we investigate if adding PEE could lead to a mechanism that could be even better than SEA mechanism[1]. In the following chapters, the introduced actuation mechanisms will be compared with SEA which was already shown to be a good candidate for active foot prostheses (see Chap. 2).

3.2 Muscle model, use of parallel elastic element (PEE)

Looking at Figs. 1.15 and 1.16 in Chap. 1, and focusing on SEA structure (Fig. 2.2), a mechanism based on the SEA concept with additional parallel elastic element (PEE) could be configured as shown in Fig. 3.1.

[1] A part of this chapter was published in IEEE International Conference on Robotics and Biomimmetics [61], and IEEE International Conference on Robotics and Automation [62].

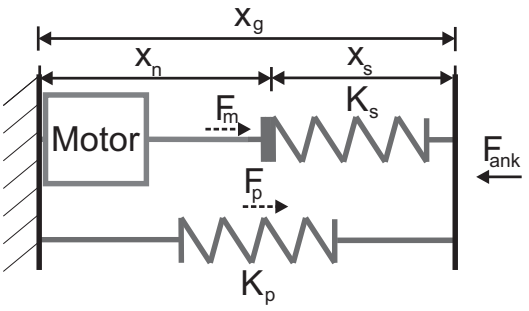

FIGURE 3.1: SEA+PS concept, PS could be in compression and/or elongation mode, PS: Parallel Spring, K_s: stiffness of series spring, K_p: stiffness of parallel spring.

This mechanism is called SEA+PS (Fig. 3.1) to show that this mechanism is a continuation of the SEA concept with an added PEE component (PS: Parallel Spring). Another similar configuration is a PEE that operates just in elongation mode and can only produce pulling forces. This mechanism is called SEA+UPS (UPS: Unidirectional Parallel Spring) and is shown in Fig. 3.2.

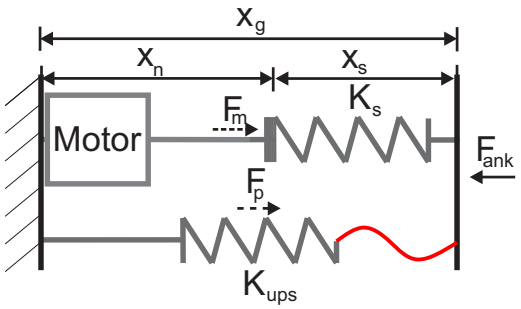

FIGURE 3.2: SEA+UPS concept, UPS could produce force only in elongation mode, UPS: Unidirectional Parallel Spring, K_{ups}: stiffness of unidirectional parallel spring (it acts like a non-linear spring).

The difference between these two configurations and its effect on PP-ER requirement will be discussed in the following sections.

3.3 Compliance

In order to investigate more comprehensively the effects of parallel elasticity (PS and UPS) we consider also the DD+PS and DD+UPS concepts (DD: Direct Drive). These concepts are shown in Fig. 3.3. In SEA+PS and SEA+UPS concepts there is elasticity in series with the motor. These systems could be considered compliant. However, in DD+PS and DD+UPS concepts, the spring is in parallel with motor, which has a high stiffness value. These systems could not be considered compliant compared to SEA+PS or SEA+UPS concepts. Therefore, for applications in active ankle prosthesis, this must be taken into consideration. Nevertheless, as it will be shown later, these concepts have relatively better results than DD concept in terms of reduction of PP-ER requirement (for some speeds they are even better than SEA concept).

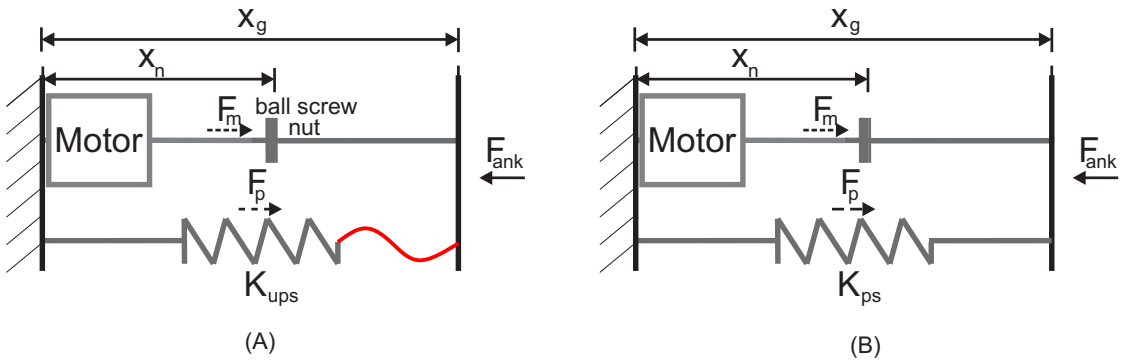

FIGURE 3.3: DD+UPS (A) and DD+PS (B) concepts.

3.4 Power-Energy requirement

In Fig. 3.4, schematic views of several active foot prostheses with PEE (parallel elastic element) are shown.

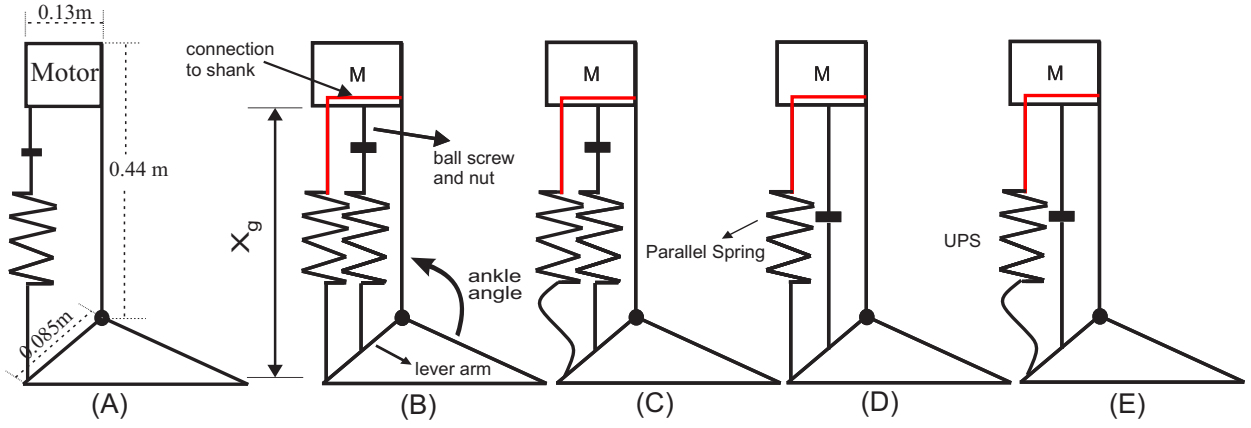

FIGURE 3.4: Schematic view of the active foot actuation concepts: SEA (A), SEA+PS (B), SEA+UPS (C), DD+PS (D), DD+UPS (E). M: Motor, PS: Parallel Spring, UPS: Unidirectional Parallel Spring, for x_g see also Figs. 3.1-3.3.

For each of these actuation candidates, the power and energy requirement will be investigated and compared for a wide range of walking and running speeds (0.5, 1, 1.6, 2.1, 2.6 m/s). First, the underlying calculations are discussed and then the results are shown and explained.

3.5 Computation of power and energy requirement

Assuming an ideal motor and transmission, the required motor power is obtained by the multiplication of the motor force F_m and (the ball screw) nut velocity $\dot{x}_n$ (Eq. 2.3) [58]. The SEA concept decreases $\dot{x}_n$ in comparison to DD (Fig. 2.6), however, intrinsically has no influence on the motor force F_m. As the required motor torque T_m is also proportional to F_m [58], consequently, the values of T_m in SEA are the same as DD.

In addition to peak power and energy, the required peak torque could cause challenges for the motor in design of active ankle prostheses (having a small motor with high rated torque and low inertia). In Fig. 3.5, it is shown that ankle peak torque and power occur almost closely to each other (late stance 49-55%, walking 1.6 m/s, [5]).

In order to improve the SEA characteristics for motor peak torque reduction, one approach could be to use the PEE component to reduce some of the load on the motor and share the force.

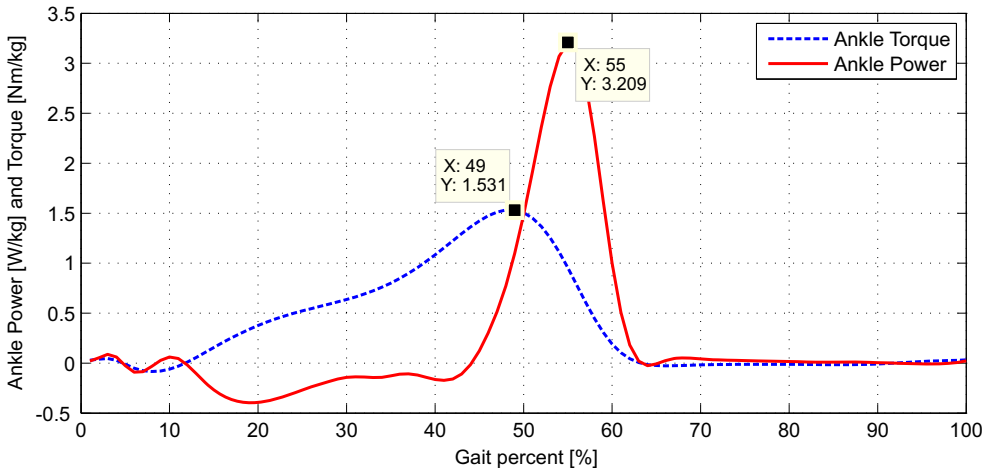

FIGURE 3.5: Peak power and torque in ankle joint (walking 1.6 m/s, [5]).

According to Fig. 3.1, the motor force (F_m) and parallel spring (PS) force (F_p) contribute to produce the ankle force F_{ank}

$$F_{ank} = F_m + F_p \tag{3.1}$$

F_p could be written as

$$F_p = K_p \cdot \Delta x_p \tag{3.2}$$

$$\Delta x_p = l_{0p} - x_g \tag{3.3}$$

l_{0p} is the free length of the parallel spring. For a motor-ballscrew drive, the required motor power P_m is calculated as [58]

$$P_m = F_m \cdot \dot{x}_n \tag{3.4}$$

$\dot{x}_n$ is the nut velocity and F_m is related to K_p by

$$F_m = F_{ank} - K_p \cdot \Delta x_p \tag{3.5}$$

on the other side, to calculate $\dot{x}_n$, we use the series spring stiffness K_s

$$F_m = K_s \Delta x_s \tag{3.6}$$

$$\Delta x_s = l_{0s} - x_s \tag{3.7}$$

where l_{0s} is the series spring free length. According to Fig. 3.1

$$x_g = x_s + x_n \tag{3.8}$$

which results in

$$x_n = x_g + \frac{F_m}{K_s} - l_{0s} \qquad \dot{x}_n = \dot{x}_g + \frac{\dot{F}_m}{K_s} \tag{3.9}$$

using Eqs. 3.4,3.5,3.9, the motor power P_m is

$$P_m = (F_{ank} - K_p(l_{0p} - x_g))(\dot{x}_g + \frac{\dot{F}_m}{K_s}) \tag{3.10}$$

Eq. 3.10 shows that P_m is related to K_p, K_s and l_{0p}. Other variables (e.g. x_g) are calculated based on human ankle data [5] and geometrical dimensions of an actuation design shown in Fig. 3.4. For each gait and speed, the power and energy (integral of power over time) requirement were calculated using Eq. 3.10 for each [K_p,K_s,l_{0p}] combination. The stiffness range for K_s was from 1 kN/m to 600 kN/m and for K_p it was from 1 kN/m to 90 kN/m (1 kN/m step size). The free length of parallel spring l_{0p} was considered from 0.390 m to 0.500 m (1 mm step size). The values of required motor peak power and energy were computed for all [K_p,K_s,l_{0p}] combinations and then compared, and finally, the minimum values of PP and ER were identified.

The selected range for l_{0p} is based on the length of x_g as shown in Fig. 3.6. The length l_{0p} was selected to be in the vicinity of the length x_g. In addition, l_{0p} values below 0.390 m increased the PP considerably. Therefore, those ranges were not considered for the calculations.

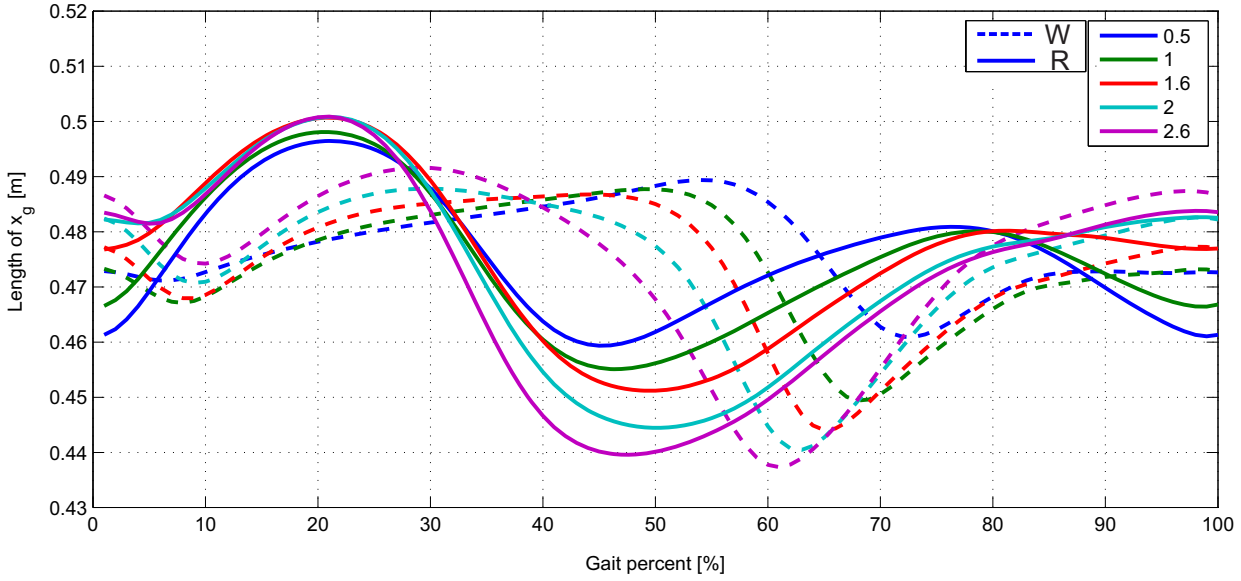

FIGURE 3.6: The actuation length x_g in walking and running gaits (0.5 m/s - 2.6 m/s), calculated based on the geometry (Fig. 3.4) and data from [5], see Figs. 3.1-3.3 for x_g.

For SEA+UPS concept (Fig. 3.2, 3.4c), the UPS comes into action only if x_g is higher than the free length of UPS (l_{0p}). If it is shorter, there will be no UPS force. Therefore, Eq. 3.5 changes to

$$F_m = \begin{cases} F_{ank} - K_{ups} \cdot \Delta x_{ups} & \text{if } x_g > l_{0p} \\ F_{ank} & \text{if } x_g < l_{0p} \end{cases} \tag{3.11}$$

all other equations mentioned above are also applied to the SEA+UPS concept.

For DD+UPS or DD+PS concepts Eq. 3.10 reduces to

$$P_m = (F_{ank} - K_p(l_{0p} - x_g))\dot{x}_g \tag{3.12}$$

the required energy E_m is the integral of power over a gait cycle. The required stride time for each speed and gait is obtained from [5] (see also Tab. 1.1).

3.6 Results

The results for the minimum required motor peak power (minimum PP) and the corresponding K_p-K_s-l_{0p} values are shown in Fig. 3.7 and Tab. 3.1. Accordingly, the results for minimum energy requirement (minimum ER) and their corresponding K_p-K_s-l_{0p} values are summarized in Fig. 3.8 and Tab. 3.2 respectively.

3.6.1 Approach for minimum required peak power (minimum PP)

3.6.1.1 General comments

In this approach, the minimum peak power (PP) requirement and their corresponding energy requirement (ER) are shown in Fig. 3.7. The results will be compared with respect to the SEA concept which was discussed in Chapter 2.

As it is seen in Fig. 3.7, for all gaits and speeds, using a PS or UPS can reduce the PP requirement in comparison to SEA. Only in running at 0.5 m/s the required PP of DD+PS and DD+UPS increased slightly in comparison to SEA. As pointed out in Chapter 2, the DD (Direct Drive) design required more PP in comparison to SEA (Fig. 2.4), however DD+PS and DD+UPS (adding a PS or UPS to DD) can reduce the PP requirement even in comparison to SEA (for slow running 0.5 m/s it increased slightly, Fig. 3.7).

The corresponding ER requirement, however, increased nearly for all speeds and reduced only in slow walking (0.5 and 1 m/s) and running (0.5 m/s, SEA+UPS) in comparison to SEA.

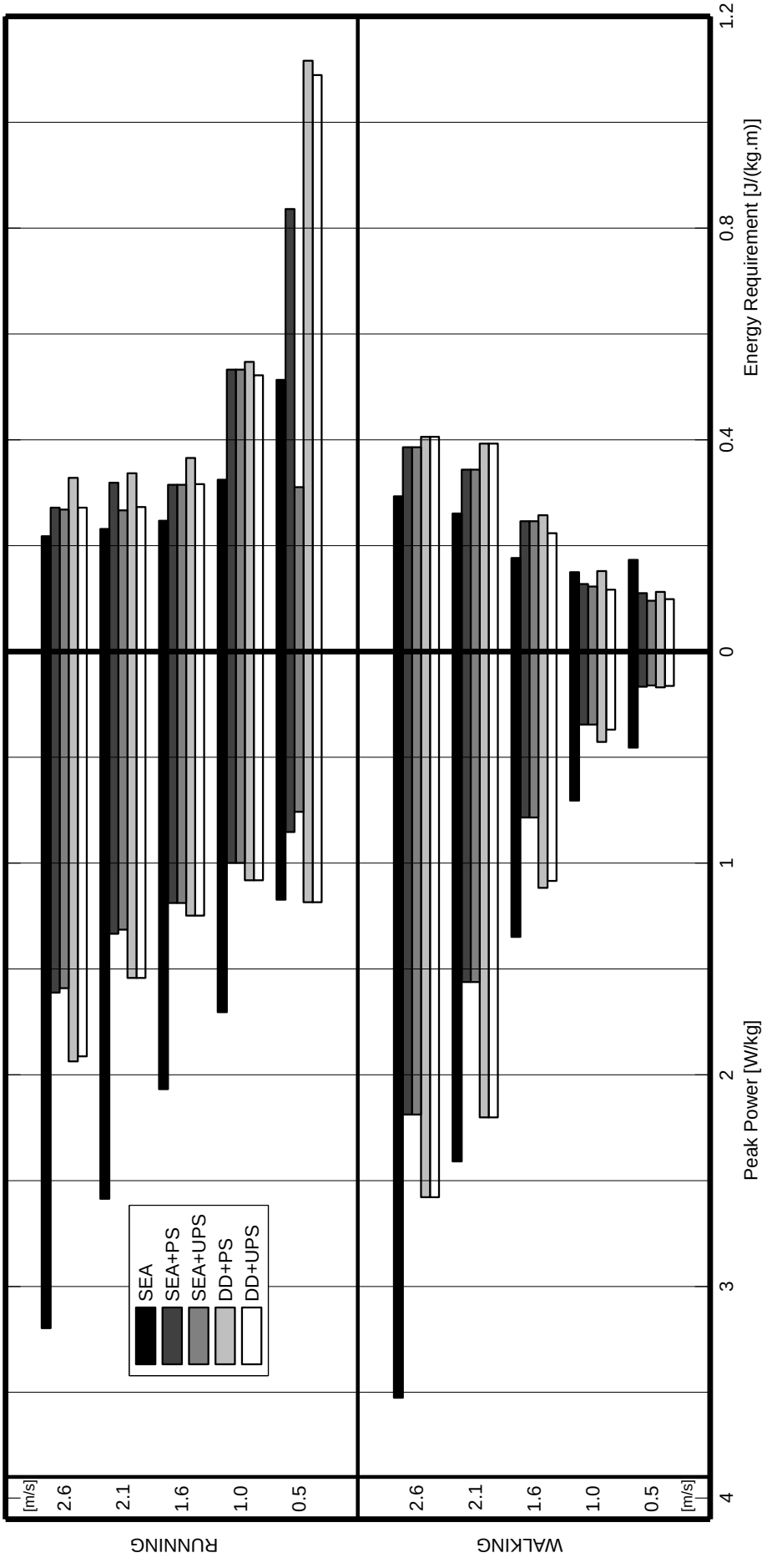

FIGURE 3.7: Comparison of calculated minimum motor peak power and their corresponding energy requirement for different actuation concepts, gaits and speeds, approach: minimum required PP.

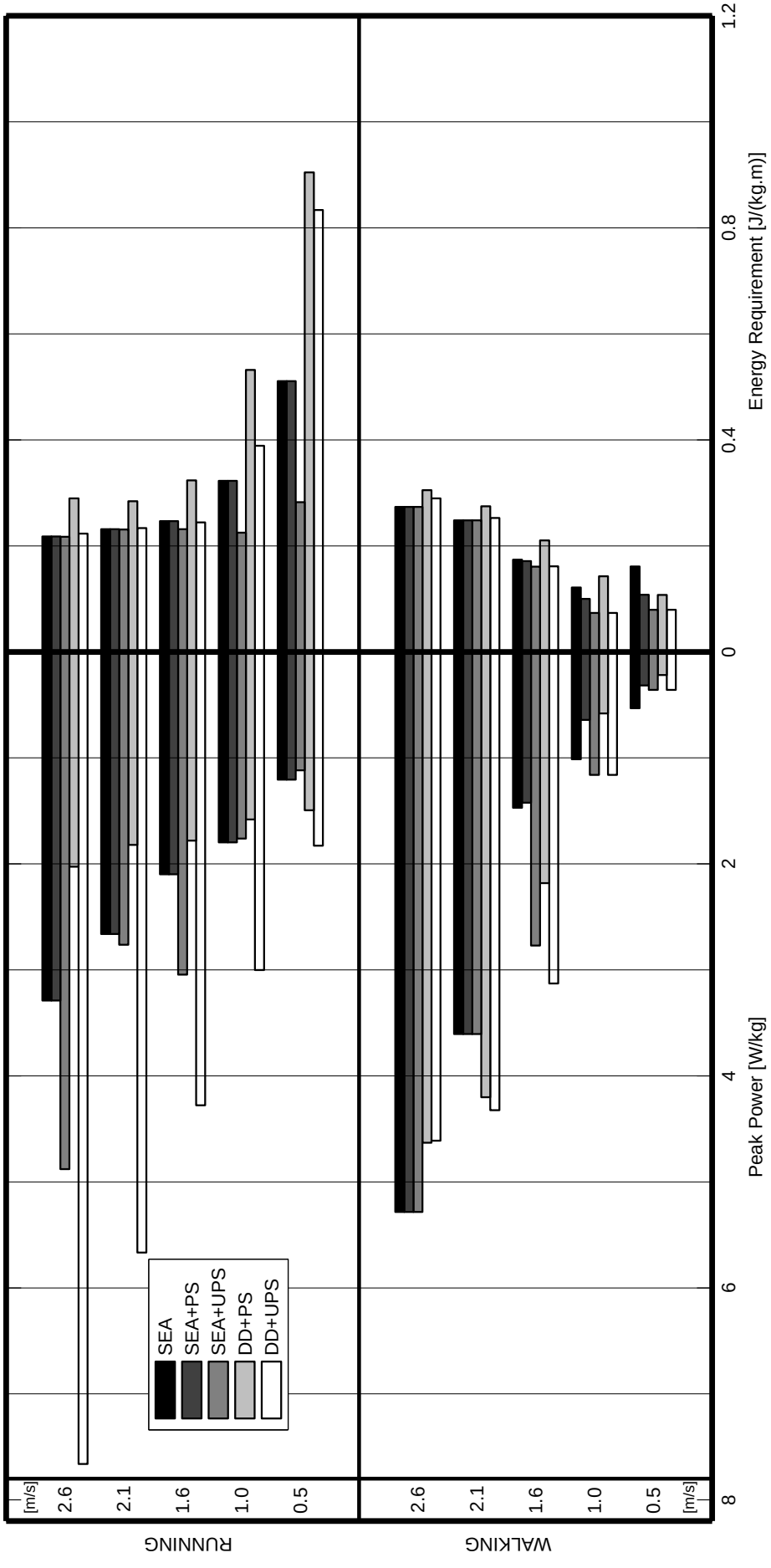

FIGURE 3.8: Comparison of calculated minimum required motor energy and their corresponding peak power requirement for different actuation concepts, gaits and speeds, approach: minimum required ER.

TABLE 3.1: The obtained optimal K_p-K_s-l_{0p} values, approach: minimum motor peak power requirement, the parallel spring stiffness values are in (parenthesis).

Gait		Walking					Running				
Speed [m/s]		0.5	1.0	1.6	2.1	2.6	0.5	1.0	1.6	2.1	2.6
Stiffness [kN/m]	SEA	78	61	80	115	143	70	74	77	77	77
	SEA+PS	279(28)	56(15)	93(7)	132(6)	137(7)	68(5)	71(8)	71(12)	237(37)	64(20)
	SEA+UPS	266(30)	56(15)	93(7)	132(6)	137(7)	61(24)	71(8)	71(12)	200(38)	197(36)
	DD+PS	(28)	(27)	(28)	(7)	(6)	(52)	(49)	(43)	(39)	(37)
	DD+UPS	(30)	(31)	(33)	(7)	(6)	(52)	(49)	(43)	(39)	(38)
l_{0p} [m]	SEA+PS	0.465	0.455	0.420	0.400	0.404	0.397	0.404	0.432	0.457	0.444
	SEA+UPS	0.466	0.455	0.420	0.400	0.404	0.489	0.404	0.432	0.458	0.454
	DD+PS	0.465	0.457	0.456	0.397	0.392	0.463	0.461	0.462	0.459	0.455
	DD+UPS	0.466	0.460	0.459	0.397	0.392	0.463	0.461	0.462	0.459	0.456

TABLE 3.2: The obtained K_p-K_s-l_{0p} values, approach: minimum energy requirement, the parallel spring stiffness values are in (parenthesis).

Gait		Walking					Running				
Speed [m/s]		0.5	1.0	1.6	2.1	2.6	0.5	1.0	1.6	2.1	2.6
Stiffness [kN/m]	SEA	66	94	73	59	40	71	77	78	76	76
	SEA+PS	53(21)	96(10)	72(2)	59(0)	40(0)	71(0)	77(0)	78(0)	76(0)	76(0)
	SEA+UPS	∞(48)	∞(67)	495(52)	59(0)	40(86)	55(29)	53(31)	55(46)	66(10)	46(47)
	DD+PS	(33)	(23)	(10)	(2)	(0)	(61)	(60)	(40)	(33)	(30)
	DD+UPS	(48)	(67)	(116)	(42)	(67)	(76)	(86)	(95)	(107)	(120)
l_{0p} [m]	SEA+PS	0.464	0.452	0.457	-	-	-	-	-	-	-
	SEA+UPS	0.469	0.470	0.473	-	0.491	0.487	0.486	0.491	0.480	0.485
	DD+PS	0.466	0.457	0.449	0.457	-	0.462	0.464	0.456	0.451	0.447
	DD+UPS	0.469	0.470	0.475	0.478	0.485	0.467	0.471	0.477	0.480	0.481

For this approach, the [Kp,K_s,l_{0p}] values are shown in Tab. 3.1. The K_p values are put between parentheses. For all speeds and gaits, the stiffness values of PS and UPS are less than their corresponding series stiffness. For some cases, the PP-ER requirement and the [Kp,K_s,l_{0p}] values in PS and UPS are similar. In these situations, PS and UPS are equivalent i.e. PS operates like a UPS.

For some cases the SEA+PS and SEA+UPS have similar results (e.g. walking 2, 2.6 m/s), however, in some other cases SEA+UPS has a better performance in terms of energy requirement (e.g. running 0.5, 2, 2.6 m/s and walking 0.5, 1, 1.6 m/s). For DD+UPS and DD+PS a similar trend is seen. Except for walking 2-2.6 m/s (that the results are similar) for other speeds the DD+UPS has a better performance than DD+PS in terms of ER reduction.

The results from gaits (two gaits), speeds (5 speeds) and actuation concepts (5 concepts) are comprehensive. Going into detail for every case would exceed the scope of this thesis. Therefore, we focus on two case studies. In addition, the walking gait will be considered and the UPS will be investigated as previously some benefits of UPS were identified. Furthermore, although DD+UPS had good performance, it will not be taken into consideration, because this concept has high stiffness and its disadvantages are more than its advantages and as the active foot prostheses is under recurring walking/running impact forces it can not be as suitable as SEA+UPS actuation. Therefore, we will compare SEA+UPS with SEA for walking at 0.5 m/s, where it had a better performance for PP and ER reduction, and walking 1.6 m/s, where the required PP was reduced however ER requirement increased in comparison to the SEA.

3.6.1.2 Case study: walking 0.5 and 1.6 m/s, SEA+UPS vs. SEA

In walking at 0.5 m/s (Fig. 3.9), the required peak motor force in SEA+UPS is much lower than that of SEA. That could explain why the required PP in SEA+UPS is lower than SEA (Fig. 3.7, 3.9C1). From Fig. 3.9A1, we see that in some part of the swing phase, after approximately 80% of the gait cycle, the motor in SEA+UPS, loads the UPS. This is a reason why unlike the SEA power curve in C1, the SEA+UPS power curve is higher. To do this, the motor requires energy. However, as seen in C1, the area under power curve of SEA+UPS is less than SEA. Therefore, in total, the ER requirement in SEA+UPS is less than SEA. For the velocity curves (B1), in push-off region (nearly 50-70%) the motor velocity in SEA+UPS is higher than SEA, however, as force was effectively reduced, this did not result in power increase as seen in C1.

In walking at 1.6 m/s (Fig. 3.9), the motor force in SEA+UPS has a smaller peak than SEA (Fig. 3.9A2). On the other hand, the motor velocities for the two concepts are not very different from each other (B2). Therefore, the peak power in SEA+UPS is less than that of SEA (C2). However, as seen from A2, for a large part of the gait cycle (approx. 1-20% and then 58-100%) the motor uses force for the loading of UPS in SEA+UPS. This operation increases the power requirement in

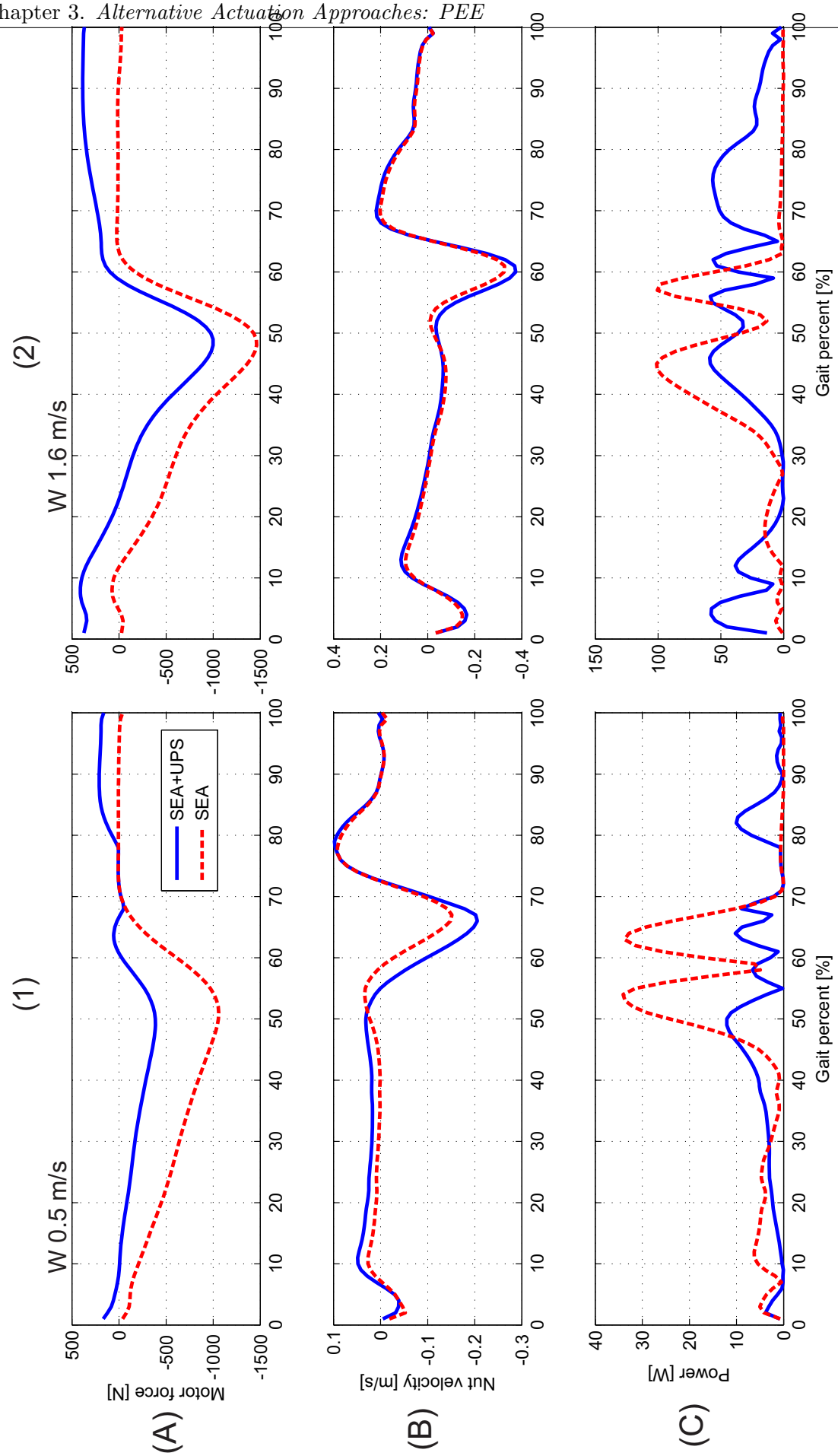

FIGURE 3.9: Comparison of calculated motor force, velocity and power between SEA and SEA+UPS actuation concepts, for walking 0.5 and 1.6 m/s, approach: minimum required PP.

these sections (C2) and consequently requires energy. This can explain the higher ER requirement in SEA+UPS than the SEA concept (Fig. 3.7).

3.6.2 Approach for minimum required energy (minimum ER)

3.6.2.1 General comments

For this approach, the minimum ER requirement and the corresponding PP requirements are comparatively shown in Fig. 3.8 for different actuation concepts, speeds and gaits. The K_s-K_p-l_{0p} values are shown in Tab. 3.2. Mainly in slow walking and running speeds, the ER requirement of SEA+PS or SEA+UPS is reduced in comparison to SEA. The DD+UPS concept required less ER (than DD+PS) for all speeds and gaits, however at the same time the corresponding PP was higher (except for walking 2.6 m/s).

In general, this approach had little advantage for construction of an active ankle prosthesis, because for the normal to fast speeds, the ER requirement in those concepts are not less than SEA. On the other hand, the corresponding PP requirement in PS/UPS concepts increased in comparison to SEA. Generally speaking, not an obvious reduction of ER was observed in comparison to the SEA concept (unlike minimum required PP approach in which for nearly all speeds the required PP reduced in comparison to the SEA).

3.6.2.2 Design considerations in minimum ER approach

As already mentioned, the minimum ER approach is not suitable for the construction of active ankle prosthesis (when talking about adding a PEE to SEA). However looking at Fig. 3.8, one might ask e.g. for running 2.6 m/s why the result of SEA+UPS did not converge to an SEA case. Because it seems that the ER requirement is the same as SEA however the corresponding PP is higher. It should be mentioned that, although the ER requirement seems the same, the precise Matlab results are not the same. In this case, the ER requirement in SEA+UPS is 0.2172 J/(kg.m) and for SEA it is 0.2177 J/(kg.m). This difference is barely visible in Fig. 3.8. However, when we look at the corresponding PP requirement for SEA+UPS it is 4.8789 W/kg and for SEA it is 3.2896 W/kg. Because of this very small reduction of ER, the software has found this result for the PP requirement.

This small reduction of ER can not mean that SEA+UPS is preferred in comparison to SEA. These issues must be taken into account for the design and construction of powered prosthetic devices.

In summary using a UPS (or even a PS) could be promising. However, the ER requirement needs to be investigated so that the reduction in PP requirement is not with the cost of a high increase in ER requirement.

3.7 General comment for design and construction

Looking back to Tab. 3.1 or 3.2, it is seen that the stiffness of parallel elastic element (PEE) is not the same for different speeds and gaits. A similar observation was found for spring stiffness in SEA (see section 2.11). Although some designs for variable stiffness are available [36, 37], the application of such mechanisms for a compact and light-weight active ankle prosthesis needs further investigation.

3.8 Summary of the chapter

Peak power, peak torque and energy requirement are amongst the important design features for powered ankle prostheses. Application of series elastic actuators (SEA) can reduce peak power and energy requirement by reducing motor speed in comparison to a Direct Drive (DD, see Chapter 2).

To enhance the SEA concept, in this chapter, a PEE (parallel elastic element) was added to SEA. The PEE could be in two design formats: (1) it could push and pull and (2) it could only pull. For the first case the PEE is called parallel spring (PS) and for the second case it is called unidirectional parallel spring (UPS).

The motor peak power (PP) and energy (ER) requirement were investigated and compared these two objectives for different active actuation concepts such as SEA, SEA+PS, SEA+UPS, DD+PS and DD+UPS. For the minimum motor peak power requirement, we found that the PEE is useful for reducing the PP in comparison to SEA. In addition, DD+PS and DD+UPS required less PP in comparison to DD (Direct Drive) and SEA. It was also found that the performance of UPS was slightly better than PS in terms of reducing the corresponding ER requirement. It is more obvious between DD+UPS and DD+PS concepts. The results also show that the PEE increases the ER requirement in comparison to SEA.

For the minimum energy requirement, however, it was found that PEE is playing a minor role in normal to fast gaits. The advantage was present in slow walking. Therefore, this approach can not be suitable for design of active ankle prostheses.

Having a PEE is useful for PP reduction, however, at the same time, a closer look into ER requirement must be done to guarantee a suitable design (for both PP and ER requirement).

Like SEA concept, the spring stiffness in PEE was not similar for different speeds and gaits. For a final construction it is recommended to investigate the specific needs of the amputee and select an optimal value for spring stiffness so that the power and energy requirements of the robotic ankle are minimal.

Chapter 4

Alternative Actuation Approaches: Damping Effects

4.1 Introduction

In Chapter 1, it was seen that the muscle model has also damping components (Figs. 1.15 and 1.16). Based on some studies this damping feature could be in series [35] or in parallel [34] with the contractile element (a motor). In this chapter, we will investigate whether a damping element could have advantage for peak power (PP) or energy (ER) reduction in active ankle prosthesis. Besides level ground locomotion, we also consider stairs ascending and descending. These types of locomotion are important as they are encountered in daily life. As contractile element, spring and damping is considered in this chapter, considering level walking, ascending and descending the stairs is also useful.

We will compare the introduced actuation mechanisms with respect to SEA mechanism. Based on the results of Chapter 2 and 3, although SEA system is a very simplified version of muscle model presented in Chapter 1 (Figs. 1.15 and 1.16), it is still an effective design approach at least for human locomotion on level ground.

A main finding of this chapter is that the stiffness is a required part of active foot prosthesis. In contrast, damping shows task specific behavior[1].

[1] A part of this chapter was published in IEEE International Conference on Rehabilitation Robotics, Seattle USA, 2013 [63].

4.2 Extension of SEA with damping characteristics

According to previous section, two actuation mechanisms that are introduced are based on muscle models (Figs. 1.15 and 1.16) and could be regarded as the extensions of SEA mechanism. The first actuator has elasticity and damping in series with CE (contractile element, or a motor). This is called *series elastic damper actuator* (SEDA actuator). For the second actuator, the damping is in parallel with the motor and the spring is in series with them. This actuator is called *parallel elastic damper actuator* (PEDA actuator). The SEDA and PEDA actuators are shown in Figs. 4.1 and 4.2 respectively.

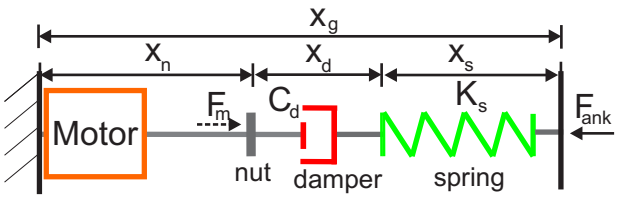

FIGURE 4.1: Model of series elastic-damper actuator (SEDA), C_d: damping coefficient.

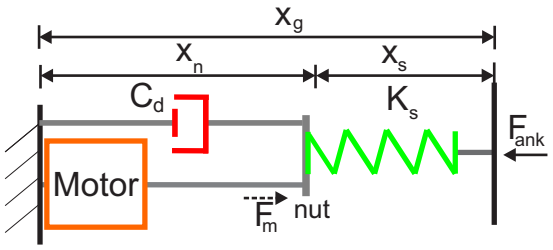

FIGURE 4.2: Model of parallel elastic-damper actuator (PEDA), C_d: damping coefficient.

In previous chapters, it was shown that the spring is a key part in the actuation mechanisms that could be used for active ankle prostheses. The elasticity of the spring allows for storing and releasing of energy during stance to support for push-off and simultaneously decrease the peak power (PP) and energy (ER) requirement in an active ankle prosthesis (with respect to DD). In this chapter, the focus is on damping to see whether or not it has a similar effect on PP and ER requirement.

In a recent patent, damper was embedded in a powered ankle prosthesis for absorbing impact energies [64]. For passive ankle prostheses (mostly for adaptation to sloped surfaces and not necessarily stair ascent-descent), the damper was used by Mauch in 70's in which prosthetic ankle could adapt to the ground slope [65]. Endolite Echelon foot-ankle is a commercially available passive hydraulic prosthesis [66]. In a recent study, the researchers investigated to use a semi-active damper in a passive foot prosthesis for negotiating on sloped surfaces to maintain stable contact and decrease the probability of falling [67].

The previous chapters mainly addressed level ground locomotion. In addition to level walking, everyday life involves additional activities such as going up or down uneven or sloped surfaces

[68] (e.g. stairs, ramps). In [69] it was found that only little signs could be found that indicate an adaptation or shift in the locomotor patterns when moving from level to stair walking. Stair locomotion is a common activity of daily living and is used in the rehabilitation of the lower extremity as a motor performance test [70, 71] to increase muscle strength and weight-bearing capabilities of the joints. Like previous chapters, we will investigate whether or not (passive) damper could reduce PP and/or ER requirement in a powered ankle prosthesis. The PP/ER requirements will be compared between SEA (Fig. 2.2), SEDA (Fig. 4.1) and PEDA (Fig. 4.2) concepts for normal level walking, ascending and descending the stairs (Fig. 4.3). In addition, for an SEA concept, we investigate whether it is good to select the spring stiffness based on level walking or stairs ascending or descending to have minimum PP/ER requirement in an active foot prosthesis. The following results are for a 75-kg person.

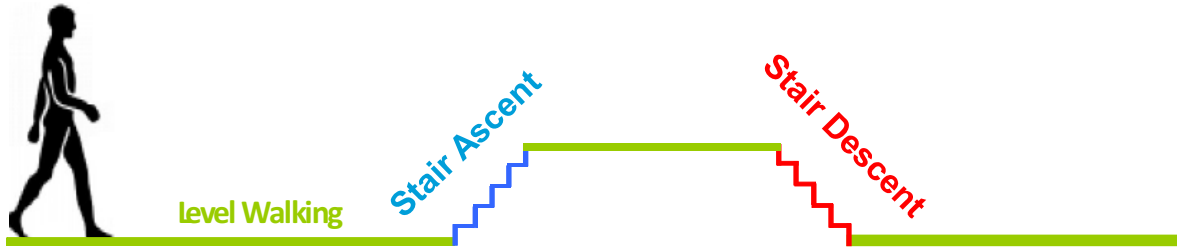

FIGURE 4.3: The power calculations will be done for a 75-kg person negotiating through level ground, ascending and descending the stairs, for SEA (Fig. 2.2), SEDA (Fig. 4.1) and PEDA (Fig. 4.2) actuation concepts.

4.3 Biomechanics of human gait in normal level walking, ascending and descending the stairs

Before designing a powered foot prosthesis for daily activities, it is necessary to understand human locomotion in different conditions like level ground, ascending or descending stairs. The ankle kinematics and kinetics of able-bodied subjects during normal level walking were obtained from [5], and for normal stairs ascending and descending from [69]. Those data correspond to healthy subjects with about the same height, body mass and age group. A comprehensive description of the experiments, data acquisition and analysis can be found in those references. In addition the joint torques were calculated by inverse dynamics (see e.g. [9]).

In Fig. 4.4, the ankle torque and ankle angle are shown in a gait cycle, together with information about negative, positive and net work of the ankle joint (W^-), (W^+), (W^{net}) for the above-mentioned gaits. The ankle torque T_{ank} is normalized to body mass. In addition, the main characteristics of human ankle biomechanics for those three gaits are shown in Tab. 4.1.

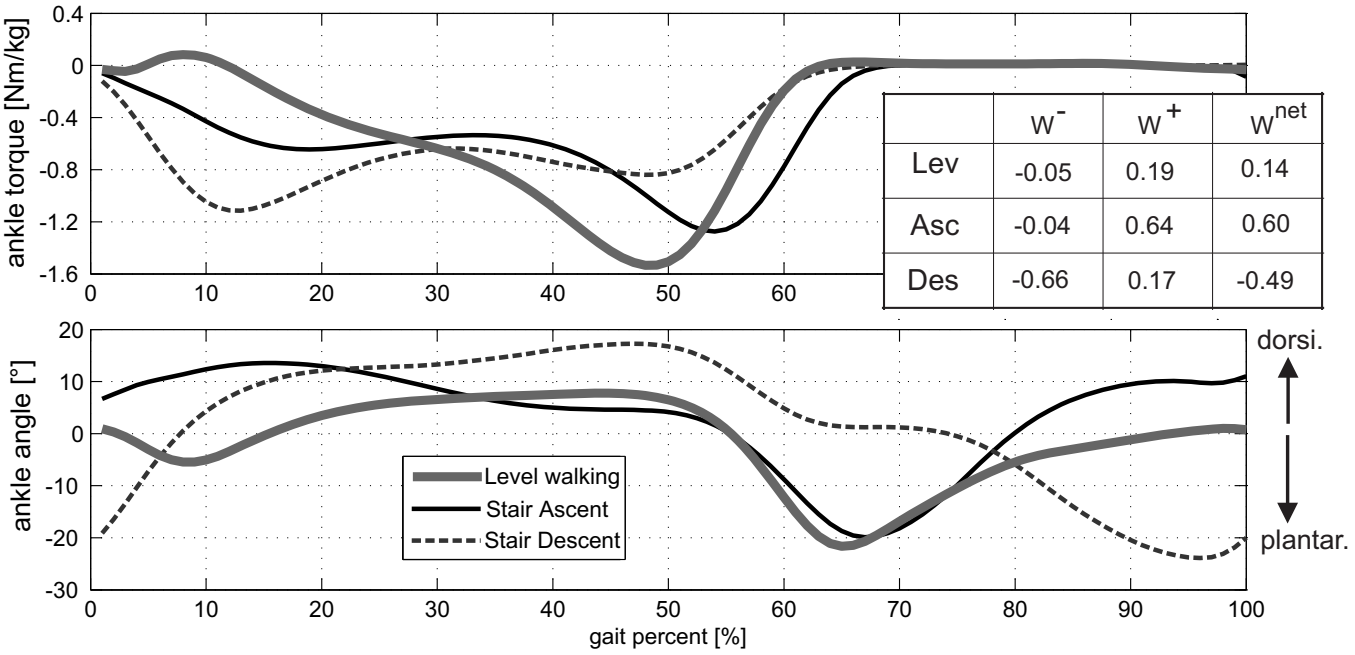

FIGURE 4.4: Human ankle torque (T_{ank}) and angle for normal level walking (1.6 m/s, [5]) and normal ascending-descending the stairs (slope 30°, [69]), with information for negative (W^-), positive (W^+) and net (W^{net}, J/(kg.m)) works in human ankle joint.

TABLE 4.1: Main features of ankle kinematics and kinetics for normal level walking [5], normal stairs ascending and descending [69], in this table when the foot and the shank are perpendicular the angle is considered zero.

Gait type	Max. Biological Power [W/kg]	Max. Torque [Nm/kg]	Range of Motion (+ = dorsi. | - = plantar.) [°]	stance until [%]	Speed, slope [m/s], [°]	cycle time [sec]
Level walking	3.2	-1.53	+7,-21	65	1.6 m/s	0.98
Stair Ascent	2.55	-1.27	+14,-20	68	0.48 m/s (30°)	1.41
Stair Descent	-2.85	-1.11	+18,-24	65	0.57 m/s (30°)	1.19

The absolute value of ankle joint net work in ascent or descent is noticeably higher than level walking. In addition, there is one peak in ankle torque for level ground locomotion, however for stair ascent-descent there are two local peaks which are mainly due to weight acceptance and propulsion. The range of motion (ROM) increases from level walking to ascent and reaches the highest in stair descent. The ankle torque T_{ank} is converted to ankle force F_{ank} using lever arm and system geometry (Fig. 4.5a). The length x_g (Fig. 4.5) is calculated by using ankle angle [5, 69] and geometrical dimensions (see Fig. 4.5a, also [61, 62]).

4.3.1 Power requirements of SEA

As the main target is to find alternative design approaches other than SEA concept for active foot prosthesis, the results of PP and ER requirement for SEDA and PEDA concepts are compared with that of SEA concept. Therefore, the power calculation for an SEA system is briefly mentioned and

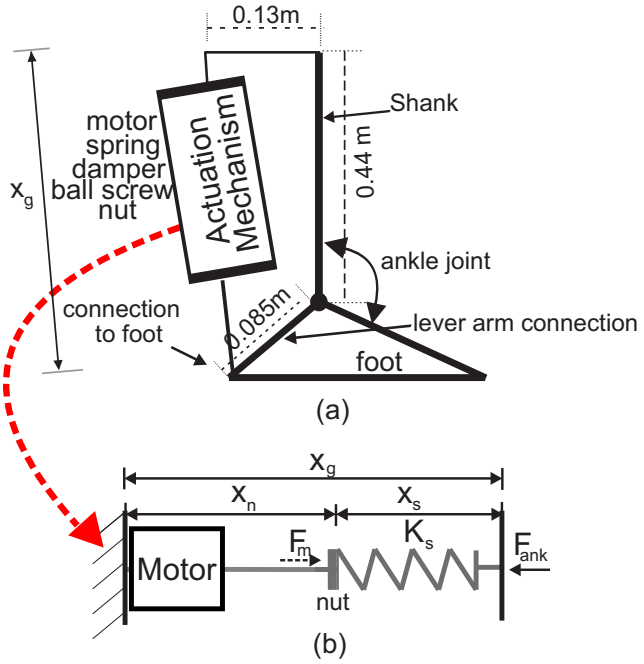

FIGURE 4.5: Schematic view of (a) the powered ankle with dimensions used for calculations (see also Fig. 2.2) and (b) model of series elastic actuator SEA [59], note that SEDA (Fig. 4.1) and PEDA (Fig. 4.2) are also the candidates for actuation mechanism.

we will focus more on the other two actuation concepts. For SEA (Fig. 4.5b), power calculation was discussed in chapter 2. The required motor power P_m for SEA is

$$P_m = F_m(\dot{x}_g + \frac{\dot{F}_m}{K_s}) \tag{4.1}$$

where K_s is the stiffness of the series spring and x_g is the length of actuator (Fig. 4.5b, see chapter 2 for detailed discussions).

4.3.2 Power requirement of the series elastic-damper actuator (SEDA)

The SEDA concept (Fig. 4.1) could be considered as an extension of SEA [59]. The required motor power P_m is obtained by the multiplication of motor Force F_m and ball screw nut velocity $\dot{x}_n$ [58]. The ankle force, motor force or nut velocity in general could be positive (to the left) or negative (to the right, Fig. 4.1). In order to have similar approach like [59], we assume if T_{ank} is negative, F_{ank} is negative (T_{ank} is known, Fig. 4.4). In SEDA, F_{ank} and F_m have similar absolute values but different signs (Newton's third law). Therefore, they are shown in different directions in Fig. 4.1. To be dynamically correct for the equations [58], as we took the left direction positive, the nut velocity could be represented by $\dot{x}_n$ but with opposite sign. Note that x_n is a distance and when elongated, $\dot{x}_n$ is naturally positive, but nut velocity would be negative according to the selected positive-negative directions. Therefore

$$P_m = F_m \, \dot{x}_n \tag{4.2}$$

Using Fig. 4.1, the length x_g (see also Fig. 4.5a) is obtained as

$$x_g = x_n + x_d + x_s \tag{4.3}$$

For spring and damper we have

$$F_m = -C_d \dot{x}_d \tag{4.4}$$

$$F_m = K_s(d_{0s} - x_s) \tag{4.5}$$

where C_d is the damping coefficient, K_s is the stiffness coefficient of series spring and d_{0s} is its free length. Using Eq. 4.3-4.5, for $\dot{x}_n$ we have

$$\dot{x}_n = \dot{x}_g + \frac{\dot{F}_m}{K_s} + \frac{F_m}{C_d} \tag{4.6}$$

based on Eq. 4.2 the required motor power P_m is calculated as

$$P_m = F_m \ (\dot{x}_g + \frac{\dot{F}_m}{K_s} + \frac{F_m}{C_d}) \tag{4.7}$$

The procedure for finding the minimum power or energy requirement will be discussed after the next subsection.

4.3.3 Power requirement of the parallel elastic-damper actuator (PEDA)

The PEDA concept (Fig. 4.2) is based on the conceptual Hill-type [33] muscle model that was also used by [72]. Using Fig. 4.2 one can write (Newton's second law, note F_{ank} is known, in Fig. 4.2 the direction of motor or ankle force are shown for an arbitrary moment)

$$F_m = -(F_{ank} + C_d \dot{x}_n) \tag{4.8}$$

and

$$F_m = K_s(d_{0s} - x_s) \tag{4.9}$$

where C_d is the damping coefficient, K_s is the series spring stiffness and d_{0s} is its free length. From Fig. 4.2

$$x_g = x_s + x_n \tag{4.10}$$

based on Eq. 4.9 and 4.10

$$x_g = (d_{0s} - \frac{F_m}{K_s}) + x_n \tag{4.11}$$

therefore $\dot{x}_n$ is

$$\dot{x}_n = \dot{x}_g + \frac{\dot{F}_m}{K_s} \tag{4.12}$$

using Eq. 4.2 together with Eqs. 4.8 and 4.12, the required motor power P_m is

$$P_m = (F_m + C_d\dot{x}_n)(\dot{x}_g + \frac{\dot{F}_m}{K_s}) \tag{4.13}$$

The required motor energy E_m is the integral of absolute required motor power over a cycle time (see Tab. 4.1)

$$E_m = \int |P_m| dt \tag{4.14}$$

Human ankle gait power can be both negative and positive [5, 69]. When it is negative, a resistance motion is applied to the ankle, and when it is positive, a propelling motion is applied [59]. A motor unit cannot typically provide negative power [58, 59], therefore it must provide power to both resist and propel human motion [58, 59]. Therefore, we consider absolute values of PP and ER requirement (see [59]). For this reason, an absolute value in Eq. 4.14 is used. In Eq. 4.7 and Eq. 4.13, the required motor power P_m is dependent on spring stiffness K_s and damping coefficient C_d. The F_{ank} and x_g are obtained by human ankle data [5, 69] and geometrical dimensions of the actuator (Fig. 4.5a). Thus, stiffness K_s and damping coefficient C_d become the only parameters that would influence the required motor power. For spring stiffness a range of 1kN/m to 500 kN/m (1 kN/m step size) was considered and for the damping coefficient a range of 25 Ns/m to 50 kNs/m (25 Ns/m step size) was selected. For each combination of K_s-C_d, the required motor power was obtained based on Eq. 4.7 and Eq. 4.13. Then the results were compared between K_s-C_d combinations and next the K_s-C_d values that result in minimum PP (peak power) or ER (energy) requirement were selected. A same method and range was used to determine minimum ER requirements for different actuators and gaits using Eq. 4.14.

4.4 Results

The power calculations are done both for the case that the motor is assumed as an ideal power source, and the case when ball screw efficiency, motor inertia and efficiency are also taken into account. Aside from rising the required peak power (which is important from design perspective), taking into account system efficiency or inertia was not changing the nature of the findings. Thus, in this section we show the results for the case when motor is assumed as an ideal power source. This is also similar to these studies [33, 59, 73]. This makes the results more general and independent of the electromechanical properties of an actuation concept.

This section is divided in two subsections. As first approach, the search was for the minimum motor PP requirements (approach PP) and as second approach we search for the minimum ER requirements (approach ER) in the SEA, SEDA and PEDA actuation concepts and for normal level walking, ascending and descending the stairs. Their corresponding energy (for PP approach) or peak power (for ER approach) requirements are also discussed in those sections. Calculations are done

based on previous section and the results will be compared here. Furthermore the values of spring stiffness and damping coefficients which minimize motor PP or ER are shown in Tabs. 4.2-4.3. Body mass is assumed 75 kg.

4.4.1 Comparison of minimum motor PP (and their corresponding energy) requirement

For this approach, the minimum required motor PP and their corresponding energy requirements are shown in Fig. 4.6 (for SEA, SEDA and PEDA concepts and for previously mentioned gaits). The corresponding K_s-C_d values for this approach are given in Tab. 4.2.

TABLE 4.2: The obtained required stiffness-damping values for different actuation concepts and different gaits, approach: minimum required PP.

Gait		level ground walking		Ascending stairs		Descending stairs	
Stiffness [kN/m] Damping [kNs/m]		K_s	C_d	K_s	C_d	K_s	C_d
Actuation concept	SEA	80	0	68	0	64	0
	SEDA	80	to ∞	68	to ∞	45	15.5
	PEDA	80	to 0	68	to 0	62	2.2

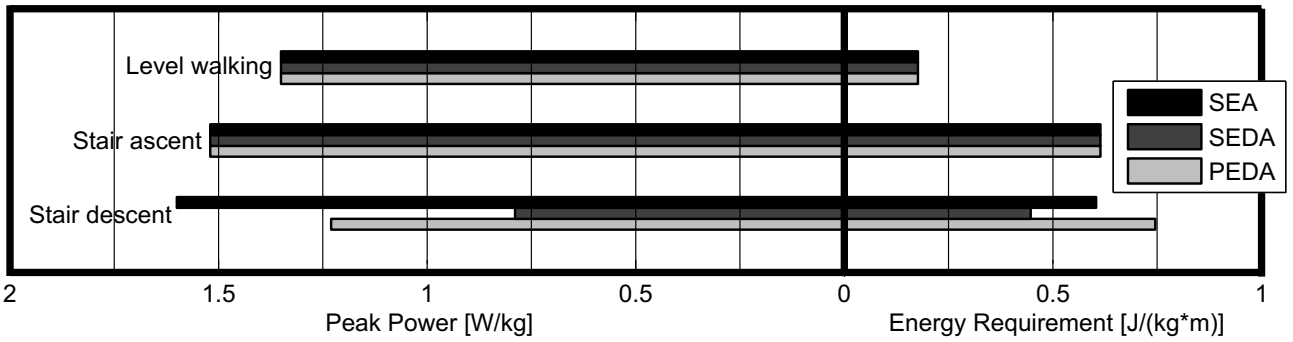

FIGURE 4.6: The calculated required minimum peak power (PP) and their corresponding energy requirements for SEA, SEDA and PEDA in level ground walking, ascending and descending the stairs, approach: the minimum required motor PP, see also Tab. 4.2.

4.4.1.1 Level ground walking

For level walking, in Fig. 4.6 and Tab. 4.2, SEA concept plays the key role for minimum required PP. The damper values for SEDA and PEDA suggest that for minimum required PP, damping is not required. Therefore, the optimal configurations of either SEDA or PEDA for level ground walking is an SEA.

For this gait (and also stair ascent), in SEDA or PEDA concept, a result for damper was not found in the mentioned range. Therefore, the lower limit and the upper limit were decreased and increased

respectively continuously. Even in this condition the result was always at the limit. Therefore, these conditions were written as 'to 0' or 'to ∞' in Tab. 4.2 (also in Tab. 4.3).

4.4.1.2 Ascending the stairs

For ascending the stairs (Fig. 4.6 and Tab. 4.2) similar to level ground walking, SEA concept again plays the key role for this gait and for a minimum required PP, the damper is not required. The required stiffness value is less than the level ground case. The required minimum PP increased by 13% and the corresponding energy requirement increased by 247% compared to level walking.

4.4.1.3 Descending the stairs

Shown in Fig. 4.6 and Tab. 4.2, for descending the stairs, the results are very different in comparison to the previous two gaits. Here, the damping characteristics are required and lead to a minimum required PP which is even less than that of SEA concept. The SEDA concept plays the key role for this gait. For SEDA, the required minimum PP and the corresponding energy requirement decreased roughly 50% and 26% respectively with respect to SEA. For PEDA, the minimum required PP has decreased about 23% however its corresponding energy requirement has increased about 22% with respect to SEA concept. SEDA concept required the least stiffness and highest damper values for this gait (Tab. 4.2). Damper value in PEDA is less than SEDA concept, in contrast its stiffness value is higher.

For the minimum PP approach, the stiffness reaches the highest value in level walking (Tab. 4.2). In addition, elasticity is required for all gaits, however damping shows 'gait specific' advantages. The SEA concept requires more PP for descending the stairs than for ascending. In fact, SEA requires its highest PP and its lowest stiffness during descent. The stiffness value gradually decreases from level walking to stair descent in all actuation concepts.[2]

4.4.2 Comparison of minimum motor ER (and corresponding peak power) requirement

For this approach, the minimum required ER and their corresponding peak power requirements are shown in Fig. 4.7 for SEA, SEDA and PEDA concepts and for level walking, ascending and descending the stairs. The corresponding K_s-C_d values for this approach are given in Tab. 4.3.

[2]In comparison to a direct drive (DD) concept (i.e. when actuator is only a motor without spring and damper), minimum required PP decreased nearly 58% for level walking, 40% for ascending (both by SEA concept) and 72% in descending (by SEDA concept).

TABLE 4.3: The obtained required stiffness/damping values for different actuation concepts and different gaits, approach: minimum required ER.

Gait		level ground walking		Ascending stairs		Descending stairs	
Stiffness [kN/m] Damping [kNs/m]		K_s	C_d	K_s	C_d	K_s	C_d
	SEA	66	0	40	0	44	0
Actuation concept	SEDA	66	to ∞	40	to ∞	38	17
	PEDA	66	to 0	40	to 0	44	to 0

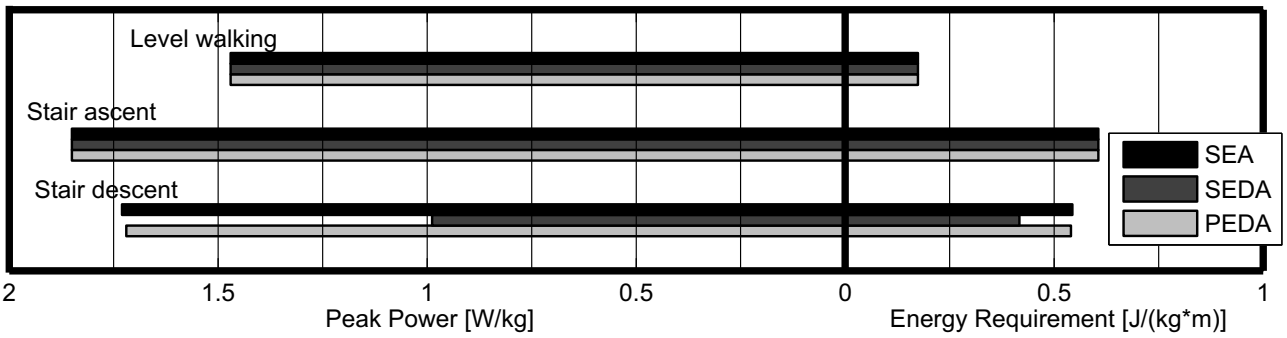

FIGURE 4.7: The calculated required minimum energy (ER) and their corresponding peak power requirements for SEA, SEDA and PEDA in level ground walking, ascending and descending the stairs, approach: the minimum required ER, see also Tab. 4.3.

4.4.2.1 Level ground walking

In this approach (i.e. minimum required ER), for level ground walking, shown in Fig. 4.7 and Tab. 4.3, SEA concept plays the key role. No benefit is found for having damping characteristics. Like minimum PP approach, in minimum ER approach, the optimal configuration of either SEDA or PEDA for level ground walking is an SEA. Compared to minimum PP approach, for ER approach in this gait, the energy requirement decreased nearly 1.5% however the corresponding peak power requirement increased nearly 8.9%.

4.4.2.2 Ascending the stairs

For ascending the stairs (Fig. 4.7 and Tab. 4.3) we see similar trend like minimum PP approach, i.e. SEA concept plays the key role for this gait as before and damping is not required. On the other side, the required stiffness value is less than that of the level ground walking. The increase of required peak power is nearly 25% however the increase for ER is nearly 248% with respect to level ground walking (in this same approach). A comparison to minimum PP approach (Fig. 4.6-Ascent) shows, for stair ascent in minimum ER approach, the energy requirement decreased nearly 1.4% and the corresponding peak power requirement increased nearly 21%.

4.4.2.3 Descending the stairs

The SEDA concept plays the key role for this gait (Fig. 4.7 and Tab. 4.3) similar to what we observed for the minimum PP approach. The decrease of peak power is nearly 42.8% and for ER it is 23% with respect to SEA. For PEDA concept, in minimum ER approach, a slight advantage was found with respect to SEA concept and it behaves similar to SEA. This is different from what we observed in minimum PP approach (see Fig. 4.6-Descent and Tab. 4.2). For SEDA concept, the required stiffness in this gait is the smallest among all actuation concepts. It is similar to the trend seen in minimum PP approach.

For the minimum ER approach, the highest stiffness value belongs to level ground walking (like in the minimum PP approach) and the highest required peak power or ER is required for ascending the stairs. Except for SEDA, the stiffness values decreased from level walking to ascent, and increased from ascent to descent (Tab. 4.3). In SEDA, the stiffness decreased gradually from level walking to descent. Like in the minimum PP approach, elasticity is always required, however damping shows task specific behavior.

4.5 Discussions

4.5.1 Approach for the minimum PP requirements vs. approach for the minimum ER requirements

For minimum required ER, the ER requirements were 'in general' only slightly less than the corresponding ER requirement of the approach for the minimum required PP. In contrast, the corresponding peak power (PP) requirements increased more noticeably (Figs. 4.6 vs. 4.7). For example for ascending gait, for minimum ER approach (Figs. 4.7), the energy requirement decreased about 1.4% in comparison to minimum PP approach (Figs. 4.6), but the corresponding peak power requirement increased nearly 21% (see Figs. 4.6-4.7). Therefore, using the minimum PP approach seems a better compromise for selecting the K_s-C_d values.

In Fig. 4.6, minimum PP and energy requirements in stair ascent increased with respect to level walking. One explanation could be that the center of mass is displaced both horizontally and vertically. In addition, the range of motion for the ankle joint is higher than level walking (Tab. 4.1). For descent, the center of mass could use the gravity for downward motion. The passive damper also helps to reduce required PP during part of stance phase where there is the first peak in ankle torque (Fig. 4.4). This could be an explanation why a lower power was required in SEDA in comparison to level walking. A main reason for higher energy requirements (in PEDA concept) is because of the passivity of the damper. It will be discussed more in Subsection 4.5.5.

4.5.2 Use of SEDA for the mixed gait (i.e. level walking+ascent+descent)

For stair descent, SEDA concept had the lowest PP requirement (Fig. 4.6). In this subsection the PP and ER requirements are compared and it is investigated whether this concept could be used for all above-mentioned gaits.

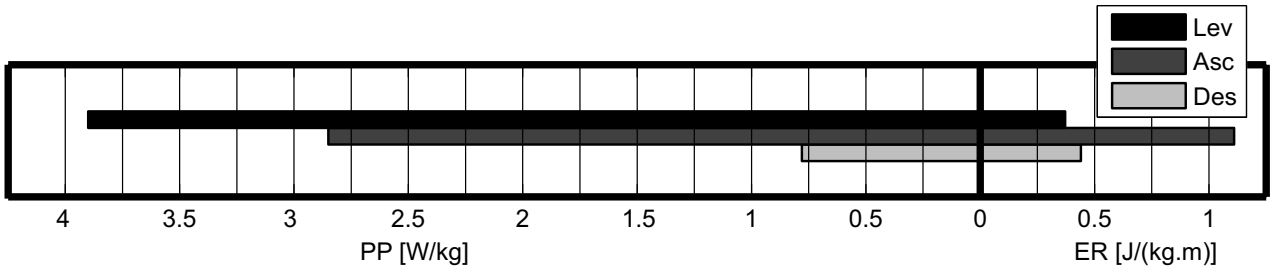

FIGURE 4.8: The calculated required PP and corresponding energy 'IF' SEDA actuation concept is used for level walking, ascending and descending the stairs, K_s=45 kN/m, C_d=15.5 kNs/m, see Tab. 4.2.

Fig. 4.8 shows the PP and corresponding energy requirements of the SEDA concept for those gaits. The K_s-C_d values are selected from Tab. 4.2, based on discussion in 4.5.1.

Comparing Fig. 4.8 with Fig. 4.6 shows that for level walking and ascent the minimum PP requirement increases 189% and 87% respectively in comparison to SEA concept (see Fig. 4.6). Increase is also seen for corresponding energy requirements. It suggests that for power and energy reducing, the SEDA is not a good concept for the mixed gaits.

4.5.3 The spring stiffness to use in case of an SEA

For level walking or stair ascending, SEA had the least PP requirements (Fig. 4.6). If an SEA is going to be used for all gaits, then it would be important to know which spring to use in it (according to Tab. 4.2, to select either from level walking, stair ascending or descending).

In Fig. 4.9, a close-up view of the graphs for the required PP versus spring stiffness is shown for SEA and for above-mentioned gaits (based on Eq. 4.1). By these graphs we can investigate the effect of spring change on the required PP in SEA for those gaits. Based on Tab. 4.2, we consider the range 60-80 kN/m.

We see in Fig. 4.9 that for ascent gait, the required PP in this range is very slightly changing. If we take K_s=68 kN/m (the corresponding stiffness in stair ascent in Tab. 4.2), we see that for stair descent, the corresponding required PP changes very slightly with respect to its minimum required PP, but for level walking the corresponding required PP increases to nearly 1.58 W/kg, which is 17% more than its minimum required PP (which is 1.35 W/kg).

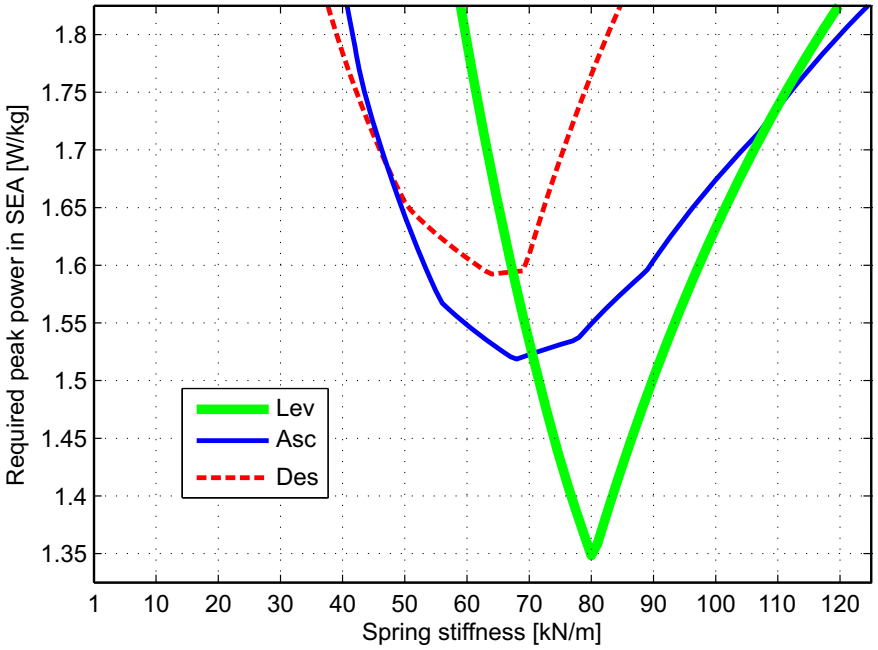

FIGURE 4.9: The (close-up view of the) variation of calculated required PP with respect to stiffness, SEA concept, based on Eq. 4.1, see also Tab. 4.2 and Fig. 4.6.

If we take K_s=64 kN/m (the corresponding stiffness for stair descent in Tab. 4.2), the required PP of level walking would be nearly 1.68 W/kg, an increase about 24% with respect to its minimum PP which is 1.35 W/kg.

If we take K_s=80 kN/m (the corresponding stiffness in level walking), we see that for stair descent, the required PP would be nearly 1.76 W/kg, an increase about 10.5% with respect to its minimum PP which is over 1.59 W/kg. Hence, if the user often uses the active ankle prosthesis for a normal level walking, it is better to select spring stiffness based on level walking and avoid the increase of required PP which was about 17-24%.

A more challenging design perspective is that the system is capable to change its stiffness by means of a mechanism. By this way, the system will always work in minimum requirements mode for any type of gait.

4.5.4 Effect of the damper on PP and ER requirements

In Fig. 4.10, motor force F_m (A) and nut velocity $\dot{x}_n$ (B) are shown for SEA, SEDA and PEDA in stair descent (approach for minimum PP, see also Fig. 4.6 and Tab. 4.2). In Fig. 4.10A, because of damper, PEDA requires less force in comparison to SEA (or SEDA) in parts of the gait cycle which there is a need for the first peak ankle force (see also Fig. 4.4). On the other hand, in Fig. 4.10B, the $\dot{x}_n$ of SEA and PEDA are very similar to each other (It could be also understood by seeing that their K_s values are close to each other, according to Tab. 4.2 and using Eq. 4.12). According to Eq. 4.13, the required motor power would be less as a result. In PEDA concept, Fig. 4.10A, in swing

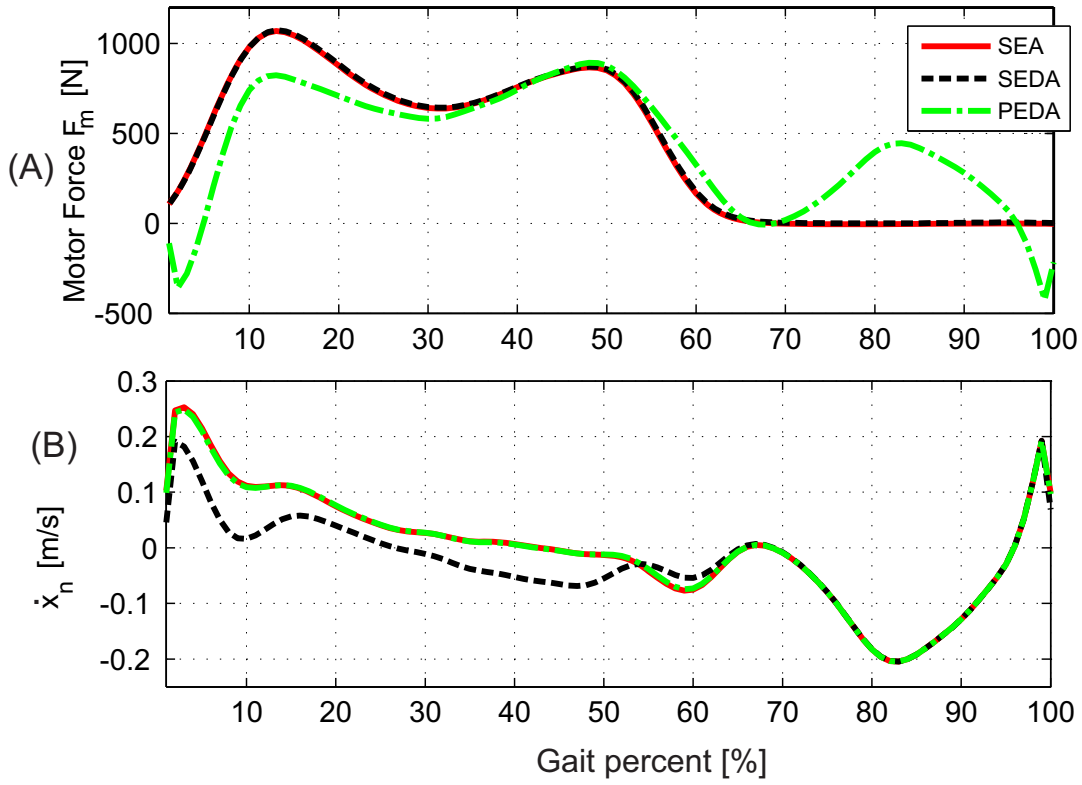

FIGURE 4.10: The calculated required motor force F_m (A) and $\dot{x}_n$ (B) for SEA, SEDA and PEDA actuation concepts in stair descent, approach for minimum PP requirements, see also Tab. 4.2 and Fig. 4.6.

phase nearly after 65%, because of the passive damper, motor uses force to regulate the total force of the ankle joint. This regulating requires motor power and hence increases energy requirements in comparison to SEA. This is in agreement with Fig. 4.6-Descent in which PEDA required more energy than SEA. In fact because of this matter, PEDA would require quite high power during swing too (for example see the motor force and $\dot{x}_n$ at 83%). This disadvantage could be resolved, if the damper in PEDA were controllable. This will be discussed in the next subsection.

For SEDA concept, the motor force is the same, however $\dot{x}_n$ is less than SEA (or PEDA) for some part of the gait cycle. According to Eq. 4.2, this results in reducing the required PP. Unlike PEDA, as motor force is very negligible in swing for SEDA, power is consequently negligible in this phase, and hence in total, energy requirement is also less than SEA (see Fig. 4.6-Descent).

4.5.5 Use of damper

The main objective of this study was to investigate on the effects of spring and passive damper on the PP and ER requirements in an active ankle prosthesis during level walking, stair ascent and descent. No benefit was found for having a damper in a powered ankle prosthesis for level walking and ascent. In contrast, for stair descent it had benefit for minimum PP or ER approach. According

to these findings and the result from 4.5.2, from the PP-ER perspective, this indicates that a damper might not be of advantage when different gaits are taken into account.

On the other side, [73] discussed that damping characteristic is embedded in human muscular structure and it is required for stability and adaptivity of muscular activities. These two points raise a question about the functionality of the damper in ankle. It appears that damper has a 'task specific' functionality i.e. when it is required it comes into action, otherwise it is off. Following these characteristics, we can use a SEDA or PEDA concept instead of an SEA, if the damper is controllable (i.e. a controllable damper). By this method, damper could be off when not required (for example in normal walking) and be on when required for example for stair descent or when a sudden stop of ankle motion is required. However, a variable damper requires additional control effort. This could be a continuation to this study.

Furthermore, energy in damper is dissipated. An efficient design approach is to have a mechanism that could have a similar effect (reducing F_m or $\dot{x}_n$, Fig. 4.10) like a damper but instead could use this effect to generate energy out of that (energy harvesting). By this approach, instead of wasting energy, it could be stored and reused for other joints or other occasions during gait cycle.

In Tab. 4.2, it is seen that the range of damping value in SEDA is from 15.5 kNs/m to ∞. It means that, if a controllable damper was used in SEDA, it should be always 'on' to change damping coefficient within the limits of the interval for different gaits, meaning that there is always a need for controlling it and providing energy for this purpose.

In contrast, for PEDA, this range is from 0 to 2.2 kNs/m. It means that a controllable damper in PEDA could be off for a gait cycle (e.g. level walking) or for a part of the gait cycle (e.g stair descent). Consequently we could avoid energy consumption for it. Therefore, from design perspective, a PEDA concept appears to be more favorable for powered ankle prosthesis.

In Section 4.5.3, it was concluded that finally K_s=80 kN/m was a better compromise to be used in SEA. Based on previous paragraph, if we want to have a PEDA concept based on this SEA, that could have a controllable damper for descent gait, there remain two parameters. One is the damping coefficient and the other is the gait percent in which the damper should get 'off'. In a simulation study for this type of PEDA concept (based on Eq. 4.13, for stair descent), it was found that a damping coefficient of ~1.98 kNs/m would be required from 1-44% of the gait cycle. After 44% the damper could be off until 100% of the stair descent gait.

In this case, the required PP and the corresponding energy requirement would be 1.28 W/kg and 0.5 J/(kg.m) respectively. Compared to PEDA concept shown in Fig. 4.6-Descent, the required PP would increase by 4% but the energy requirement would decrease nearly 33%. From section 4.5.3, it is seen an SEA required nearly 1.76 W/kg for stair descent at K_s=80 kN/m (Fig. 4.9). It means by using PEDA in the above-mentioned way, the required PP decreases by 27% in stair descent in comparison to SEA (Fig. 4.9).

By this approach, it could be possible to have a powered ankle prosthesis that though not perfect, would work in a compromise condition for all gaits. For level walking and stair ascent it operates like SEA and for stair descent, with a controllable damper, it could reduce power and energy requirements through PEDA concept.

As previously mentioned, a more efficient and challenging design approach is to have controllable spring and damper in the system. This makes the system operate with minimum requirements for all gaits. However, this requires additional mechanisms and control efforts to change the stiffness or damping values. This is not in line with a compact and light weight powered robotic foot.

4.6 Summary

In this chapter, we investigated whether or not a passive damper could reduce peak power (PP) and energy (ER) requirement in an active ankle prosthesis. To do this, aside from SEA, we introduced SEDA and PEDA concepts that in addition to spring have damper in series or parallel to motor. We calculated the minimum PP-ER requirements of these concepts in normal walking, ascending and descending the stairs. It was found that like a spring, a passive damper could also have a major role to reduce required PP and ER. However, it was useful for descent gait and SEDA had the least PP and ER requirement. Furthermore, for a mixed gait of level walking+ascent+descent, the SEA concept was still the best compromise regrading power-energy issues. On the other side, studies showed that damping is required for stable muscular activities. This raises a question for the functionality and control method of the damper in muscle to provide stability and adaptivity for the human gait. Therefore, it was suggested to have a controllable damper together with an SEA (through PEDA concept, Fig. 4.2). By this approach, it could be possible to develop a powered ankle prosthesis that would work in a compromise condition for all gaits. For level walking and stair ascent it is an SEA and for stair descent, with a controllable damper, it would reduce power and energy requirement in comparison to an SEA system.

Chapter 5

Design of Active Ankle Prosthesis with Bi-articular Passive Spring: A Macroscopic View

5.1 Introduction

The approaches for design of active foot prosthesis could be divided into two main categories:

1. Microscopic view
2. Macroscopic view

5.1.1 Microscopic view

In the previous chapters (2,3,4), the main concentration was to use the muscle models suggested by [34] (Fig. 1.15) and [35] (Fig. 1.16) as a template for actuation mechanisms in active foot prostheses. There, we investigated the effect of these models on power and energy requirement in the corresponding derived actuation concepts. This was a *microscopic view* since we considered the internal structure of the actuator itself regardless of the assembly and number of the actuators (or equivalently muscles) that could actuate the foot.

5.1.2 Macroscopic view

From the human body perspective, in current designs of active foot prostheses the research is concentrated on mimicking the functionality and structure of Soleus muscle (SOL, Fig. 5.1) in humans by using a series elastic actuator (SEA) [26, 44, 59, 60].

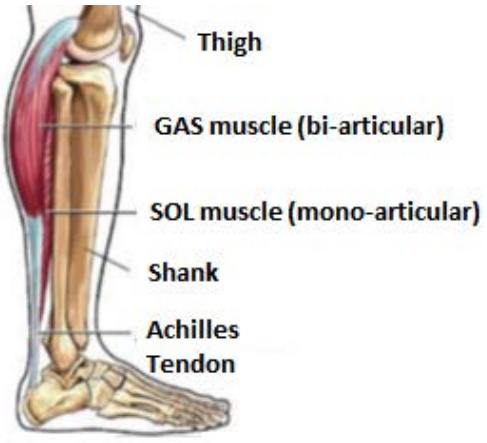

FIGURE 5.1: Human Soleus-Gastrocnemius musculo-skeletal structure, note to the assembly of the SOL and GAS muscles [74].

SOL is a mono-articular muscle i.e. it passes just one joint (ankle joint) [1] (see also Fig. 5.2A,B,C). In humans, one end of SOL is attached to the shank and the other end is connected to the Achilles tendon and hindfoot. In contrast to the current trends for mono-articular active feet, in [75] the authors argue that "the restoration of normal gait kinematics and kinetics" to the amputees was not possible using the active foot due to the mono-articulation of the active device.

In addition to SOL muscle, the human lower extremity consists of Gastrocnemius muscle (GAS) which collaborates with SOL to plantarflex the foot (Fig. 5.2A,C). Unlike SOL, GAS is a bi-articular muscle i.e. it passes two joints (ankle and knee joints, Fig. 5.2A,C). One end of GAS is on the thigh and the other end with SOL ends up to Achilles tendon which is connected to the hindfoot [1].

According to this biomechanical characteristic, a bipedal robot and an externally powered orthosis (with hydraulic mechanism) were constructed [76, 77] using bi-articular schemes. Improvement of operation, safety in locomotion and weight savings are among the advantages that the authors mention regarding their bi-articular design.

In [78] the authors simulated an arm with mono- and bi-articular actuators, assuming nonlinear and time-varying stiffness characteristics. It was shown this can considerably simplify the control structure for serial arms without the need for inverse dynamics computations, although, construction of such a varying system is complex. A planar jumping robot was developed in [79] for performing vertical jump experiments that used a bi-articular spring which connected thigh to the heel. The authors concluded that the performance of jumping and other fast explosive robot movements could be improved using the bi-articular approach.

In this perspective, the cooperation of different muscles to actuate a joint comes more into attention. In robotics this phenomenon is called *over-actuation*. The importance of over-actuated robots could be seen from two perspectives. One is what would be their effect on the control structure of the system. Could such a system simplify the control algorithm? The next is, what is the effect of such an assembly on power-energy requirements of a robotic system? The latter aspect is the main

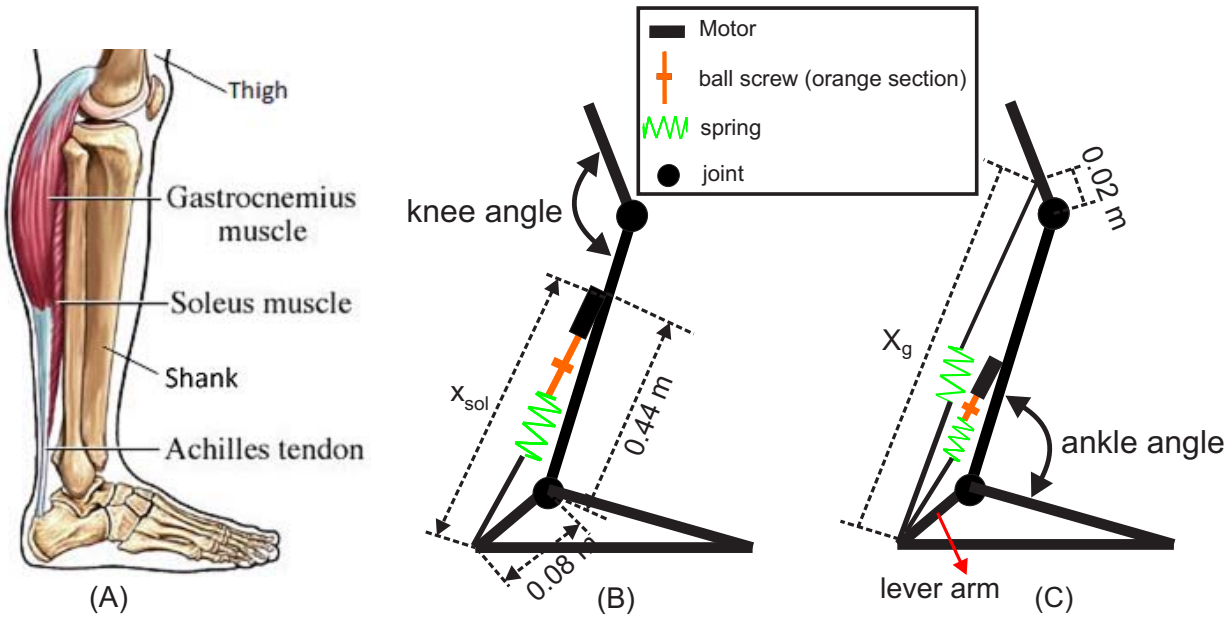

FIGURE 5.2: A: Human Soleus-Gastrocnemius musculo-skeletal structure with the assembly of the muscles and their connection points, B: The active ankle prostheses equipped with SEAS concept (mimicking a motorized Soleus), C: The active ankle prostheses equipped with SEAS+G concept (schematic representation of muscle group mimicking a motorized (active) Soleus and a passive (motorless) Gastrocnemius)

topic of this chapter. Here, we would like to know if a bi-articular foot actuation could reduce the power and /or energy requirements in a powered foot prosthesis in comparison to a mono-articular actuation scheme.

To investigate this topic, the actuation unit could consist of a motor and a series spring (i.e. the SEA concept). However, more complicated models could also be considered. The hypothesis is that not only similarity to muscular structure (Chapters 2, 3, 4) is of importance to reduce the energetics requirement but also the cooperation of different muscles that actuate a joint (the scope of this chapter).

As a first step toward this goal, in this chapter, we will focus on the effects of bi-articular actuation concept in active foot prostheses. The actuation configuration is analogous to the SOL-GAS structure in human lower extremity as shown in Fig. 5.2A,C. We would like to know the effects of this arrangement on the peak Power (PP) and energy (ER) requirement of such robotic prostheses. A lower PP or ER requirement will lead to a smaller motor or battery, hence, making it possible to increase the performance capacity of these active devices. The result of this investigation is fundamental for development, design and construction of more efficient prosthetic robots.

In the previous chapters it was shown that the spring stiffness plays a key role in PP and ER requirement of the active foot prostheses. To obtain a desired value for stiffness, one approach could be to search for stiffness values that minimize PP or ER requirement. In previous chapters,

it was seen that selecting stiffness based on minimizing PP was a preferred approach for mono-articular active ankle prostheses. This was the case because at the same time its corresponding energy requirement was slightly higher than the minimum energy requirement. In current study we see that for a bi-articular actuation concept, minimizing PP or ER requirement might not be necessarily the preferred method. Therefore another intuitive method will be used for the selection of optimal stiffness. In order to concentrate only on the effects of the GAS spring, normal level walking (1.6 m/s) and running (2.6 m/s) are considered.

In the following, we calculate and compare the power-energy requirement between mono- and bi-articular actuators for an active ankle prosthesis at normal walking (1.6 m/s) and running (2.6 m/s) (for each concept and for each type of locomotion). Then the minimum requirements are analyzed and methods for obtaining the springs' stiffness are compared and discussed. In addition, we make suggestions for the development and design of active foot prostheses based on the findings of our study.

5.1.3 Human ankle biomechanics in normal walking and running

In this chapter, we would focus mainly on normal walking (1.6 m/s) and running (2.6 m/s). The purpose is to discuss more on the result of the bi-articulation actuation rather than discussing the results of a wide range of speeds. At the end of the chapter the results for a wide range of walking and running speeds are given. In Fig. 5.3, the ankle torque T_{ank} and angle are shown for normal walking (1.6 m/s) and running (2.6 m/s) [5]. In addition, the main characteristics of human ankle biomechanics for those gaits are shown in Tab. 5.1. The ankle torque T_{ank} is normalized to body mass. The angle shown is the angle between foot and shank ([5], see also Fig. 5.2C). The gait cycle starts with heel contact and ends with the next contact of the same foot. Ankle torque T_{ank} is converted to ankle force F_{ank} using lever arm and is calculated by system geometry (Fig. 5.2B,C).

TABLE 5.1: The main features of ankle kinematics and kinetics for normal level walking and running [5]

gait type	max. ankle power [W/kg]	max. torque [Nm/kg]	stance until [%]	cycle time [sec]
walking 1.6 [m/s]	3.20	-1.53	65	0.98
running 2.6 [m/s]	8.67	-2.25	44	0.75

5.2 Power calculations

The model of the mono-articular active foot prosthesis is called as SEAS (Fig. 5.2B). This means it uses the SEA concept which emulates the SOL muscle function (and also Tibialis-anterior TA, a

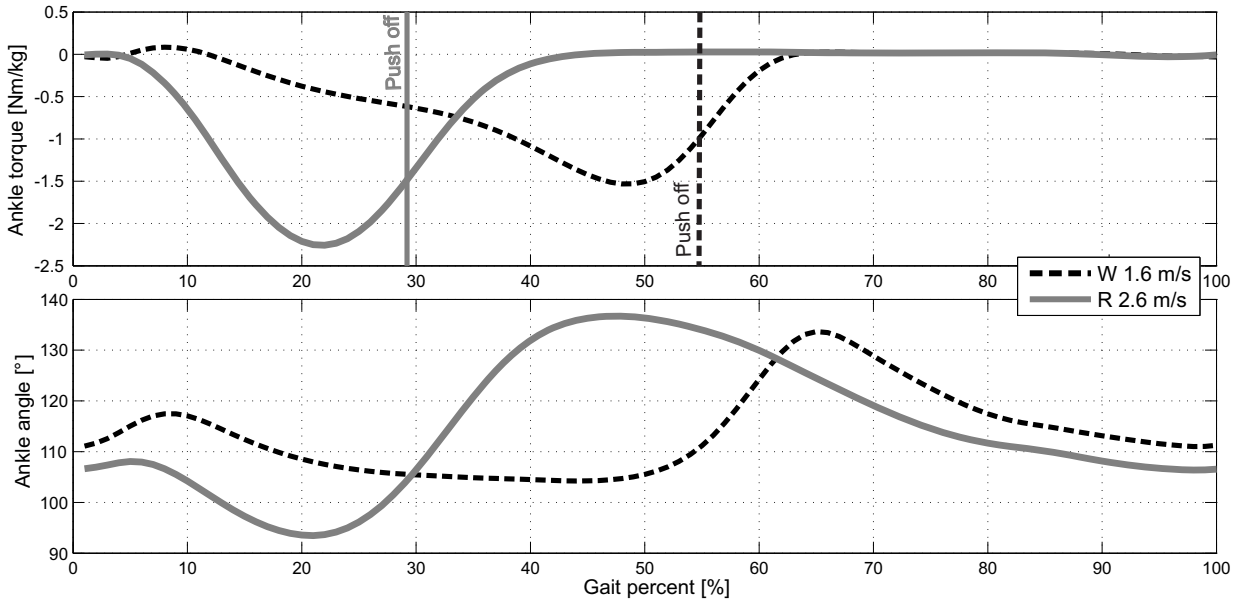

FIGURE 5.3: Human ankle torque (T_{ank}) and angle for normal level walking (W 1.6 m/s) and running (R 2.6 m/s) [5]. Vertical lines denote the instance of push-off.

dorsi-flexor muscle) such as in humans (Fig. 5.2A) (plantar-flexion: the foot wants to go away from the shank, dorsi-flexion: the foot wants to get closer to the shank).

The bi-articular active foot is called SEAS+G (Fig. 5.2C). SEAS+G resembles the SOL and GAS structure in humans (Fig. 5.2A). For both models, SOL is considered to be active. In SEAS+G concept, GAS is considered passive. In [80] it is concluded that, when optimally designed, unpowered passive elastic devices can substantially reduce the required active power and force in joints and may allow independent locomotion in patients with large deficits in muscle function. In addition, this will reduce the complexity of the system for final construction and helps to determine the possible advantages of a passive GAS. This would also eliminate the corresponding control efforts.

5.2.1 The required motor power in SEAS

The required motor power P_m for SEAS is discussed in chapter 2. After a short review of this design, we will focus on the SEAS+G concept here in this chapter. The required motor power P_m in SEAS is

$$P_m = F_m \ (\dot{x}_{sol} + \frac{\dot{F}_m}{K_s}) \tag{5.1}$$

x_{sol} is the length of SOL (Fig. 5.4), K_s is the stiffness of the series SOL spring and F_m is the motor force. For a mono-articular actuation (Figs. 5.2B, 5.4), F_{ank} is equal to F_m. The length x_{sol} (Fig. 5.4) is calculated by using ankle angle (Fig. 5.3) and geometrical relations (Fig. 5.2B,C). Angle and torque data were obtained from [5].

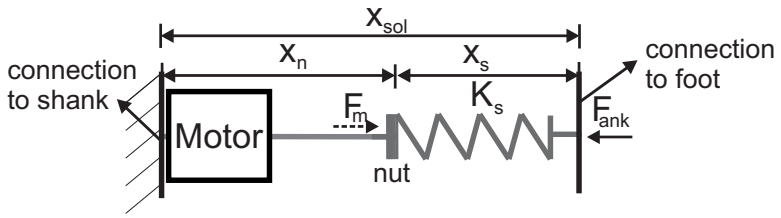

FIGURE 5.4: Model of SEAS concept, This structure resembles the Soleus muscle (a mono-articular mechanism), see also Fig. 5.2B

5.2.2 The required motor power in SEAS+G

The transmissions in active ankle prostheses are typically ball screws [26, 44, 60]. Therefore, we also assume the power calculations for this type of mechanism. In a motor-ballscrew mechanism, the required motor power P_m is obtained by [58]

$$P_m = F_m \, \dot{x}_n \tag{5.2}$$

where F_m is the motor force and $\dot{x}_n$ is the (ball screw) nut velocity (Fig. 5.5).

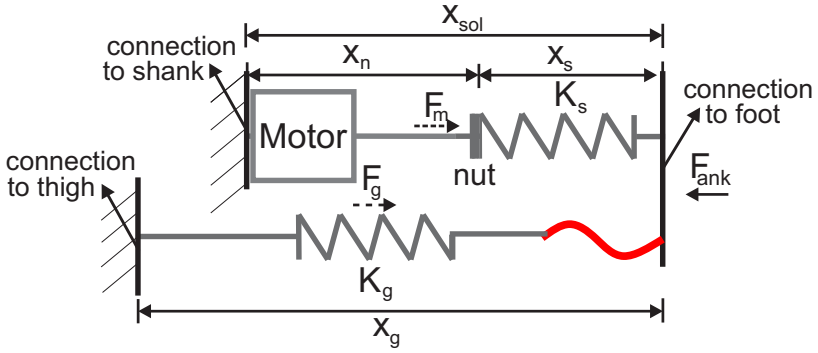

FIGURE 5.5: Model of SEAS+G concept, this structure emulates the function of the Soleus-Gastrocnemius complex (a bi-articular mechanism), see also Fig. 5.2C, note that GAS spring could create force only in elongation mode which is shown like a loose string (red section), see also chapter 3 for UPS definition.

In SEAS+G concept, both SOL and GAS would contribute to exert torque on the ankle joint (T_{ank}, Fig. 5.2C, Fig. 5.5). Hence

$$T_{ank} = T_g + T_s \tag{5.3}$$

T_{ank} is known by ankle torque data [5]. T_g is the torque of GAS and T_s is the torque of SOL

$$T_g = F_g \, L_{g\perp} \tag{5.4}$$

$L_{g\perp}$ is the length of the lever arm with respect to ankle joint and perpendicular to GAS force F_g. This is calculated by geometry of the robotic system (Fig. 5.2C) and ankle angle [5]. F_g is

$$F_g = K_g \, \Delta x_g \tag{5.5}$$

where

$$\Delta x_g = l_{0g} - x_g \tag{5.6}$$

K_g and l_{0g} are the stiffness and free length of GAS spring. x_g is the length of the GAS (Fig. 5.5) and is calculated by the geometry of the system (Fig. 5.2C) and ankle and knee angles [5], therefore it is a known parameter. The GAS spring is considered uni-directional. This is shown like a red loose string in Fig. 5.5. It means that GAS spring produces force F_g only when elongated. If it were bi-directional (i.e. GAS spring could be both elongated or compressed) the motor in SOL would need to fight against the GAS spring in some part of the gait and expend energy unnecessarily. This difference of uni-directional versus bi-directional spring was previously shown in chapter 3. Hence we would have

$$F_g = 0 \qquad if \quad x_g < l_{0g} \tag{5.7}$$

The SOL torque T_s on the ankle is

$$T_s = F_s L_{s\perp} \tag{5.8}$$

F_s is the SOL force which is equal to the motor force F_m (Fig. 5.2C). $L_{s\perp}$ is the length of the lever arm with respect to ankle joint and perpendicular to SOL force F_s. Based on Eq. 5.3-5.8, we obtain

$$F_s = (T_{ank} - K_g\ \Delta x_g\ L_{g\perp})/L_{s\perp} \tag{5.9}$$

On the other side, SOL spring deflection is also dependent on F_s, hence we have

$$F_s = K_s\ \Delta x_s \tag{5.10}$$

and

$$\Delta x_s = l_{0s} - x_s \tag{5.11}$$

x_s is the length of SOL spring and l_{0s} is its free length. According to Fig. 5.5 we have

$$x_{sol} = x_s + x_n \tag{5.12}$$

x_{sol} is the length of SOL (Fig. 5.5) and is calculated by geometry of the system and ankle angle data, therefore, it is a known parameter. x_n is the ball screw nut position (Fig. 5.5). From Eq. 5.10-5.12, $\dot{x}_n$ is obtained as

$$\dot{x}_n = \dot{x}_{sol} + \frac{\dot{F}_s}{K_s} \tag{5.13}$$

from Eqs. 5.9,5.13 and 5.2, the required motor power P_m of the SOL motor in SEAS+G concept is

$$P_m = F_s\ \dot{x}_n \tag{5.14}$$

$$= ((T_{ank} - K_g\ \Delta x_g\ L_{g\perp})/L_{s\perp})(\dot{x}_{sol} + \frac{\dot{F}_s}{K_s}) \tag{5.15}$$

The required motor energy E_m is the integral of absolute required motor power over a cycle time (see Tab. 5.1 for cycle time)

$$E_m = \int |P_m| \, dt \tag{5.16}$$

The power of human ankle can be both negative and positive during gait [5, 26]. When it is negative, a resistance motion is applied to the ankle, and when it is positive, a propelling motion is applied. A motor unit cannot typically provide negative power [26, 58], therefore, it must provide power to both resist and propel human motion. Therefore, we considered absolute values of PP and energy requirement in this study. For this reason, an absolute value in Eq. 5.16 is used.

The two parts of Eq. 5.14 i.e. F_s and $\dot{x}_n$ are related to K_g and K_s by Eqs. 5.9 and 5.13. For any given value of K_g and l_{0g}, the SOL force F_s (which is the same as motor force) is determined by Eq. 5.9. Subsequently its derivative $\dot{F}_s$ would be known. Other variables like x_{sol} or x_g are calculated by joint angles [5] and geometrical dimensions of the actuation concept (Fig. 5.2B,C). Thus, the values K_g, l_{0g} and K_s become the only parameters that would influence the motor power requirement P_m in SEAS+G concept (since other variables are constant or obtainable).

For K_s a stiffness range of 1 $\frac{kN}{m}$ to 200 $\frac{kN}{m}$ (1 $\frac{kN}{m}$ step size) was considered and for K_g the range was from 1 $\frac{kN}{m}$ to 60 $\frac{kN}{m}$ (1 $\frac{kN}{m}$ step size). The range of l_{0g} was assumed from 0.390 m to 0.520 m (1 mm step size). This range for l_{0g} was selected according to the length of x_g as shown in Fig. 5.6.

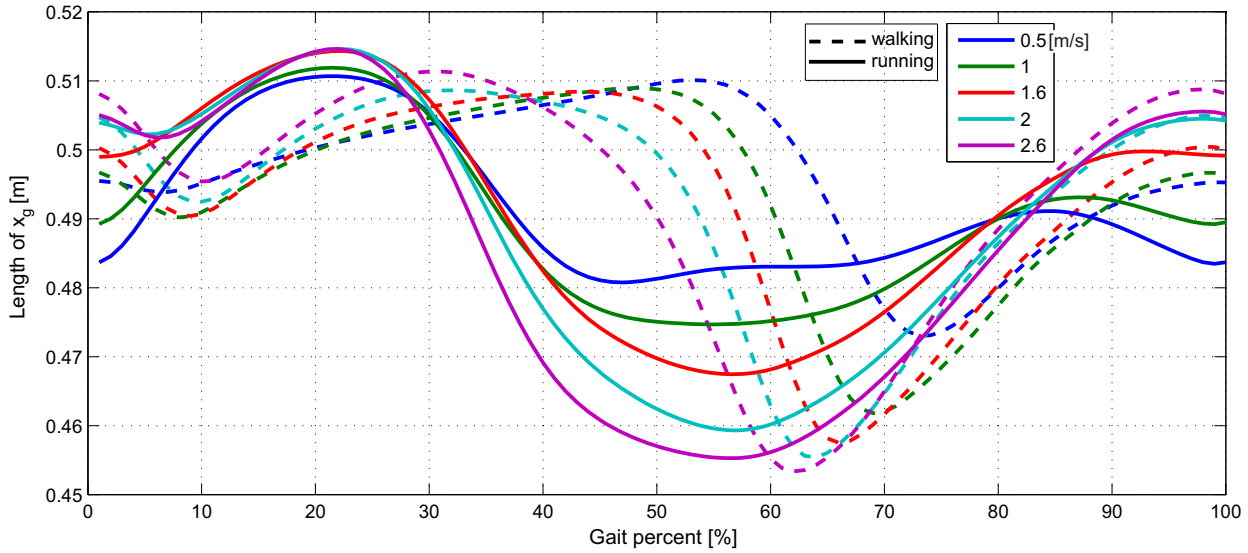

FIGURE 5.6: The length of x_g (see Fig. 5.5) in walking (dashed) and running (solid) gaits (0.5 $\frac{m}{s}$ - 2.6 $\frac{m}{s}$), calculated based on geometry Fig. 5.2 and ankle and knee angles [5].

For each combination of [K_g,K_s,l_{0g}], the required motor power was obtained based on Eq. 5.14 through afore-mentioned procedure. Then the results were compared between [K_g,K_s,l_{0g}] combinations and then the K_g-K_s-l_{0g} values that result in minimum PP were selected. A same method and range was used to determine minimum energy requirement for different actuation concepts, gaits and speeds. The programming was done in Matlab.

5.2.3 The weighted sum approach

It was found out that to search for minimum PP or energy requirement might not be a good approach for the selection of stiffness and design of active feet that are based on bi-articular actuation scheme (see Figs. 5.7 and 5.8). As it was seen, in minimum PP requirement, the reduction of the ER requirement was not satisfactory and for minimum ER requirement, the reduction of PP requirement was not satisfactory. Instead, searching for minimum sum of PP and ER requirement might be a better approach. Therefore, it was decided to use a criteria like

$$min(\lambda \times \frac{PP}{1\ W/kg} + (1-\lambda) \times \frac{ER}{1\ J/(kg.m)}) \quad 0 \leq \lambda \leq 1 \tag{5.17}$$

for reaching acceptable amount of PP and ER requirement and selecting the stiffness. λ is a weighting factor. By this factors, we could regulate the influence of PP or ER requirement. This factor works like tuning parameter and depends on a specific design objective for the amount of PP or ER requirement.

For each combination of [K_g,K_s,l_{0g}], the motor PP and corresponding ER were obtained like before. Then multiplied by the factors (λ and $1-\lambda$). Next the minimum weighted sum and the corresponding K_g-K_s-l_{0g} values were obtained. Note that when $\lambda = 1$ this approach is like to search for the minimum PP and when $\lambda = 0$ it is like to search for minimum ER requirements. In addition, the two terms of sum in Eq. 5.17 are dimensionless parameters.

In general, different weighting factors could be selected. If λ is very low or high, it means that one aspect (either PP or ER) would be more important for the designer. However, in this study, we select the weighting factors in a way that the two terms of Eq. 5.17 could be nearly equivalent and in the same order of magnitude (meaning that both PP and ER are important).

5.3 Results

This section is divided to three subsections. The results are shown for normal walking (1.6 m/s) and running (2.6 m/s) speeds. The SEAS concept has been studied in Chapter 2. Therefore, we consider it as a basis and compare it with the bi-articular concept (SEAS+G). Body mass is assumed 75 kg.

5.3.1 Approach for minimum motor PP requirement, $\lambda = 1$

In this approach, we search for the K_g, K_s, l_{0g} values that minimize the PP requirement in SEAS and SEAS+G concepts. The minimum PP and their corresponding energy (ER) requirement for those concepts are shown in Fig. 5.7. The corresponding K_g, K_s, l_{0g} values are in Tab. 5.2.

TABLE 5.2: The obtained required stiffness in SEAS and SEAS+G concepts. The K_g values are in (Parenthesis), approach: minimum PP requirement $\lambda = 1$.

Gait		Walking	Running
Speed [m/s]		1.6	2.6
Stiffness $[\frac{kN}{m}]$	SEAS	80	77
	SEAS+G	94 (8)	81 (18)
l_{0g} [m]	SEAS+G	0.443	0.448

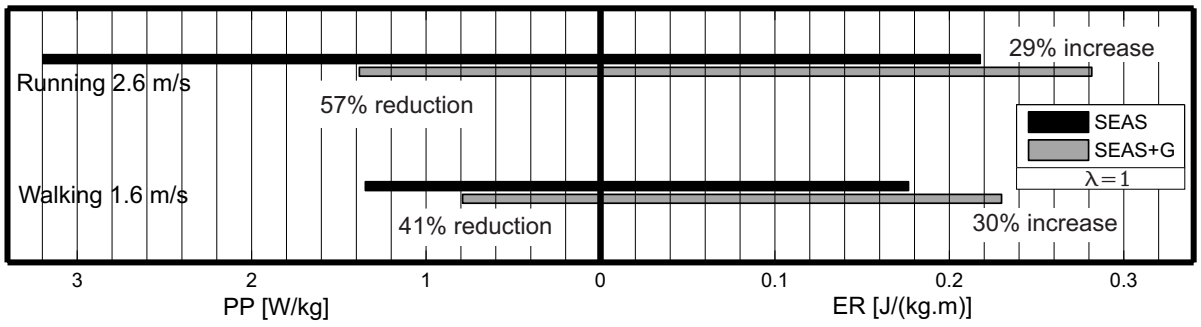

FIGURE 5.7: The minimum PP and their corresponding ER requirement for SEAS and SEAS+G actuation concepts in normal walking and running, approach: minimum PP requirement $\lambda = 1$, see also Tab. 5.2.

For walking 1.6 m/s, the PP requirement in SEAS+G decreased about 41% in comparison to SEAS (Fig. 5.7). On the other hand, its corresponding energy requirement increased by 30%. In running gait, the PP requirement of SEAS+G decreased about 57% in comparison to SEAS, and its corresponding energy requirement increased about 29%. The stiffness of SOL spring in SEAS+G concept is higher than that of SEAS concept for both gaits. Meanwhile, the GAS stiffness K_g is much less than SOL stiffness K_s.

5.3.2 Approach for minimum ER requirement, $\lambda = 0$

For this approach, the K_g, K_s, l_{0g} values that minimize the ER requirement in SEAS and SEAS+G concepts were calculated. The minimum ER requirement and their corresponding peak power for those concepts are shown in Fig. 5.8. The corresponding K_g, K_s, l_{0g} values are brought in Tab. 5.3.

In this approach, for walking gait, in SEAS+G concept the ER requirement decreased about 2% in comparison to SEAS. At this time its corresponding peak power decreased about 5% in comparison to SEAS. In running gait, the ER and its corresponding peak power requirement for SEAS+G concept decreased about 15% and 31% respectively in comparison to SEAS. Unlike the minimum PP approach, in this approach it was found that both ER and peak power requirement of SEAS+G decreased in comparison to SEAS. However reduction in peak power is not as noticeable as what we see in the approach for the minimum required PP (compare Fig. 5.8 vs. Fig. 5.7).

TABLE 5.3: The obtained required stiffness in SEAS and SEAS+G actuation concepts. The K_g values are in (Parenthesis), approach: minimum ER requirement $\lambda = 0$.

Gait		Walking	Running
Speed [m/s]		1.6	2.6
Stiffness	SEAS	73	76
$[\frac{kN}{m}]$	SEAS+G	72(2)	108(24)
l_{0g} [m]	SEAS+G	0.465	0.466

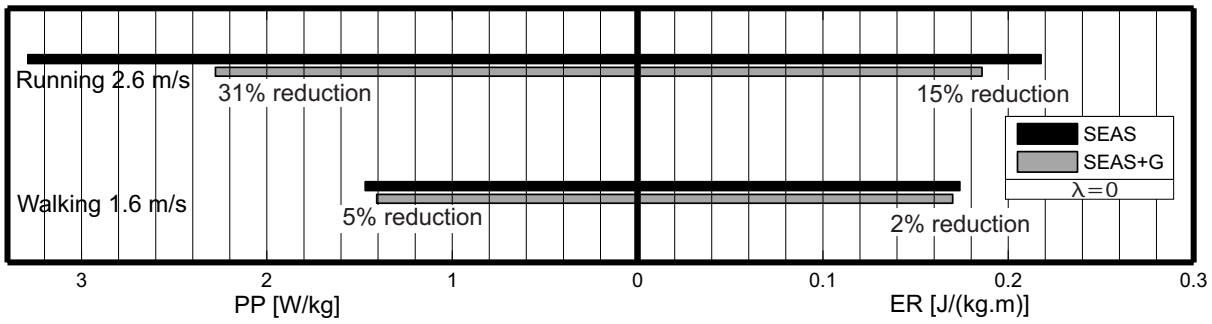

FIGURE 5.8: The minimum ER requirement and their corresponding PP for SEAS and SEAS+G actuation concepts in normal walking and running, approach: minimum ER requirement $\lambda = 0$, see also Tab. 5.3.

5.3.3 Approach for minimum weighted sum of PP and ER requirement, $\lambda = 0.25$

According to Fig. 5.7, in the minimum required PP approach, the minimum required PP of SEAS+G reduced considerably in comparison to SEAS but not the corresponding ER requirement. On the other hand, in minimum ER approach, both PP and ER requirement reduced, however, the reduction was not that noticeable.

As previously mentioned, this led us to use another method based on Eq. 5.17. To do that, it was required to choose the weighting factors. Looking at Fig. 5.7, the values of PP and the corresponding energy requirement are not in the same order. Therefore, in this approach, we selected $\lambda = 0.25$ so that the two terms of Eq. 5.17 are numerically equivalent (to reach a similar order of magnitude, it means that PP and ER requirement have the same importance, as previously mentioned if the weighting factor is at the limit, it means that one of the requirements was considered less important).

TABLE 5.4: The obtained required stiffness in SEA and SEAS+G actuation concepts. The K_g values are in (Parenthesis), approach: the minimum weighted sum, $\lambda = 0.25$.

Gait		Walking	Running
Speed [m/s]		1.6	2.6
Stiffness	SEA	80	77
$[\frac{kN}{m}]$	SEAS+G	84(13)	74(25)
l_{0g} [m]	SEAS+G	0.464	0.465

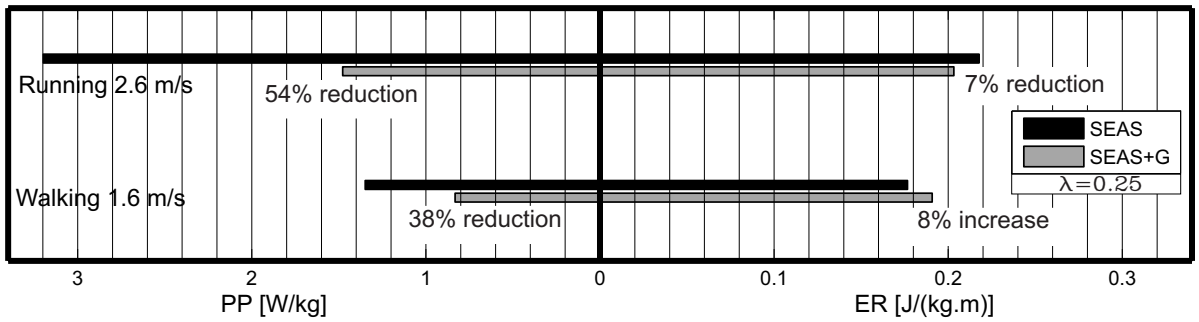

FIGURE 5.9: The obtained PP and their corresponding ER requirement for SEAS and SEAS+G actuation concepts in normal walking and running, approach: the minimum weighted sum $\lambda = 0.25$, see also Tab. 5.4.

The corresponding values of K_g, K_s, l_{0g} that minimize Eq. 5.17 are found in Tab. 5.4. In this approach, the corresponding PP and their ER requirement for SEAS and SEAS+G concepts are shown in Fig. 5.9.

In walking, the required PP of SEAS+G concept decreased about 38% in comparison to SEAS. On the other hand, its ER requirement increased about 8% in comparison to SEAS.

In running, both ER and PP requirement of SEAS+G decreased nearly 7% and 54% respectively in comparison to SEAS concept.

5.3.4 Power requirement during a gait cycle in minimum weighted sum approach

In Figs. 5.10 and 5.11, the power requirements of DD, SEAS and SEAS+G actuation concepts for a whole gait cycle in walking (1.6 m/s) and running (2.6 m/s) are shown to illustrate the distribution of the power requirement in a gait cycle. As it is seen, in the SEAS+G concept, during some part of the swing phase, the motor requires power to load the GAS spring.

5.4 Discussion

5.4.1 Comparison between the approaches

Only in minimum ER approach Fig. 5.8, we found that both PP and ER requirement of SEAS+G concept (bi-articular actuation) could be reduced in comparison to SEAS (mono-articular scheme). However the reduction of PP was not that large. On the other side, in minimum PP approach, the reduction of PP was noticeable, however the corresponding ER requirement increased.

In order to combine the advantages of the two approaches, we used another criteria to minimize the weighted sum of PP and ER requirement (see Eq. 5.17).

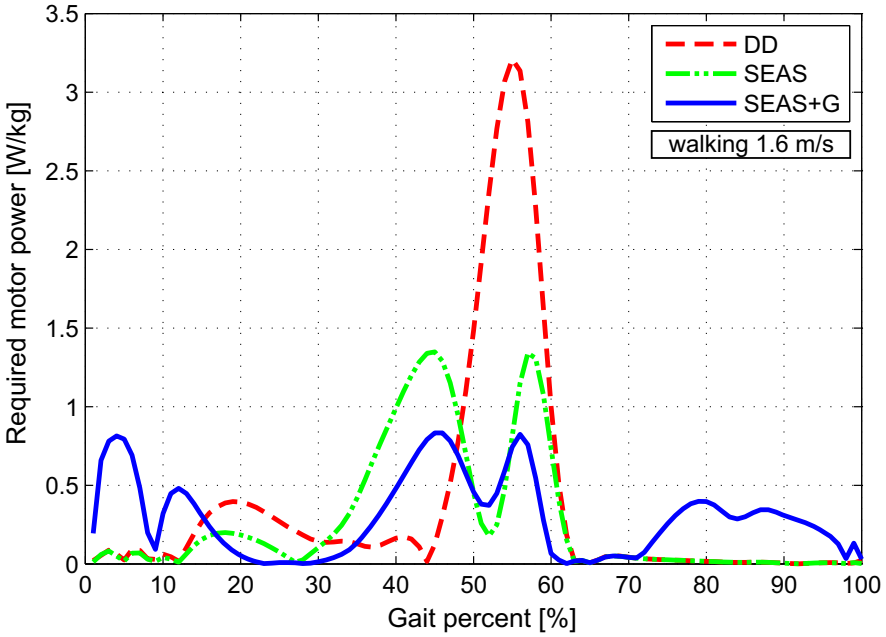

FIGURE 5.10: Comparison of the required motor power between DD, SEA and SEAS+G actuation concepts for walking 1.6 m/s ($\lambda = 0.25$, see also Fig. 5.9 and Tab. 5.4).

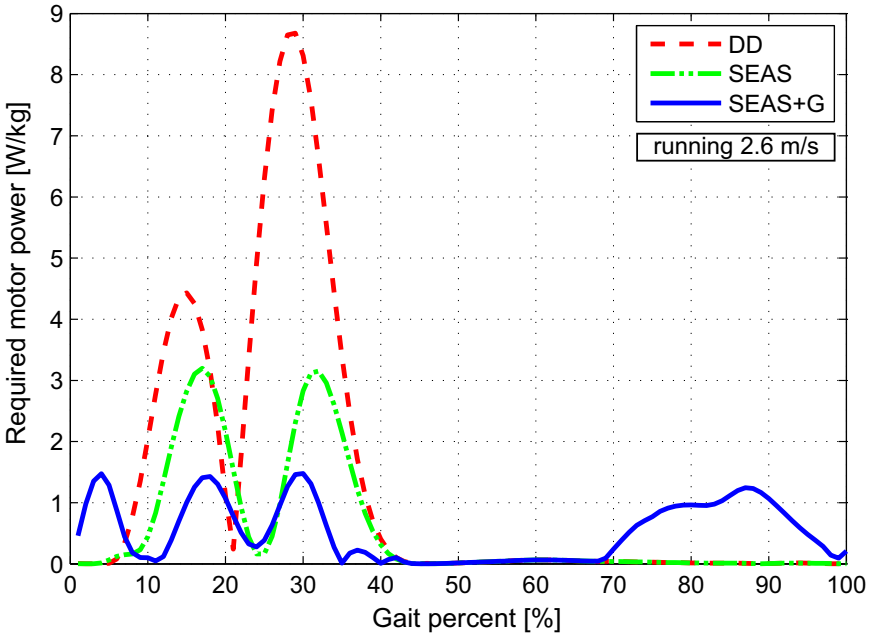

FIGURE 5.11: Comparison of the required motor power between DD, SEA and SEAS+G actuation concepts for running at 2.6 m/s ($\lambda = 0.25$, see also Fig. 5.9 and Tab. 5.4).

Comparison between Fig. 5.7 (minimum peak power approach) and Fig. 5.9 (minimum weighted sum approach) shows that in running gait the required PP in SEAS+G in the weighted sum approach is nearly 7% more than that of the minimum PP approach (for SEAS+G). However, the corresponding energy requirement in weighted sum approach is nearly 28% less than the corresponding energy requirement of the minimum PP approach. Such a similar trend was also found for walking.

According to Fig. 5.9, the weighted sum approach had no obvious effect on the mono-articular SEAS

concept (compare the results of SEAS concept in Fig. 5.7 vs. Fig. 5.9 and Tab. 5.2 vs Tab. 5.4). This fact might suggest that for a mono-articular SEAS structure the minimization of PP might be already the proper approach regarding the stiffness and power-energy requirements. Instead, in a bi-articular scheme like SEAS+G the weighted sum approach can be used to balance and reduce PP-ER requirement for an active foot prostheses.

In some early studies, it was hypothesized that bi-articular muscles may play a role in saving energy expenditure in human locomotion [81, 82]. The hypothesis was also discussed in [83], in which it was shown that bi-articular muscles like GAS transport energy from proximal (e.g. knee joint) to distal joints (e.g. ankle) during jumping. The results presented in this chapter also show that the GAS could be a key structure for transferring a flow of power-energy from knee to the ankle joint. This structure could be potentially used in design of the powered foot prostheses. In a way, if we consider both gaits together, we see that we could be reducing the required PP at about the same ER requirement (SEAS vs. SEAS+G). It means a reduced mass (smaller motor or biologically a smaller Soleus) is expected.

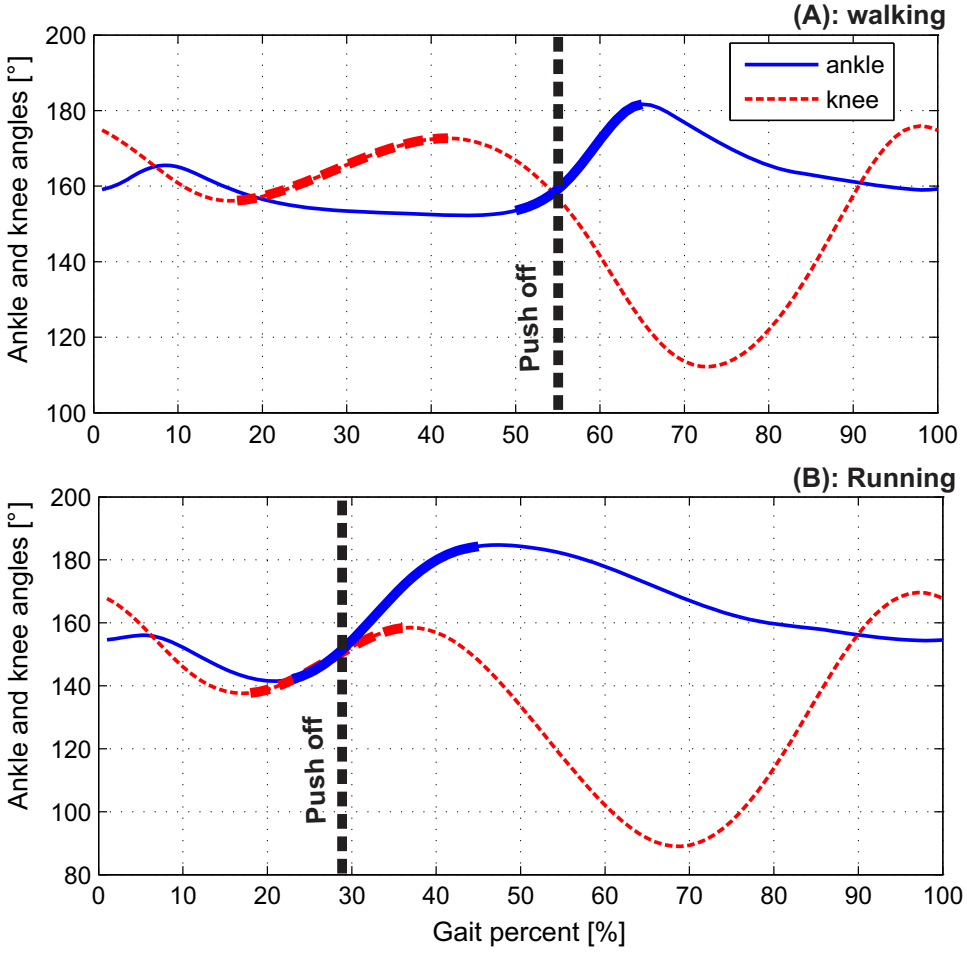

FIGURE 5.12: Comparison of ankle and knee angles for normal walking (1.6 m/s) and running (2.6 m/s), during late stance phase the extension of ankle and knee are thickened, (for the ease of comparison, 50° were added to the values of ankle angle from [5]).

In Fig. 5.9 (the weighted sum approach) it is seen in walking that the ER requirement in SEAS+G was higher than SEAS concept by 8%. One reason could be λ value was not appropriate for this gate. However when the interval of search was increased for the weighting factor, no better solution was found. Another reason could be that an alternative criteria should be used in walking instead of the one used in Eq. 5.17. Then, suitable weighting factor could be adapted for this gait. The kinematic relationship between the knee and ankle joints could also be a reason. In [84] the authors argue that a simultaneous knee extension and ankle plantar flexion could be a reason for the transfer of power and energy from knee to ankle through the GAS muscle and helps for ankle push-off. In Fig. 5.12 the ankle and knee angles are shown for walking (1.6 m/s) and running (2.6 m/s). As seen, in running, the ankle and knee angle operate in phase (parallel) during late stance when ankle plantar flexion coincides with the knee extension (the thickened section). This concurrence, however, is not seen for the walking gait approximately in late stance (near push-off). We may note that other reasons might also exist as the cooperation between different muscles during human locomotion is still under investigation by the research community.

5.4.2 Spring stiffness

As seen from Tabs. 5.2, 5.3, 5.4, the optimal stiffness in walking and running gaits differ from each other. In fact, this is one of the problematic issues in building active prostheses. If the prosthesis is using a constant stiffness, then it would work optimally for a specific speed and gait. It would be of importance to have a compact mechanism that could change to the optimal stiffness for different gaits and speeds. Some groups have suggested mechanisms for changing the spring stiffness [36, 37], however integrating such mechanisms in a compact prosthetic system requires more considerations. Any addition to a prosthetic system should be always evaluated to see if the added mechanism is necessary and compact. Note that the optimal lengths for GAS spring (l_{0g}) are also slightly different for different gaits and speeds.

5.4.3 The effect of GAS spring on the knee joint

As previously mentioned, the GAS spring is attached to the thigh at one end (Fig. 5.2 A,C). Therefore it could create torque also on the knee joint. In this subsection, we investigate the effects of the GAS on the knee torque if a transtibial amputee would wear the active foot prosthesis equipped with the SEAS+G concept.[1]

To this end, in Fig. 5.13, the knee torques of an able-bodied human [5] and the estimated knee torque of a transtibial amputee (who is assumed to wear an active foot with SEAS+G concept) are shown for walking 1.6 m/s and running 2.6 m/s. The estimated knee torque was calculated based on the data from [5] and the ankle and knee dynamics. As seen in Fig. 5.13, for both gaits the knee

[1] note that it is an estimation, the exact effect needs to be determined by gait experiments.

torques of the two cases (able-bodied vs. estimated) are similar to each other. However, a more realistic comparison could be achieved based on the experiments with a transtibial amputee wearing the active foot (with SEAS+G concept).

In Fig. 5.13, the effect of GAS on the knee torques was not very noticeable. One reason is the geometry of the robotic system. Looking back to Fig. 5.2, we see that the lever arms related to the ankle and knee are very different (0.08 m vs. 0.02 m). Hence the same force in GAS results in different torques in the ankle and knee joints. Further investigations on the importance of geometry (e.g. lever arms) and the attachment point on the thigh, could be considered in future studies.

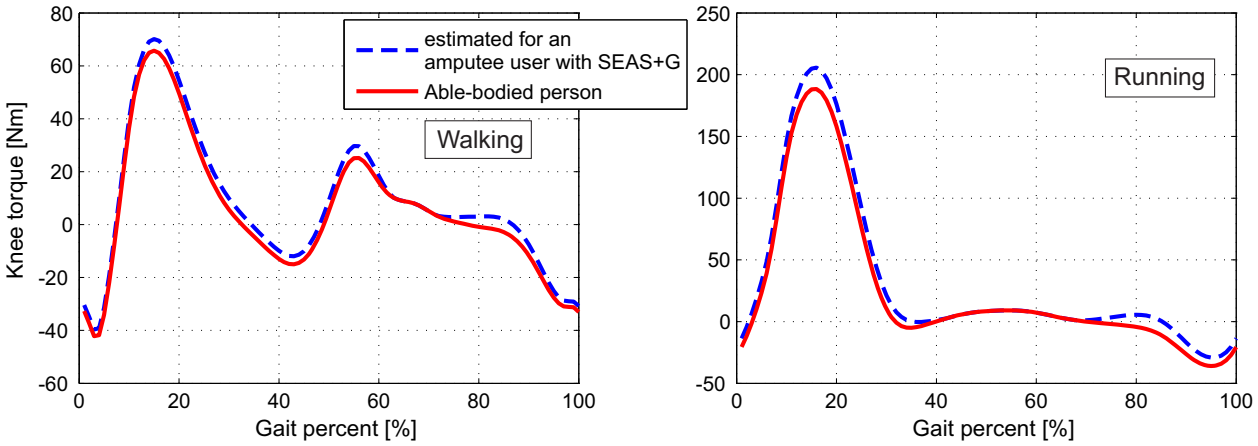

FIGURE 5.13: Comparison of knee torque between able-bodied subject [5] and estimated knee torque for an imaginary amputee with an active foot prosthesis based on SEAS+G concept, graphs for (A) walking 1.6 m/s and (B) running 2.6 m/s (approach: minimum weighted sum, $\lambda = 0.25$, see also Fig. 5.9 and Tab. 5.4).

5.4.4 Difference to the UPS approach seen in Chapter 3

Although the GAS spring is assumed to be unidirectional, the results of such a spring in bi-articular scheme is different from what we saw in SEA+UPS concept in Chapter 3. For example in minimum ER approach, we saw that both PP and ER requirement of SEAS+G concept reduced in comparison to SEAS concept (Fig. 5.8). This result, however, is not seen in Fig. 3.8 from Chapter 3. It could be concluded that for mono-articular actuation the intensity is on power minimization, however, for bi-articular actuation the intensity is to minimize power and energy with a higher attention to energy i.e. through weighted sum approach.

5.5 Further investigation on the minimum weighted sum approach for other speeds

In this section, we will apply the weighted sum approach for a wide range of walking and running speeds. As shown in Fig. 5.14, the selected weighting factor ($\lambda = 0.25$) is still effective and could

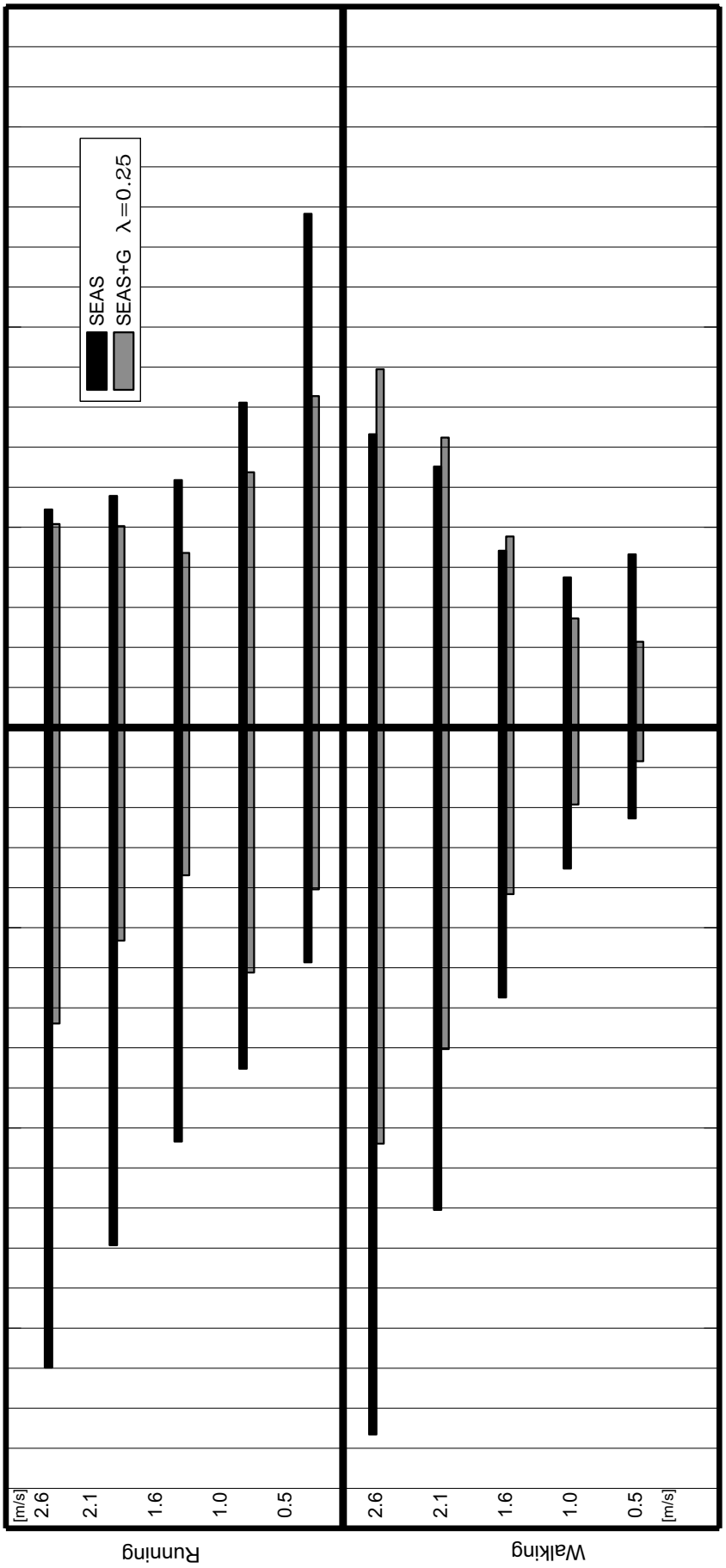

FIGURE 5.14: The required PP and their corresponding ER for SEAS and SEAS+G actuation concepts for a wide range of walking and running speeds, approach: the minimum weighted sum $\lambda = 0.25$, for the ratio of PP and ER requirements between SEAS+G and SEAS concepts look at Tab. 5.5.

TABLE 5.5: The obtained required stiffness in SEAS and SEAS+G concepts for different walking and running speeds. The K_g values are in (Parenthesis), the minimum weighted sum approach $\lambda = 0.25$, the last rows show the ratio of the required peak power and energy in SEAS+G concept with respect to SEAS concept (see also Fig. 5.14).

Gait		Walking					Running				
Speed [m/s]		0.5	1.0	1.6	2.1	2.6	0.5	1.0	1.6	2.1	2.6
Stiffness [kN/m]	SEA	78	61	80	115	143	70	74	77	77	77
	SEAS+G	195(33)	70(13)	84(13)	119(12)	71(11)	62(44)	64(44)	78(47)	72(29)	74(25)
l_{0g} [m]	SEAS+G	0.484	0.469	0.464	0.456	0.438	0.506	0.507	0.479	0.469	0.465
PP_{SEAS+G}/PP_{SEAS}		0.36	0.55	0.62	0.67	0.59	0.69	0.72	0.36	0.41	0.46
ER_{SEAS+G}/ER_{SEAS}		0.49	0.72	1.08	1.11	1.22	0.64	0.78	0.70	0.86	0.93

reduce the peak power and energy requirements of SEAS+G in comparison to SEAS for a wide range of speeds. The only exceptions are walking at 1.6, 2 and 2.6 m/s. However, even for these cases the PP requirement reduced in comparison to SEAS concept.

The corresponding values of K_g, K_s, l_{0g} for those speeds and gaits (that minimize Eq. 5.17) are given in Tab. 5.5. The corresponding PP and their ER requirement for SEAS and SEAS+G concepts are shown in Fig. 5.14.

This approach (weighted sum) provided a useful method for the mechanical design of SOL/GAS for a powered foot prosthesis. In the future more advanced optimization criteria than the one suggested in Eq. 5.17 could be developed for a comprehensive approach to minimize power and energy requirements in these active devices.

5.6 Summary

Current designs of active ankle prostheses try to mimic the functionality of human Soleus muscle (SOL) by using a series elastic actuator (SEA) [26, 44, 59, 60]. However, humans utilize a bi-articular actuation scheme in their lower extremities. In this study we investigated on having a bi-articular actuation scheme in active ankle prostheses. For design of these robotic systems, peak power (PP) and energy (ER) requirement are two important design factors. Lower PP or ER requirement lead to a small motor and/or battery. We compared minimum PP and ER requirement of mono- and bi-articular actuation concepts for active ankle prosthesis. The results show that reduction about 50% in PP requirement is possible by bi-articular scheme in comparison to mono-articular actuation. At the same time, in running gait, reduction in ER requirement was possible by 7%, however, for walking gait, it increased by 8%.

In contrast to mono-articular actuation (Chapters 2, 3, 4), in which the PP minimization was the desired approach for design and selecting the spring stiffness, for bi-articular actuation this approach

was not appropriate. Therefore, we used an intuitive approach called *the weighted sum approach*. It was found that it is possible to have nearly the same peak power requirement as in minimum PP approach but with less energy requirement.

Another important matter, is when both actuators are active. A main consideration here goes toward the procedure of the force distribution between the actuators and to investigate whether the bi-articular actuation could have less requirement than mono-articular actuation.

Chapter 6

Control and Laboratory Experiments

6.1 Introduction

This chapter describes the laboratory experiments on the PAKO platform (Powered Ankle Knee Ortho-prosthesis). The first aim is to see if the robotic foot is following the kinematic and kinetic trajectory for slow walking (0.5 m/s). The fist results are summarized in this chapter. Having obtained understanding of the system's characteristics and limitations, further experiments are planned for the future.

6.2 Controller structure

As described in Chapter 1, the controller for a powered foot could be divided to slave controller and master controller (see Fig. 1.18).

6.2.1 Slave controller

The slave controller is the motor position control. Different position controllers could be used. We will start from a general approach and narrow it down to controller equation we used for PAKO control. To obtain a final command for motor control, we start from the equation of motion for the motor. The equation of motion for the motor is presented as

$$T_m - T_l = I_m \ddot{\theta}_m \tag{6.1}$$

where T_m, T_l, I_m and $\ddot{\theta}_m$ are the applied motor torque, external (load) torque, motor (rotor) inertia and motor angular acceleration respectively. Rotor inertia could be obtained from the manufacturer's

catalog (Appendix A). T_l is due to load force F_l

$$T_l = \frac{F_l L}{2\pi\eta} \tag{6.2}$$

where L and η are the lead and efficiency[1] of the ball screw [58]. In a powered foot with SEA, the load is related to the spring force (see previous chapters). In the PAKO robot a ball screw is used as transmission mechanism for converting the angular motion of the motor to the linear motion of the nut. In Figs. 6.1 and 6.2, the working principle of a ball screw and its usual structure are shown.

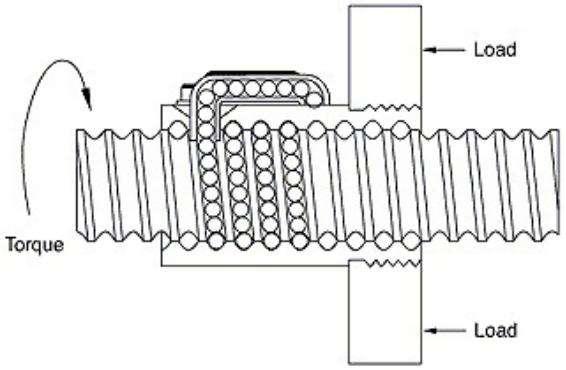

FIGURE 6.1: The working principle of ball screw: when there is an external horizontal load, upon exerting a certain torque, the load moves back and forth [85].

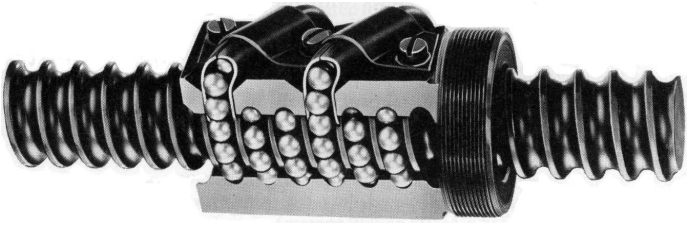

FIGURE 6.2: The structure of a ball screw [86].

In robotics, in order to impose a desired motion on the motor, a mass-spring-damper relationship for the error dynamics is usually used (a linear error dynamics is imposed),

$$M\ddot{e} + K_p\, e + K_v\, \dot{e} = 0 \tag{6.3}$$

where $e = \theta_{des} - \theta_m$ and θ_{des} is the desired value of the motor angular position and M, K_p and K_v are the mass, position and velocity gains (or in some texts as stiffness and damping gains). For simplicity, M could be replaced by I_m. According to Eqs. 6.1, 6.2 and 6.3, a command signal to the motor could be extracted

$$T_{com} = K_p\, e + K_v\, \dot{e} + I_m\, \ddot{\theta}_{des} + \frac{F_l L}{2\pi\eta} \tag{6.4}$$

[1] ball screws usually have high efficiency (80-90%), however in general it depends on the friction and the pitch angle [58].

this method of creating a command signal for motor is called *computed torque method* (CTM). Different versions of Eq. 6.4 could be used in a robotic system to simplify the command (see robotics textbooks). For example, a simple form of

$$T_{com} = K_p\ e - K_v\ \dot{\theta}_m \tag{6.5}$$

is also suggested in some textbooks to avoid derivative kick [87]. Different algorithms were tested to evaluate the least controller requirements.

6.2.2 Master controller

From Eqs. 6.3 and 6.4, in order to make the command signal, we see that it is required to provide the desired values (θ_{des}) of the control variable (e.g. θ_m). As pointed out in chapter 1, to provide those values, the *gait*, *speed* and *phase* (*gait percent*) of a specific locomotion should be identified. These three pieces of information are obtained via the master controller.

Generally at first the type of the person's gait (i.e. walking, running etc.) is determined. Then, the speed at which the person is performing that gait is identified. Next, the gait percent within the corresponding gait and speed should be determined. The gait detection procedure is schematically shown in Fig. 6.3.

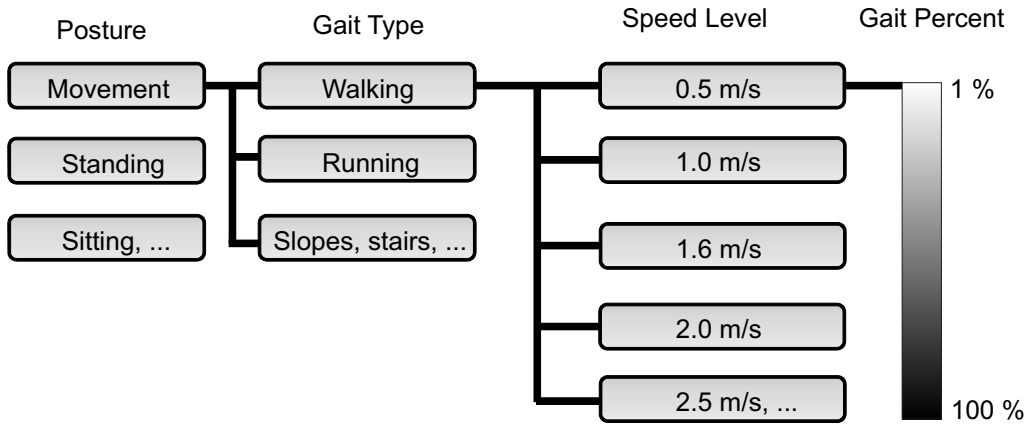

FIGURE 6.3: Gait detection procedure.

In general there are different methods to determine those objectives (see Chapter 1). In this chapter, we first discuss the method suggested in [46]. The advantage of this controller is that it needs just one sensor in order to determine the speed and the phase in a gait cycle. Therefore, we will check if this controller could be used for the PAKO platform and to evaluate the possible limitations of this controller.

The controller is based on the measurement of the angular velocity of the user's shank[2] by a gyro sensor. The angular velocity is then integrated to obtain the shank angle. The shank angle (θ_{sh}, (A)) and angular velocity ($\dot{\theta}_{sh}$, (B)) for walking 0.5 m/s are shown in Fig. 6.4.

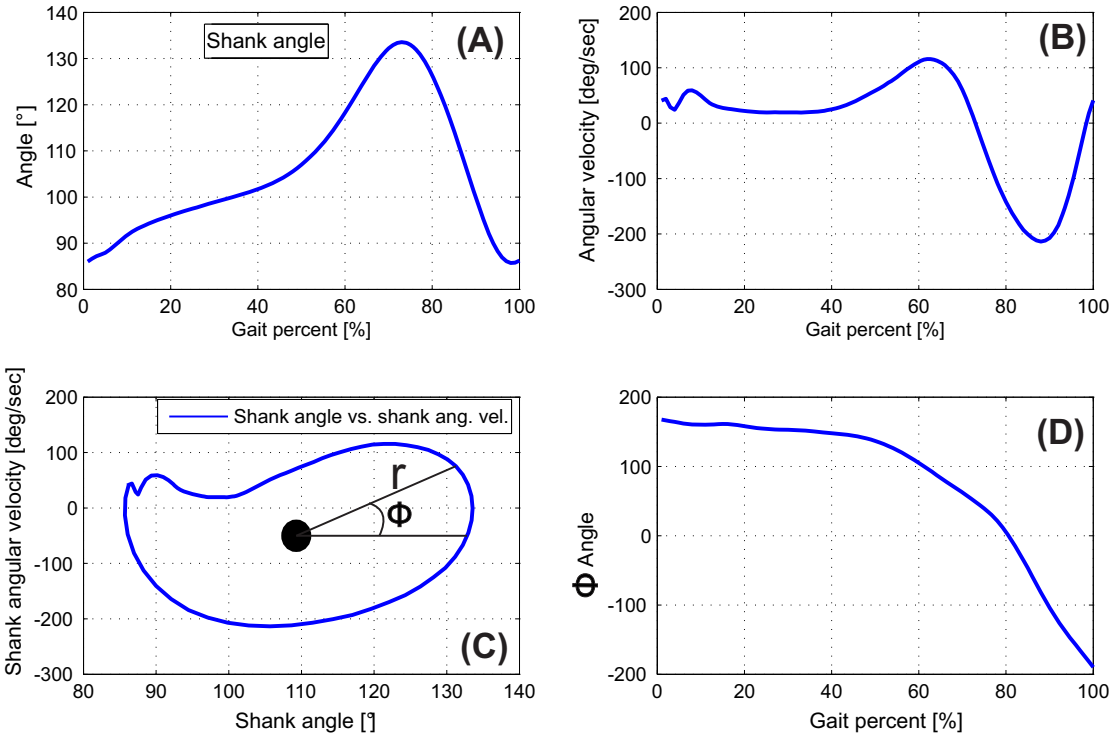

FIGURE 6.4: Shank angle and angular velocity, together with the description of ϕ-method (phase plane method) (walking 0.5 m/s, angle data from [5]).

In Fig. 6.4C, the shank angle and angular velocity are plotted together. As seen this creates a pseudo-circular graph. Hence, it could be used to determine the location of each point by having the angle ϕ and the distance r. We will show later that the distance r could be used for speed identification. Looking back to Fig. 6.4C we see that because of the pseudo-circular graph, there could be a one-to-one relationship between the ϕ angle and the location of each (θ_{sh},$\dot{\theta}_{sh}$) (however, this is not valid for *all* points).

Therefore, for the entire gait cycle a one-to-one graph could be obtained that relates the ϕ angle (and hence each (θ_{sh},$\dot{\theta}_{sh}$)) to each gait percent. In this manner, by knowing the ϕ angle, the gait percent would be determined. The corresponding graph is shown in Fig. 6.4D.

Having determined the gait percent, the corresponding desired values of θ_{des} and $\dot{\theta}_{des}$ are selected and then the command signal in Eq. 6.4 is produced (the other variables are obtained based on the on-line sensor measurements). The desired value of θ_{des} or equivalently the desired value of nut position could be obtained by Eq. 2.7.

[2]Note that the transtibial amputee has lost a part of the shank and not all of it.

6.2.2.1 Challenges of the phase plane control structure

Although the phase plane method explained in the previous subsection, provides almost a simple method for the detection of the gait percent, the data processing for this purpose has some difficulties in the way ahead.

1. The integration challenge (integration of the shank angular velocity)

Unlike Simulink that a $\frac{1}{s}$ block could be used for integration for simulation purposes, the integration of online sensory data from shank angular velocity for real world application is not so straight forward. The output from the gyro sensor (that is used for the measurement of the shank angular velocity) could not be directly used for integration and obtaining the shank angle. This is due to *integration drift*. This fact is shown in Fig. 6.5. Using ordinary integration method by $\frac{1}{s}$ shows that after a while (nearly 20 sec) the graph for the shank angle goes down. In other words the output of the integration block $\frac{1}{s}$ gets unstable.

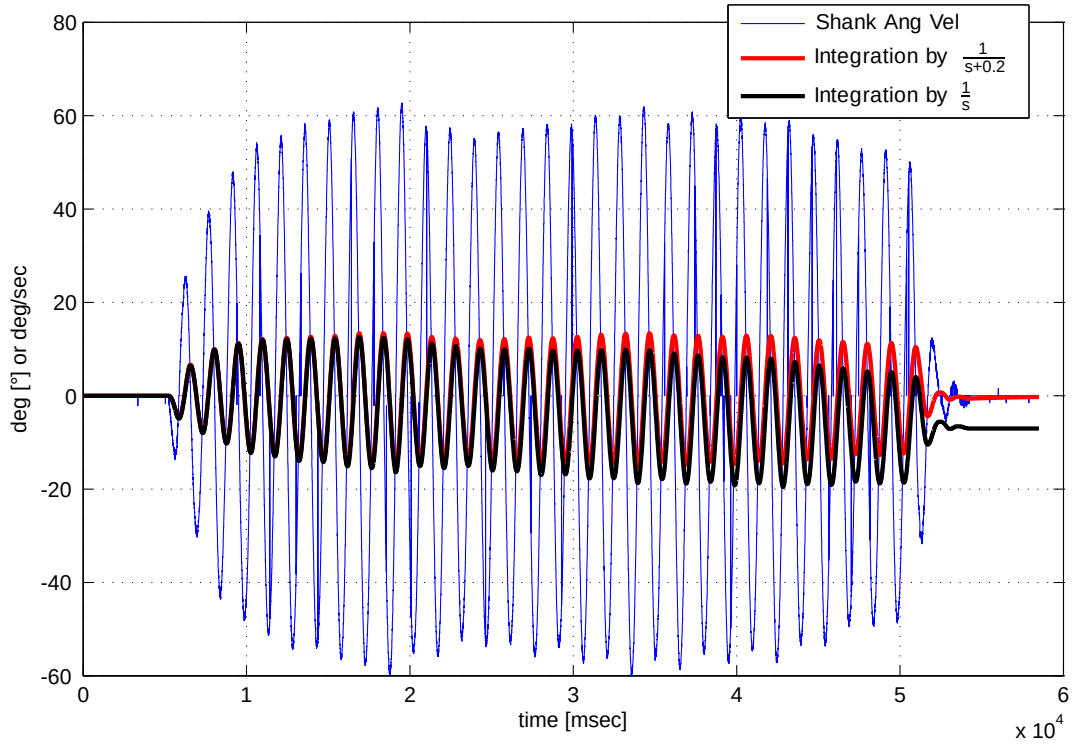

FIGURE 6.5: Integration drift, the comparison between integration with $\frac{1}{s}$ and integration with $\frac{1}{s+0.2}$.

The transfer function of the integrator in frequency domain ($\frac{1}{s}$) has a pole in 0. This might be an explanation why the output of the integration shows instability with time (see Fig. 6.5, the integrator output deviates from what it should be when the time increases).

To overcome this problem, a transfer function similar to $\frac{1}{s}$ but more stable was used instead. From frequency domain point of view, this means to move the pole of the transfer function to the left.

Therefore, $\frac{1}{s+a}$ was selected as a possible candidate for integration. It is more stable than $\frac{1}{s}$ and not too much different if appropriate values are selected for a. However, in this case it is really not an integrator for all frequencies. To achieve this, a was selected 0.2. The Bode plots of $\frac{1}{s}$ and $\frac{1}{s+0.2}$ are shown in Fig. 6.6.

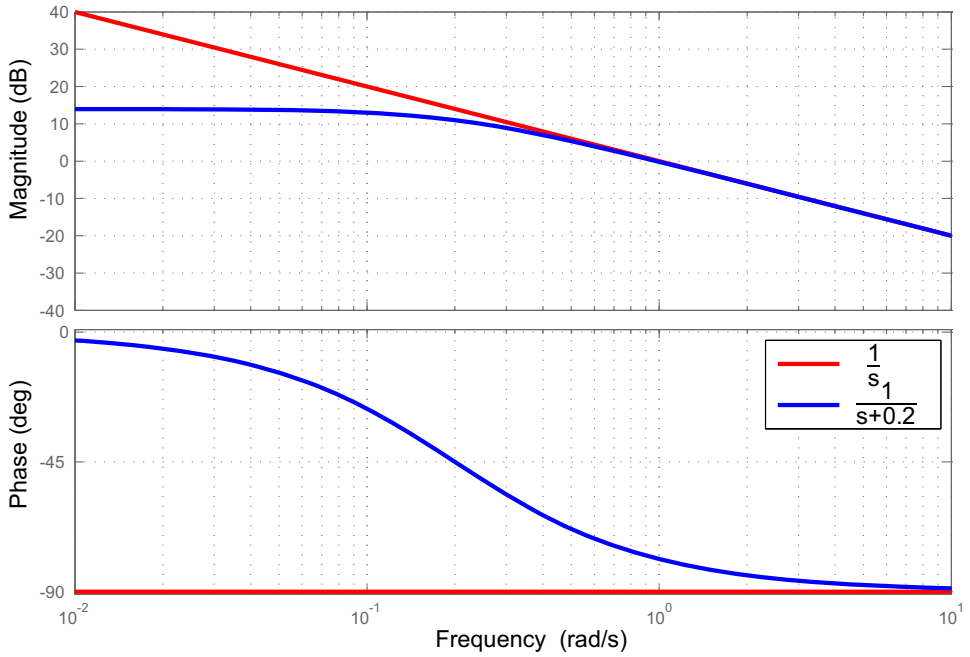

FIGURE 6.6: The Bode plots of $\frac{1}{s}$ and $\frac{1}{s+0.2}$, note that in high enough frequencies (angular velocities) (e.g. more than 3 rad/s) the behavior of $\frac{1}{s+0.2}$ is similar to $\frac{1}{s}$.

Using $\frac{1}{s+0.2}$, it is shown in Fig. 6.5 that the drift was removed. Note that based on Fig. 6.6, $\frac{1}{s+0.2}$ cannot be used for integration in low frequencies as its behavior is very different from the integrator $(\frac{1}{s})$.[3]

2. Obtaining ϕ curve in Fig. 6.4D

The curve shown in Fig. 6.4D, is dependent on the definition of the origin point in Fig. 6.4C. The ideal curve of the 6.4C is when it is very steep without any plateau-like regions. To obtain such a curve, it is required to manipulate the origin point and use weighting factors to magnify or attenuate the $x-y$ axes (values) in Fig. 6.4C.

[3]Note that using the concept of frequency response analysis, the magnitude of the transfer functions $\frac{1}{s+0.2}$ and $\frac{1}{s}$ are very different at very low frequencies

$$G(s) = \frac{1}{s+0.2} \implies |G(\omega i)| = \frac{1}{\sqrt{\omega^2+0.04}} \tag{6.6}$$

for higher frequencies, it is seen that $\frac{1}{\sqrt{\omega^2+0.04}} \simeq \frac{1}{\omega}$ as previously predicted by Fig. 6.6 (the magnitude curves). From the phase point of view, at low frequencies like (0.6 Hz) the phase of the G(s) would be

$$\phi = \angle G(s) @\ 0.6\ Hz\ \simeq -87^\circ \tag{6.7}$$

in principle it should have been -90° to match the integration characteristics (compare the phase curves in Fig. 6.6).

Unfortunately, for each walking or running speed, this must be regulated. This makes the algorithm more individual. This challenge is shown in Fig. 6.7 for walking 0.5 m/s and 1 m/s. As seen in Fig.

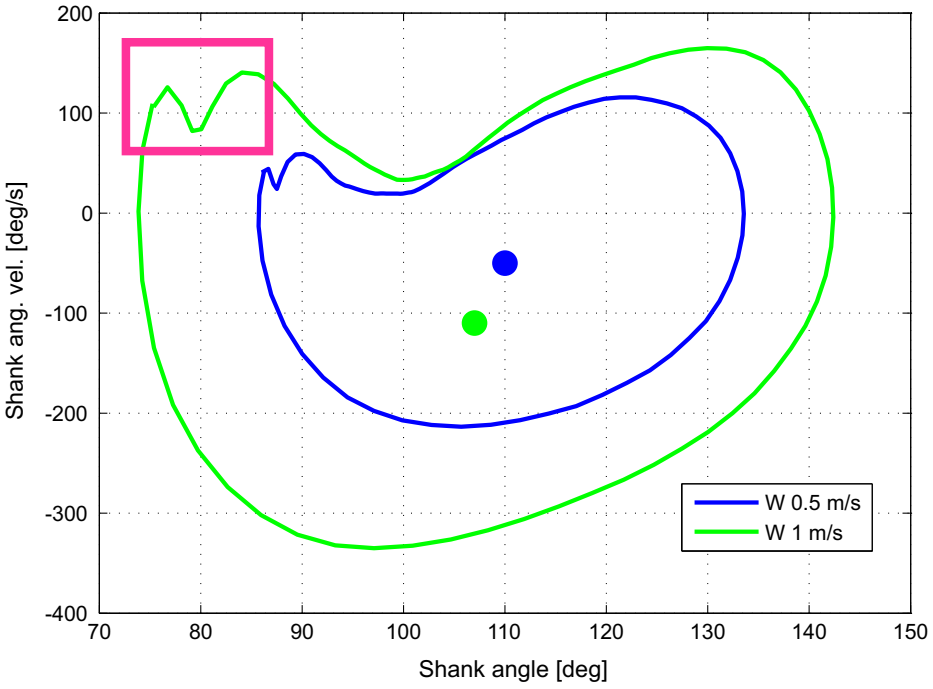

FIGURE 6.7: The desirable origin points to create the ϕ curve in Fig. 6.4D for walking speeds of 0.5 m/s and 1 m/s.

6.7 the desirable origin points to create the ϕ curve in Fig. 6.4D are different for walking 0.5 m/s and 1 m/s.

Another issue is shown in pink rectangle (Fig. 6.7). As seen in that region it is possible to find two different points with the same ϕ angle. This means that the ϕ curve in Fig. 6.4D could not be one-to-one. This creates problem for selecting a real gait percent and feed it to the controller in Eq. 6.4.

3. Overlap in Fig. 6.4C for different speeds

As previously mentioned, the distance r from the defined origin[4] could be used for the identification of the gait speed. However, as shown in Fig. 6.8 in some regions it is not possible to establish a one-to-one relationship between a certain r and a specific speed. This happens due to the intersection of the curves.

The problem is that it causes chattering between the real and false desired values in a certain gait.

4. The existence of loops in Fig. 6.4C for different speeds

As shown in Fig. 6.9, obtaining the correct r-ϕ values is more complicated in running. Other than overlap of the curves, in some regions there are loops that make it hard to obtain just one ϕ angle

[4]In case a same origin is selected for all speeds.

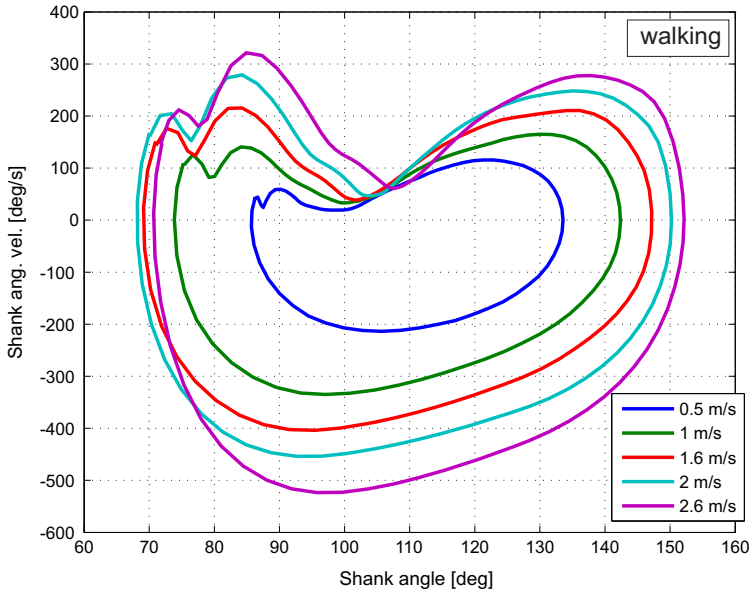

FIGURE 6.8: The overlap of θ_{sh} vs. $\dot{\theta}_{sh}$ curves for different walking speeds, in some regions it is difficult to identify the correct locomotion speed based on a certain distance r, see also Fig. 6.4C.

in a specific speed. Like before, the problem is that it causes chattering between the real and false

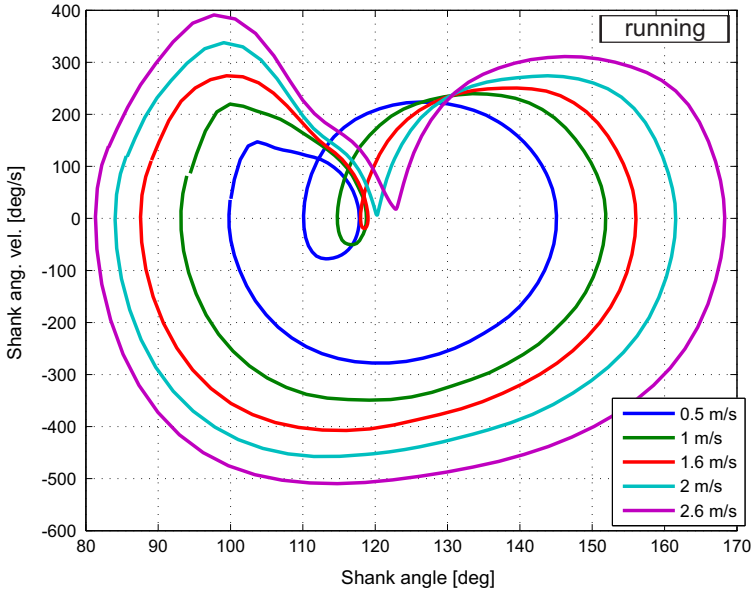

FIGURE 6.9: The existence of loops and overlap of θ_{sh} vs. $\dot{\theta}_{sh}$ curves for different running speeds. In some regions it is challenging to identify the correct locomotion speed and gait percent based on a certain distance r and ϕ angle, see also Fig. 6.4C.

desired values in a certain gait (e.g. the desired values jump from one speed to another speed or jump from one gait percent to another gait percent within a specific gait).

Despite having these problems, provided that the speed is known this controller could be still used for experiments with PAKO to estimate the gait percent.

6.3 Experiments with PAKO

The first experiment was to test the PAKO robot on a treadmill at the gait lab. The experiments were conducted for the slow walking of 0.5 m/s.

In the following graphs the nut position (Fig. 6.10), ankle angle (Fig. 6.11), SEA force (Fig. 6.12) and ankle power (Fig. 6.13) and the detected gait percent (shown later in Fig. 6.15) are shown. In these graphs, the obtained results from the PAKO experiments are shown and compared with those of the desired data (i.e. the data that we had from human experiments presented in [5]).

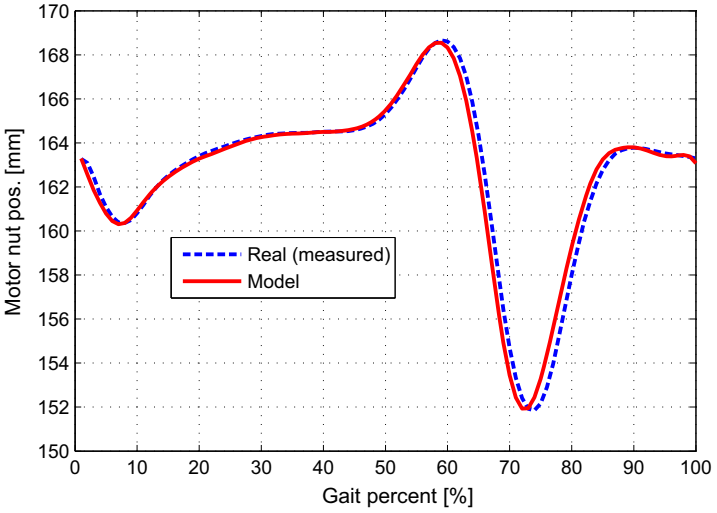

FIGURE 6.10: The desired and real (measured) nut position for PAKO experiments (walking 0.5 m/s).

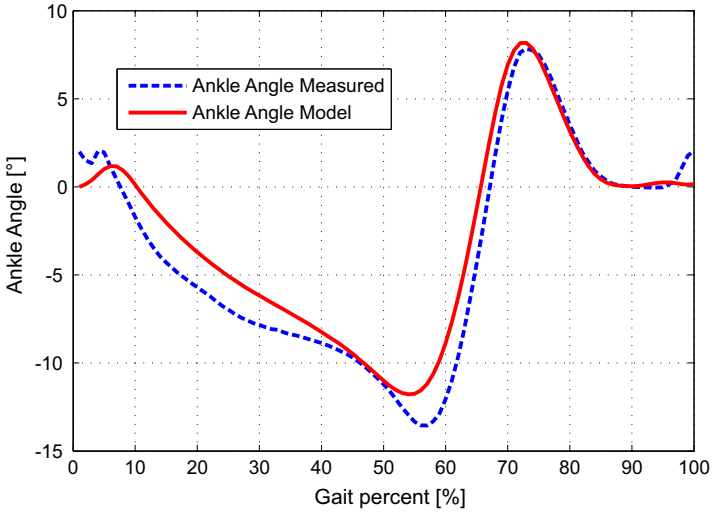

FIGURE 6.11: The desired and real (measured) ankle angle for PAKO experiments (walking 0.5 m/s).

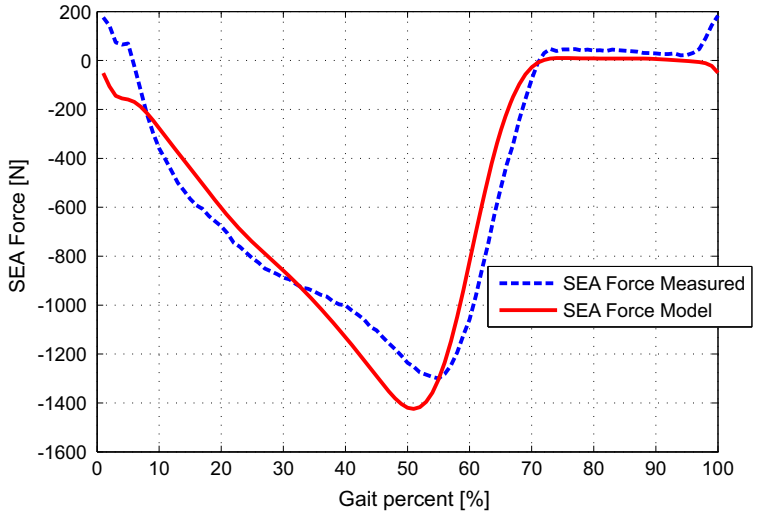

FIGURE 6.12: The desired and real (measured) SEA force for PAKO experiments (walking 0.5 m/s).

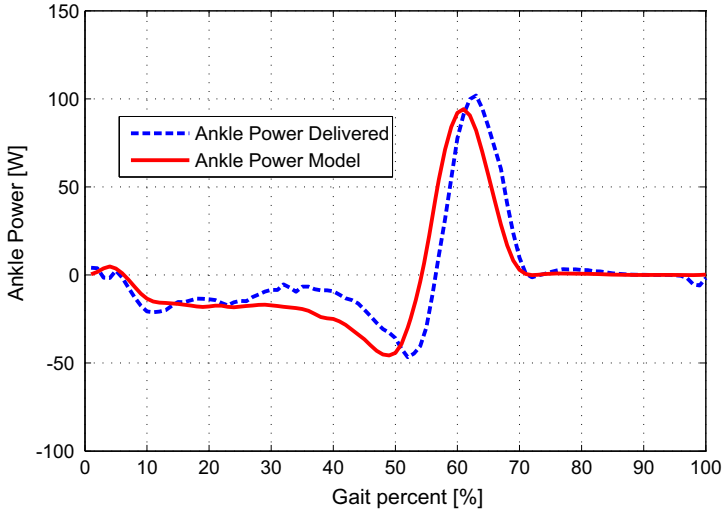

FIGURE 6.13: The desired and real ankle joint power for PAKO experiments (walking 0.5 m/s).

6.3.1 Improvement of the gait recognition method

During the experiments with PAKO, it was observed that the gait recognizer was not producing the desired gait percent as precisely as we expected. For the calculation of the ϕ-curve, it was required to have a curve for shank angle versus shank angular velocity. This curve was obtained based on a mean of measured (i.e. shank angular velocity) and calculated (i.e. shank angle) values. This means necessarily the real on-line curves might not match that mean curve. This is illustrated in Fig. 6.14.

In Fig. 6.14 at some points a sharp edge is observed. This is due to the measurements made by the sensor of shank angular velocity. The peaks were much higher than this at these points, however Kalman filter was used to reduce these effects and at the same time not to change the real

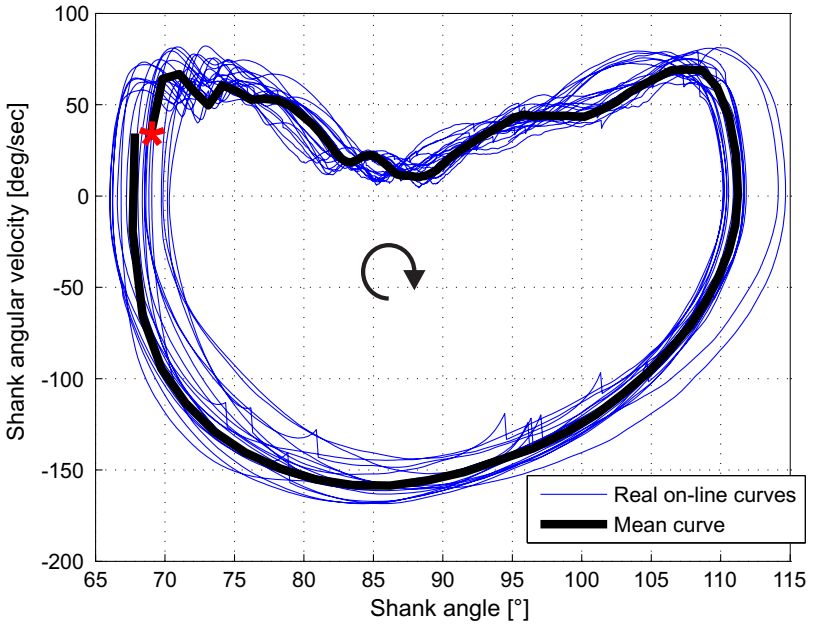

FIGURE 6.14: The mean and on-line shank angular velocities and angles for PAKO experiments (walking 0.5 m/s). The red asterisk * shows the start of the gait and the arrow shows the course of the curve.

measurements too much. Due to these points, the obtained gait percent has some deviations from the precise desired one as seen in Fig. 6.15. Therefore, it was decided to modify this approach.

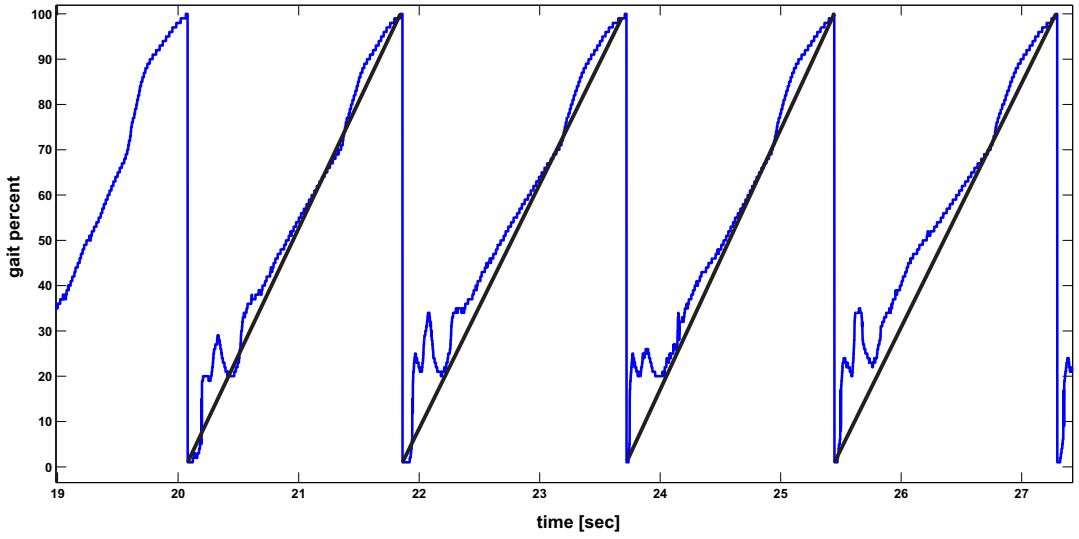

FIGURE 6.15: The detected gait percent by the gait detection method using ϕ-curve (see Fig. 6.14), the black lines show the correct precise (desired) gait percent detection (walking 0.5 m/s).

6.3.2 Modified ϕ-curve approach

In this method, the ϕ-curve approach was used for the detection of the heel strike only, and then the time between two successive heel strikes was divided to 100 representing each gait percent. However, even in this approach there are a number of limitations. For example for the gait percent

determination, there is a need for a priori information about the time of the first stride when the user wants to start the locomotion from the heel strike. Another point is that this controller uses the steptime of the previous stride for the current stride which might cause problems for applications in outdoors. Nevertheless, its performance for gait detection was clearly improved (Fig. 6.16).

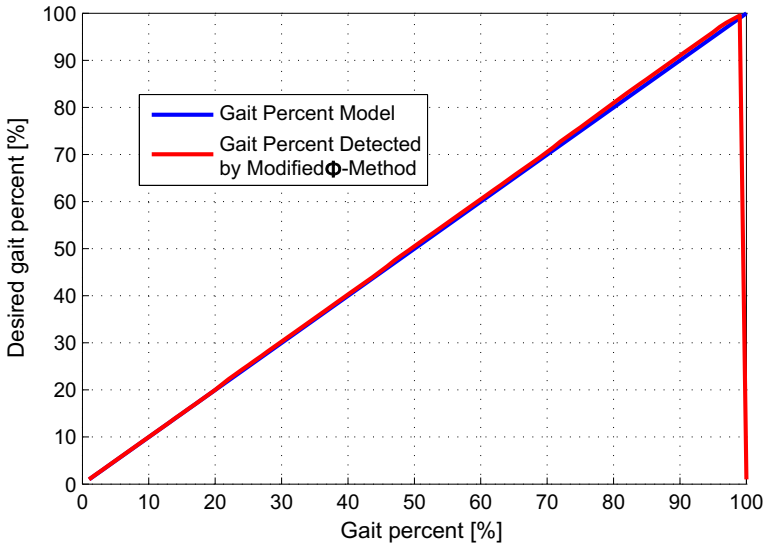

FIGURE 6.16: The detected gait percent by the modified ϕ approach (walking 0.5 m/s), compare with Fig. 6.15.

In Fig. 6.16 it is seen that the red line (the curve for modified ϕ approach) has a sudden break nearly at the end of gait cycle. This could happen because the gait detection procedure can not exactly predict the beginning of the next gait cycle. The results of the PAKO experiments shown in Figs. 6.10, 6.11, 6.12 and 6.13 are based on the modified ϕ approach.

6.3.3 Other approaches for speed and gait percent detection

Depending on the available sensory information, other approaches could also be used for gait percent detection. For example, one approach would be to use a third parameter (other than shank angle and angular velocity) in order to identify the gait. This, however, is with the cost of adding a sensor for the required corresponding measurement. To do this, the knee joint angle (θ_k) could be added to the shank angle and angular values and create a 3D plot as shown in Fig. 6.17.

For this case the procedure for finding the possible gait percent is different from what was explained in the previous method (ϕ or modified ϕ method). In this case, for each set of $[\theta_{sh},\ \dot{\theta}_{sh},\ \theta_k]$, a measurement set is compared with the desired saved values (off-line values) and then the possible gait is detected based on *the minimum distance* between the on-line sensor data and the desired ones as expressed in Eq. 6.8.

$$min(\sqrt{(\theta_{sh}-\theta_{sh,des})^2+(\dot{\theta}_{sh}-\dot{\theta}_{sh,des})^2+(\theta_k-\theta_{k,des})^2}\ ) \tag{6.8}$$

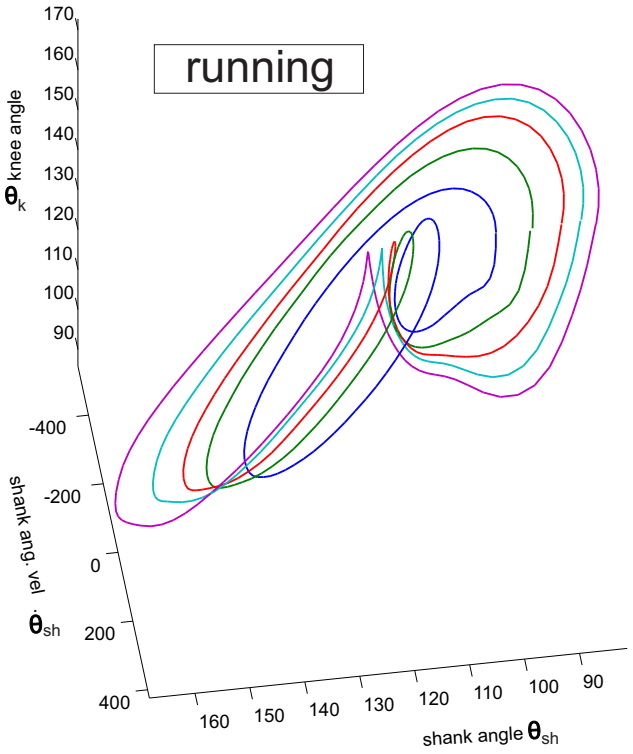

FIGURE 6.17: Another method for gait percent detection based on *the minimum distance* between the sensor data and the desired values of $[\theta_{sh}, \dot{\theta}_{sh}, \theta_k]$.

Note that in this method the intersections between the curves are eliminated to a great extent because of the using of three values (compare Fig. 6.9 with Fig. 6.17). In this method, both gait percent and gait speed are determined based on *the minimum distance* concept.

6.4 The modified transpose Jacobian (MTJ) control as slave controller

The MTJ controller [88] is a control method similar to a PD control approach with smaller gains and a priori information of the exerted torque (force) by the actuator. For the MTJ controller, the K_p and K_v gains we selected 60% and 80% respectively in comparison to the PD controller that was used for nut position control. The controller uses a delayed command signal together with the modified PD gains. This controller has been shown to have better results than PD control in case of dynamic situations [88]. The command signal in this method is written as

$$T_{com} = K_p\ e + K_v\ \dot{e} + K\ Q|_{t-\triangle t} \tag{6.9}$$

where

$$K = exp(-(\frac{|e|}{e_{max}} + \frac{|\dot{e}|}{\dot{e}_{max}})) \tag{6.10}$$

e_{max} and $\dot{e}_{max}$ are sensitivity threshold for position and velocity errors.

Other than PD control, PAKO was tested with this type of controller in order to see if there is any noticeable advantage. However the results showed that the performance of the PD and MTJ controllers are quite similar. Therefore, the results of MTJ controller are not shown here to avoid repetition.

6.5 Design limitations

6.5.1 The required motor power

In Fig. 6.18, the required motor power and the predicted curve by model are shown. As it is seen the power requirement for the slow walking is very high. A main reason is the inertia of the rotor. Also note that during late stance and start of swing motor encounters power saturation. This is not a good design characteristic.

The current version of PAKO was designed by a company before the author joins the group. The simulations and modellings presented in this thesis, showed and predicted (see Chapter 2 e.g. Tab. 2.8 for simulation results of ThinGap motor for motor power requirements) that the current design of PAKO is not desirable due to high power demands. Therefore, based on the results in this thesis, it is recommended to change the motor of the PAKO platform. An alternative could be to use Maxon motors. They are usually prompt enough and have acceptable torque densities.

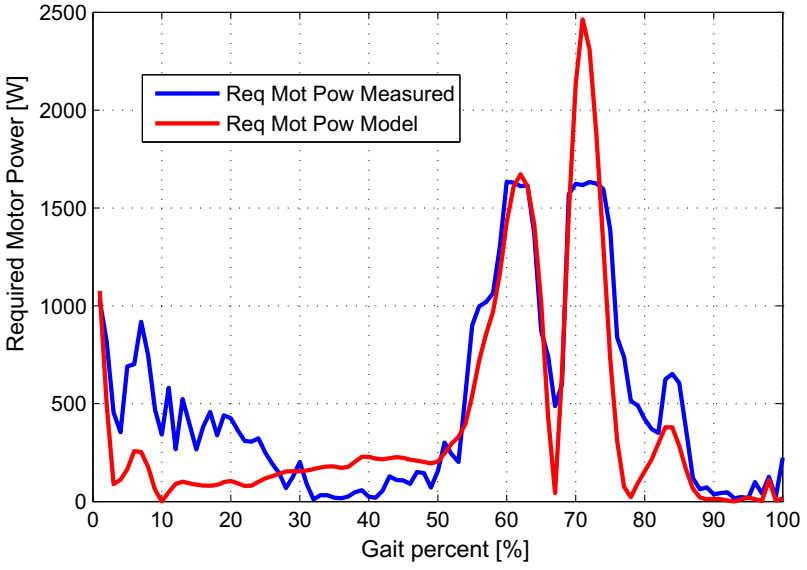

FIGURE 6.18: The required motor power versus model (for walking 0.5 m/s).

6.5.2 The overall ratio of output/input power

Another drawback of the current design, is the very low overall ratio of output/input power of the PAKO platform. A good evaluation approach for understanding how much the robotic ankle is efficient could be the comparison between the input electrical power $P_{e,in}$ which is

$$P_{e,in} = V_m \; . \; I_m \tag{6.11}$$

where V_m and I_m are the motor voltage and current respectively and the ultimate output power P_{out} which I define here as the ankle joint power

$$P_{out} = T_{ank} \; . \; \dot{\theta}_{ank} \tag{6.12}$$

where θ_{ank} is the ankle angular velocity and T_{ank} is the ankle torque.

For current experiments, in order to deliver a 100 W power to the ankle joint, more than 2000 W of electrical power is required (see Figs. 6.13 and 6.18). Therefore the ratio between output power and input power is very low (less than 0.05). Ideally this overall ratio should go to infinity meaning a very low requirement of the input electrical power.

6.6 Summary

In this chapter, we discussed the control of active foot prosthesis with respect to master and slave controllers. We explained the possible methods for control of the active foot prostheses PAKO. The first laboratory experiments and their results for kinematics and kinetics were discussed and at the end different opinions for improvement of the system were explained.

Chapter 7

Summary, Conclusion and Future Works

The overall goal of this work was to achieve novel comprehensive designs for active foot prostheses. In the following, I would like to make conclusions and to give suggestions for future research.

7.1 Muscle model to be used in a mono-articular active foot prosthesis

The outcomes of this study, suggest that for a mono-articular active foot prosthesis, the SEA mechanism is an effective yet simple actuation concept that can be used for active foot prosthesis in a wide range of gaits.

Only for some gaits and speeds like slow walking and running (Chapter 3) or descending the stairs (Chapter 4) it was not the most desirable actuation concept.

Based on these facts, it depends on the designer's intention and design's constraints which actuation scheme could be used. The pros and cons of several actuation concepts have been discussed in this thesis. These findings can directly be used for designs of future prostheses.

Alternative design approaches could be the PEDA (Fig. 4.2) or SEA+UPS (Fig. 3.2) systems. The drawback of these actuation concepts are that they require a variable damper or spring length and stiffness in these approaches (see Chapter 2 and 4). This would add to the versatility of the device and at the same time its complexity.

One important point is that these designs are closer to muscle models presented in Chapter 1 (Figs. 1.15 and 1.16) than the SEA mechanism.

7.2 Bi-articular actuation

In order to be closer to the human musculo-skeletal structure, another suggested design approach would be an active bi-articular mechanism emulating the SOL and GAS muscles in human lower extremities.

In Chapter 5, we saw that both PP and ER requirement could be reduced using this actuation scheme (even by an elastic passive GAS, see Fig. 5.14, this holds for most of the speeds).

The key question here, is the force distribution between the SOL and GAS actuators (motors) when both are active. One could use optimization approaches to investigate on the best possible cooperation between the actuators in a way that both PP and ER requirement are less than that of a mono-articular actuation scheme. This is currently under investigation.

7.3 Master controller for gait detection in various terrains

The main concentration of this thesis was on level ground locomotion such as walking and running. However, in daily situations, people often encounter uneven or rough terrains like stairs or slopes. Therefore, a more general and comprehensive master controller is required to *identify and recognize the intention of the user* for such more specific tasks.

A possible starting point for this purpose, is to use the notion of *principal component analysis* (PCA) and benefit from the intact limbs of the user. One option is to use the motion of the remaining limbs and based on them, predict the motion of the missing limbs. More investigations in this field are currently being carried out.

7.4 The role of bi-articular actuation concept in controlling human locomotion

As seen in Fig. 5.14, for normal and fast walking speeds, we could not find ER reduction in comparison to the SEAS concept. Although different reasons could be responsible for this (like λ value, the minimizing criteria, etc.), this issue needs to be investigated in more detail.

One approach, could be to search for the role of bi-articular actuators in control of human locomotion. To do this, the concept of the PAKO platform could be used as a research tool for future investigations.

Appendix A

Motor Properties

maxon DC motor

RE 40 ∅40 mm, Graphite Brushes, 150 Watt

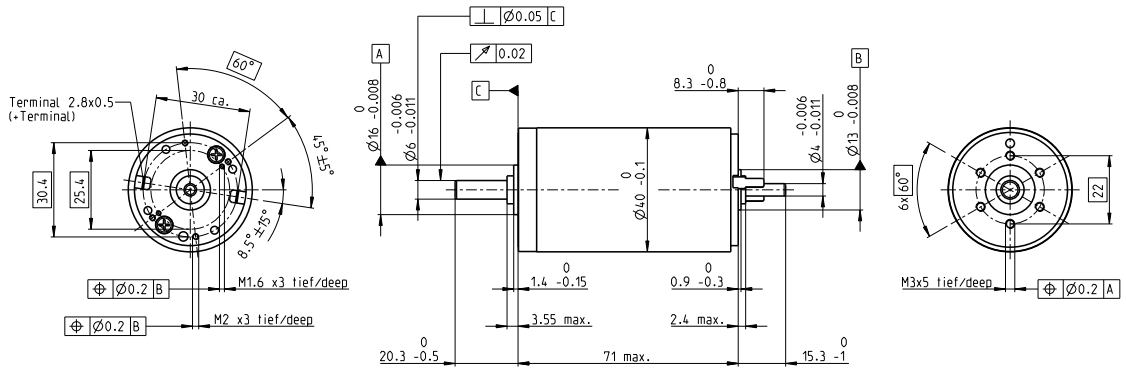

M 1:2

Stock program
Standard program
Special program (on request)

Order Number	148866	148867	148877	218008	218009	218010	218011	218012	218013	218014
Motor Data										
Values at nominal voltage										
1 Nominal voltage V	12.0	24.0	48.0	48.0	48.0	48.0	48.0	48.0	48.0	48.0
2 No load speed rpm	6920	7580	7580	6420	5560	3330	2690	2130	1710	1420
3 No load current mA	241	137	68.6	53.7	43.7	21.9	16.7	12.5	9.67	7.77
4 Nominal speed rpm	6370	6930	7000	5810	4920	2700	2050	1500	1080	774
5 Nominal torque (max. continuous torque) mNm	94.9	170	184	183	177	187	187	189	189	188
6 Nominal current (max. continuous current) A	6.00	5.77	3.12	2.62	2.20	1.38	1.12	0.898	0.721	0.593
7 Stall torque mNm	1680	2280	2500	1990	1580	995	796	641	512	415
8 Starting current A	102	75.7	41.4	28.0	19.2	7.26	4.68	3.00	1.92	1.29
9 Max. efficiency %	88	91	92	91	91	89	88	87	86	85
Characteristics										
10 Terminal resistance Ω	0.117	0.317	1.16	1.72	2.50	6.61	10.2	16.0	24.9	37.1
11 Terminal inductance mH	0.0245	0.0823	0.329	0.460	0.612	1.70	2.62	4.14	6.40	9.31
12 Torque constant mNm / A	16.4	30.2	60.3	71.3	82.2	137	170	214	266	321
13 Speed constant rpm / V	581	317	158	134	116	69.7	56.2	44.7	35.9	29.8
14 Speed / torque gradient rpm / mNm	4.15	3.33	3.04	3.23	3.53	3.36	3.39	3.35	3.37	3.44
15 Mechanical time constant ms	6.03	4.81	4.39	4.36	4.35	4.31	4.31	4.31	4.31	4.32
16 Rotor inertia gcm²	139	138	138	129	118	123	121	123	122	120

Specifications

Thermal data

17	Thermal resistance housing-ambient	4.65 K / W
18	Thermal resistance winding-housing	1.93 K / W
19	Thermal time constant winding	41.6 s
20	Thermal time constant motor	1120 s
21	Ambient temperature	-30 ... +100°C
22	Max. permissible winding temperature	+155°C

Mechanical data (ball bearings)

23	Max. permissible speed	12000 rpm
24	Axial play	0.05 - 0.15 mm
25	Radial play	0.025 mm
26	Max. axial load (dynamic)	5.6 N
27	Max. force for press fits (static)	110 N
	(static, shaft supported)	1200 N
28	Max. radial loading, 5 mm from flange	28 N

Other specifications

29	Number of pole pairs	1
30	Number of commutator segments	13
31	Weight of motor	480 g

Values listed in the table are nominal.
Explanation of the figures on page 49.

Option
Preloaded ball bearings

Operating Range

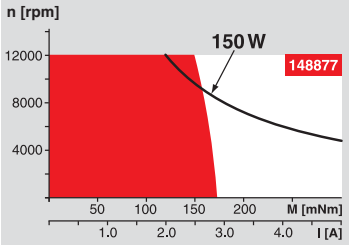

Comments

Continuous operation
In observation of above listed thermal resistance (lines 17 and 18) the maximum permissible winding temperature will be reached during continuous operation at 25°C ambient.
= Thermal limit.

Short term operation
The motor may be briefly overloaded (recurring).

Assigned power rating

maxon Modular System

Overview on page 16 - 21

Planetary Gearhead
∅42 mm
3 - 15 Nm
Page 237

Planetary Gearhead
∅52 mm
4 - 30 Nm
Page 240

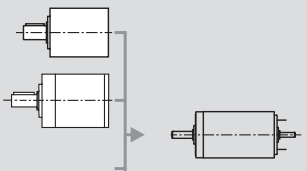

Encoder MR
256 - 1024 CPT,
3 channels
Page 263

Encoder HED_ 5540
500 CPT,
3 channels
Page 266 / 268

Brake AB 28
24 VDC
0.4 Nm
Page 318

Industrial Version
Encoder HEDL 9140
Page 271
Brake AB 28
Page 319

Recommended Electronics:

ADS 50/5	Page 282
ADS 50/10	283
ADS_E 50/5	283
ADS_E 50/10	283
EPOS2 24/5	305
EPOS2 50/5	305
EPOS2 70/10	305
EPOS2 P 24/5	308
Notes	**18**

May 2011 edition / subject to change

FIGURE A.1: The full properties of Maxon RE 40

ThinGap®

Brushless
TG2320 BLDC Motor

- **425 oz-in. peak torque**
- **1025 watts continuous power**
- **Weight 16.5 oz**
- **73% peak system efficiency**
- **Smooth, controllable power**
- **No cogging or hysteresis torque**
- **3 mounting options available**
- **8 Pole, Y Coil**

TG2320 BRUSHLESS MOTOR					
	UNITS	IMPERIAL		SI	
Peak torque[1]	Tpk	425	oz-in.	3.0	Nm
Peak current	Ipk	86.7	amps		
Maximum Continuous rating:[2]					
Torque -	Tc	85	oz-in.	0.60	Nm
Speed -	Wc	16305	rpm		
Current -	Ic	17.65	amps dc		
Voltage -	Vc	80	Volts dc		
Shaft Power	Pc	1025	watts		
Maximum Locked Rotor Torque[2]	Tlr	45	ozin	0.32	Nm
Maximum Locked Rotor Current	Ilr	9.2	Amps		
No load speed	Wnl	21,800	Rpm		
No load voltage	Vnl	80	Volts		
No load current	Inl	1.1			
Motor constant	Km	8.8	oz-in./sqrt (W)	0.062	Nm/sqrt(W)
Torque constant -trap drive	Kt	4.9	oz-in./amp	0.035	Nm/amp
Back EMF constant	Kv	0.036	v/rad./s		
Back EMF constant	Ke	264	rpm/volt		
Terminal resistance	Rt	0.31	ohms		
Cogging and hysteresis torque	Tc, Th	0	oz-in.		
Viscous drag torque	Tac	0.22	oz-in./krpm	1.55	mNm/krpm
Friction torque	Tfr	0.05	oz-in.	0.35	mNm
Stator inductance	L	10	micro H		
Mechanical time constant	Tm	42	mS		
Electrical time constant	Te	0.032	mS		
Maximum system Efficiency	Efficiency	73	%		
Motor weight, total	Wt. Total	16.5	oz	468	grams
Rotor inertia	J	2.31E-02	oz-in.-sec2	1.63E-04	Kg-m^2
Max rotor temperature[3]	Temp rotor	70	°C		
Max stator winding temperature[3]	Temp wdg	110	°C		

NOTES:
1-Torque vs current is linear and limited to short duration
2-Tested with the motor on a 3"x.375"x8" bracket using a 50amp, 80volt amplifier with 65uH inductors added per phase.
3-Limited by magnet temperature stability at a fixed torque load.

FIGURE A.2: The full properties of ThinGap 2320 series

Bibliography

[1] Michael W Whittle. *Gait analysis: an introduction*. 2003.

[2] Aaron M Dollar and Hugh Herr. Lower extremity exoskeletons and active orthoses: challenges and state-of-the-art. *IEEE Transactions on Robotics*, 24(1):144–158, 2008.

[3] R.H. Rozendal. Human poly-articular muscles: An anatomical comment. *Human Movement Science*, 13(5):557–568, 1994. ISSN 0167-9457.

[4] URL https://myhealth.alberta.ca/health/pages/conditions.aspx?hwid=ug3002. Access Dec 2013.

[5] S.W. Lipfert. *Kinematic and dynamic similarities between walking and running*. Verlag Dr. Kovac, Hamburg, 2010. ISBN: 9783-8300-50308.

[6] Daan J.J. Bregman. *The Optimal Ankle Foot Orthosis*. PhD thesis, Vrije Universiteit Amsterdam, 2011.

[7] René Jimenez-Fabian and Olivier Verlinden. Review of control algorithms for robotic ankle systems in lower-limb orthoses, prostheses, and exoskeletons. *Medical engineering & physics*, 34 (4):397–408, 2012.

[8] URL http://biometrics.derawi.com/?page_id=38. Access May 2014.

[9] M. Günther, VA Sholukha, D. Keßler, V. Wank, and R. Blickhan. Dealing with skin motion and wobbling masses in inverse dynamics. *Journal of Mechanics in Medicine and Biology*, 3 (3-4):309–335, 2003.

[10] Heydar Sadeghi. Local or global asymmetry in gait of people without impairments. *Gait & Posture*, 17(3):197–204, 2003.

[11] URL http://www.esbiomech.org/?page_id=1819#10. European Society of Biomechanics, Access Feb. 17th 2014.

[12] URL www.toc-reha.de/amputation.php. Access: June 6th 2013.

[13] Institut für das Entgeltsystem im Krankenhaus GmbH (InEK).

[14] . URL www.amputee-coalition.org/fact_sheets/diabetes_leamp.pdf. Access Feb. 18th 2014.

[15] . URL www.cdc.gov/diabetes/statistics/lea/. Access Feb. 18th 2014.

[16] URL www.biom.com. Access May 2014.

[17] K Postema, HJ Hermens, J De Vries, HFJM Koopman, and WH Eisma. Energy storage and release of prosthetic feet part 1: Biomechanical analysis related to user benefits. *Prosthetics and Orthotics International*, 21(1):17–27, 1997.

[18] RL Waters, Jacquelin Perry, DANIEL Antonelli, and Helen Hislop. Energy cost of walking of amputees: the influence of level of amputation. *J Bone Joint Surg Am*, 58(1):42–46, 1976.

[19] NH Molen. Energy/speed relation of below-knee amputees walking on a motor-driven treadmill. *Internationale Zeitschrift für angewandte Physiologie einschließlich Arbeitsphysiologie*, 31(3): 173–185, 1973.

[20] David J Sanderson and Philip E Martin. Lower extremity kinematic and kinetic adaptations in unilateral below-knee amputees during walking. *Gait & posture*, 6(2):126–136, 1997.

[21] Christopher M Powers, Sreesha Rao, and Jacquelin Perry. Knee kinetics in trans-tibial amputee gait. *Gait & posture*, 8(1):1–7, 1998.

[22] John G Buckley. Biomechanical adaptations of transtibial amputee sprinting in athletes using dedicated prostheses. *Clinical Biomechanics*, 15(5):352–358, 2000.

[23] Ronald D Snyder, Christopher M Powers, C Fountain, and Jacquelin Perry. The effect of five prosthetic feet on the gait and loading of the sound limb in dysvascular below-knee amputees. *Journal of rehabilitation research and development*, 32:309–315, 1995.

[24] GK Klute, J Czerniecki, and B Hannaford. Development of powered prosthetic lower limb. In *Proceedings of the 1st National Meeting, Veterans Affairs Rehabilitation Research and Development Service*, 1998.

[25] S. Au. *Powered Ankle-Foot Prosthesis for the Improvement of Amputee Walking Economy*. PhD thesis, MIT, 2007.

[26] K.W. Hollander and TG Sugar. Design of the robotic tendon. In *Design of Medical Devices Conference*, 2005.

[27] Frank Charles Sup. *A Powered Self-contained Knee And Ankle Prosthesis For Near Normal Gait In Transfemoral Amputees*. PhD thesis, Vanderbilt University, 2009.

[28] Matthew Aaron Holgate. *Control Of A Robotic Transtibial Prosthesis*. PhD thesis, Arizona State University, 2009.

[29] Rocket Powered Prosthetic Feet May Outrun Natures Best. URL http://www.medgadget.com/2012/11/rocket-powered-prosthetic-feet-may-outrun-natures-own-best.html.

[30] K Alex Shorter, Géza F Kogler, Eric Loth, William K Durfee, and Elizabeth T Hsiao-Wecksler. A portable powered ankle-foot orthosis for rehabilitation. *J Rehabil Res Dev*, 48(4):459–72, 2011.

[31] Martin Noël, Benoit Cantin, Sébastien Lambert, Clément M Gosselin, and Laurent J Bouyer. An electrohydraulic actuated ankle foot orthosis to generate force fields and to test proprioceptive reflexes during human walking. *IEEE Transactions on Neural Systems and Rehabilitation Engineering*, 16(4):390–399, 2008.

[32] Gregory S Sawicki, Keith E Gordon, and Daniel P Ferris. Powered lower limb orthoses: applications in motor adaptation and rehabilitation. In *IEEE International Conference on Rehabilitation Robotics*, pages 206–211, 2005.

[33] A.V. Hill. The heat of shortening and the dynamic constants of muscle. *Proceedings of the Royal Society London*, pages 136–195, 1938.

[34] W.K. Durfee and K.I. Palmer. Estimation of force-activation, force-length, and force-velocity properties in isolated electrically stimulated muscle. *IEEE Trans. on Biomedical Eng.*, 41: 205–216, 1994.

[35] Michael Günther, Syn Schmitt, and Veit Wank. High-frequency oscillations as a consequence of neglected serial damping in hill-type muscle models. *Biological Cybernetics*, 97(1):63–79, 2007.

[36] Antonio Gonzalez Rodriguez, Nestor Eduardo Nava Rodriguez, and Angel Gaspar Gonzalez Rodriguez. Design and validation of a novel actuator with adaptable compliance for application in human-like robotics. *Industrial Robot: An International Journal*, 36(1):84–90, 2009.

[37] K. W. Hollander, T. G. Sugar, and D. E. Herring. A robotic "jack spring"^{TM} for ankle gait assistance. *ASME Conference Proceedings*, 2005(47446):25–34, 2005.

[38] John DW Madden, Nathan A Vandesteeg, Patrick A Anquetil, Peter GA Madden, Arash Takshi, Rachel Z Pytel, Serge R Lafontaine, Paul A Wieringa, and Ian W Hunter. Artificial muscle technology: physical principles and naval prospects. *IEEE Journal of Oceanic Engineering*, 29 (3):706–728, 2004.

[39] Joseph Hamill and Kathleen M Knutzen. *Biomechanical basis of human movement*. Lippincott Williams & Wilkins, 2006.

[40] D.G. Caldwell. Polymeric gels: Pseudo muscular actuators and variable compliance tendons. In *lEEE/RSJ International Conference on Intelligent Robots and Systems*, volume 2, pages 950–957, 1992.

[41] E. T. Esfahani. Developing an active ankle foot orthosis based on shape memory alloys. Master's thesis, University of Toledo, Toledo, OH, 2007.

[42] Takashi Maeno and Toshiyuki Hino. Miniature five-fingered robot hand driven by shape memory alloy actuators. In *Proc. of the 12th IASTED Int. Conf. on Robotics and Applications*, pages 174–179, 2006.

[43] M Shahinpoor. Conceptual design, kinematics and dynamics of swimming robotic structures using ionic polymeric gel muscles. *Smart Materials and Structures*, 1(1):91, 1992.

[44] S.K. Au, J. Weber, and H. Herr. Powered Ankle-Foot Prosthesis Improves Walking Metabolic Economy. *IEEE Transactions on Robotics*, 25(1):51–66, 2009. ISSN 1552-3098.

[45] Huseyin Atakan Varol. Progress towards the intelligent control of a powered transfemoral prosthesis. Master's thesis, 2007.

[46] M.A. Holgate, T.G. Sugar, and AW Bohler. A novel control algorithm for wearable robotics using phase plane invariants. In *Robotics and Automation, 2009. ICRA'09. IEEE International Conference on*, pages 3845–3850. IEEE, 2009.

[47] H.A. Varol, F. Sup, and M. Goldfarb. Real-time gait mode intent recognition of a powered knee and ankle prosthesis for standing and walking. In *Biomedical Robotics and Biomechatronics, 2008. BioRob 2008. 2nd IEEE RAS & EMBS International Conference on*, pages 66–72. IEEE, 2009.

[48] Francis HY Chan, Yong-Sheng Yang, FK Lam, Yuan-Ting Zhang, and Philip A Parker. Fuzzy emg classification for prosthesis control. *IEEE Transactions on Rehabilitation Engineering*, 8 (3):305–311, 2000.

[49] Samuel K Au, Paolo Bonato, and Hugh Herr. An emg-position controlled system for an active ankle-foot prosthesis: an initial experimental study. In *IEEE International Conference on Rehabilitation Robotics*, pages 375–379, 2005.

[50] DL Grimes, WC Flowers, and M Donath. Feasibility of an active control scheme for above knee prostheses. *Journal of Biomechanical Engineering*, 99:215, 1977.

[51] *Össur Prosthetics Product Catalogue 2007-2008.*

[52] Aykut Mehmet Oymagil, Joseph K Hitt, Thomas Sugar, and Jennifer Fleeger. Control of a regenerative braking powered ankle foot orthosis. pages 28–34, 2007.

[53] Jared Markowitz, Pavitra Krishnaswamy, Michael F Eilenberg, Ken Endo, Chris Barnhart, and Hugh Herr. Speed adaptation in a powered transtibial prosthesis controlled with a neuromuscular model. *Philosophical Transactions of the Royal Society B: Biological Sciences*, 366(1570): 1621–1631, 2011.

[54] Hartmut Geyer and Hugh Herr. A muscle-reflex model that encodes principles of legged mechanics produces human walking dynamics and muscle activities. *IEEE Transactions on Neural Systems and Rehabilitation Engineering*, 18(3):263–273, 2010.

[55] Michael F Eilenberg, Hartmut Geyer, and Hugh Herr. Control of a powered ankle-foot prosthesis based on a neuromuscular model. *IEEE Transactions on Neural Systems and Rehabilitation Engineering*, 18(2):164–173, 2010.

[56] Michael Frederick Eilenberg. *A neuromuscular-model based control strategy for powered ankle-foot prostheses*. PhD thesis, Massachusetts Institute of Technology, 2009.

[57] G.A. Pratt and M.M. Williamson. Series elastic actuators. In *Intelligent Robots and Systems 95.'Human Robot Interaction and Cooperative Robots', Proceedings. 1995 IEEE/RSJ International Conference on*, volume 1, pages 399–406. IEEE, 2002. ISBN 0818671084.

[58] JE Shigley and CR Mischke. *Standard handbook of machine design*. McGraw-Hill, New York, 1986.

[59] K. W. Hollander, R. Ilg, T.G. Sugar, and D. Herring. An efficient robotic tendon for gait assistance. *ASME Jour. of. Biomech. Eng.*, 128:788–791, 2006.

[60] F. Sup, H.A. Varol, J. Mitchell, T.J. Withrow, and M. Goldfarb. Self-contained powered knee and ankle prosthesis: Initial evaluation on a transfemoral amputee. In *IEEE ICORR*, pages 638–644, 2009.

[61] M. Eslamy, M. Grimmer, and A. Seyfarth. Effects of unidirectional parallel springs on required peak power and energy in powered prosthetic ankles: Comparison between different active actuation concepts. *IEEE RoBio*, pages 2406–2412, 2012.

[62] M. Grimmer, M. Eslamy, S. Gliech, and A. Seyfarth. A comparison of parallel- and series elastic elements in an actuator for mimicking human ankle joint in walking and running. In *IEEE ICRA*, pages 2463–2470, 2012.

[63] M. Eslamy, M. Grimmer, S. Rinderknecht, and A. Seyfarth. Does it pay to have a damper in a powered ankle prosthesis? a power-energy perspective. *IEEE Int'l Conf. on Rehab. Robo.*, pages 1–8, 2013.

[64] H.M. Herr, S.K. Au, P. Dilworth, and D.J. Paluska. Artificial ankle-foot system with spring, variable-damping, and series-elastic actuator components, January 11 2012 US Patent App. 13/348,570.

[65] H.A. Mauch. The development of artificial limbs for lower limbs. *Bulletin of prosthetics research*, pages 158–166, 1974.

[66] URL www.endolite.com. Access May 2014.

[67] A. LaPrè and F. Sup. A semi-active damper design for use in a terrain adaptive ankle prosthesis. ASME IMECE, 2011.

[68] B.J. McFadyen and D.A. Winter. An integrated biomechanical analysis of normal stair ascent and descent. *Journal of biomechanics*, 21(9):733–744, 1988.

[69] R. Riener, M. Rabuffetti, and C. Frigo. Stair ascent and descent at different inclinations. *Gait & posture*, 15(1):32–44, 2002.

[70] H.C. Lin, T.W. Lu, and H.C. Hsu. Comparisons of joint kinetics in the lower extremity between stair ascent and descent. *Journal of Mechanics*, 21(01):41–50, 2005.

[71] K. Pfeifer and W. Banzer. Motor performance in different dynamic tests in knee rehabilitation. *Scandinavian journal of medicine & science in sports*, 9(1):19–27, 1999.

[72] D.F.B. Haeufle, M. Günther, R. Blickhan, and S. Schmitt. Can quick release experiments reveal the muscle structure? a bionic approach. *Journal of Bionic Engineering*, 9(2):211–223, 2012. ISSN 1672-6529.

[73] DFB Haeufle, S. Grimmer, and A. Seyfarth. The role of intrinsic muscle properties for stable hopping stability is achieved by the force–velocity relation. *Bioinspiration&biomimetics*, 5(1), 2010.

[74] URL http://edu.obgynmenopause.com/ItemPopup.aspx?HWID=tp10578&SEC=tp10578-sec. Access Dec 2013.

[75] Abbie E Ferris, Jennifer M Aldridge, Christopher A Rábago, and Jason M Wilken. Evaluation of a powered ankle-foot prosthetic system during walking. *Archives of physical medicine and rehabilitation*, 93(11):1911–1918, 2012.

[76] Yukio Saito, Kazuya Kikuchi, Hiroshi Negoto, Toru Oshima, and Toshimasa Haneyoshi. Development of externally powered lower limb orthosis with bilateral-servo actuator. In *IEEE International Conference on Rehabilitation Robotics*, pages 394–399, 2005.

[77] Yukio Saito, Takeshi Matsuoka, and Hiroshi Negoto. Study on designing a biped robot with bi-articular muscle type bilateral servo system. In *IEEE International Workshop on Robot and Human Interactive Communication*, pages 490–495, 2005.

[78] Kenji Tahara, Zhi-Wei Luo, and Suguru Arimoto. On control mechanism of human-like reaching movements with musculo-skeletal redundancy. *IEEE International Conference on Intelligent Robots and Systems*, pages 1402–1409, 2006.

[79] Jan Babič, Bokman Lim, Damir Omrčen, Jadran Lenarčič, and FC Park. A biarticulated robotic leg for jumping movements: theory and experiments. *ASME Journal of Mechanisms and Robotics*, 2009.

[80] A.J. Van Den Bogert. Exotendons for assistance of human locomotion. *Biomedical engineering online*, 2(17), 2003.

[81] Herbert Elftman. The function of muscles in locomotion. *American Journal of Physiology–Legacy Content*, 125(2):357–366, 1939.

[82] Herbert Elftman. The work done by muscles in running. *American Journal of Physiology–Legacy Content*, 129(3):672–684, 1940.

[83] L Gregoire, HE Veeger, PA Huijing, and GJ van Ingen Schenau. Role of mono-and biarticular muscles in explosive movements. *International Journal of Sports Medicine*, 5(06):301–305, 1984.

[84] GJ van van Ingen Schenau, MF Bobbert, and RH Rozendal. The unique action of bi-articular muscles in complex movements. *Journal of Anatomy*, 155:1, 1987.

[85] . URL www.roton.com/page.aspx?id=28. Access Feb 2014.

[86] . URL www-mdp.eng.cam.ac.uk/web/library/enginfo/textbooks_dvd_only/DAN/threads/mechanics/mechanics.html. Access May 2014.

[87] Katsuhiko Ogata and Yanjuan Yang. Modern control engineering. *Prentice-Hall Englewood Cliffs*, 1970.

[88] S Ali A Moosavian and Evangelos Papadopoulos. Modified transpose jacobian control of robotic systems. *Automatica*, 43(7):1226–1233, 2007.

Mahdy Eslamy

Résumé

Research Interests

Human-Centered Design, Control, Robotics, Mechanism Design

Education

09/2005 Bachelor of Eng. in Applied Design, Dept. of Mechanical Engineering, Iran University of Science and Technology (IUST), Tehran, Iran.

Final Thesis: *Motion-Vibration Analysis of a Flat Plate Excited by a Reciprocating Semi-Conical Cam.*

04/2008 Master of Eng. in Control and Robotics, Dept. of Mechanical Engineering, Khaje Nasir Toosi University of Technology (KNTU), Tehran, Iran.

Final Thesis: *Control and Dynamics of Wheeled Mobile Robots (with Manipulators) with/without Suspension Systems considering Object Manipulation Tasks.*

Current Activity

PhD candidate (about to finish), Lauflabor, Locomotion Laboratory, Technical University of Darmstadt, Germany, working on

Mechanical Representations of Human Muscle for application in Active foot Prostheses,

And,

Design Improvement, Control and Laboratory Experiments of a Robotic Ankle/Knee Ortho-Prosthesis,

(supported by German Research Foundation (DFG)), a video of my work could be found at: `https://www.youtube.com/watch?v=i7N3L6RsNNU`

Thesis Supervisors: Prof. Dr. Andre Seyfarth, Prof. Dr. Ing. Stephan Rinderknecht.

Other Activities

Supervising master project for human gait detection based on Machine Learning together with Prof. Jan Peters from Computer Eng. Faculty, 2014(1)

Supervising bachelor projects for design of active knee prosthesis: 2013(1), 2014(1)

Over-actuation in Robotic Systems with application in Prosthetics

Proposal Writing: 1. Co-author of a grant for instrumented stairs for investigations on human locomotion on stairs, TU Darmstadt internal grant, 75000 €, Germany 2013-2014

2. Co-author for DFG proposal, human like bi-articular actuation in prosthetics

✉ m.eslamy@gmail.com

Experience

06/2003 - 08/2003 Apprenticeship "Neka Steam Power Plant".

06/2005 - 06/2006 Technical Translator, "Rah-avard sana't Tarjome", affiliated with car manufacturing companies in Iran, part time.

06/2005 - 08/2008 Researcher of R&D department, "Noavaran Design Institute", Tehran, Iran, part time, design of injection pumps for cars

2007-2010 Teaching at Azad University of Sari, Iran, teaching: Dynamics, Linear Control Systems, Dynamics and Vibration Lab, SolidWorks/Matlab for BSc students.

08/2008 - 02/2010 R&D researcher, Shomal Institute of Technology, Iran

since 12/2010 Researcher at Lauflabor Locomotion Laboratory at TU Darmstadt, Germany, Active Prostheses for Lower Extremities.

since 2013 Supervising students for bachelor and master theses at Lauflabor Locomotion Laboratory at TU Darmstadt, Germany. The theses are about biomedical robotics.

active knee prosthesis: 2013(V. Grabosch), 2014(P. Scholl).

human gait detection based on Machine Learning: 2014(S. Reinhardt).

Computer Skills

SolidWorks, MSC.ADAMS, familiar with ANSYS

MATLAB, SimuLink, Maple, C++

TwinCAT PLC: The Windows-based Industrial Control Software

MS Office

Publications

2014 Mahdy Eslamy, Martin Grimmer and Andre Seyfarth, *The Comparison of Power and Energy Requirement between Mono- and Bi-articular Actuation in Active Foot Prostheses*, IEEE Humanoids 2014.

Grimmer, M., Eslamy, M. and Seyfarth, A. *Energetic and Peak Power Advantages of Series Elastic Actuators in an Actuated Prosthetic Leg for Walking and Running*, Actuators 2014.

2013 Mahdy Eslamy, Martin Grimmer, Stephan Rinderknecht and Andre Seyfarth, *Does it pay to have a damper in a powered ankle prosthesis? A Power-Energy Perspective*, IEEE Int'l Conf. on Rehab. Robotics, ICORR 2013, Seattle USA.

2012 Mahdy Eslamy, Martin Grimmer and Andre Seyfarth, *Effects of Unidirectional Parallel Springs on Required Peak Power and Energy in Powered Prosthetic Ankles: Comparison between Different Active Actuation Concepts*, IEEE RoBio, pp. 2406-2412, 2012.

Mahdy Eslamy, Martin Grimmer and Andre Seyfarth, *Effects of Unidirectional Parallel Springs on Required Peak Power and Energy in Martin Grimmer, Mahdy Eslamy and Andre Seyfarth, A Comparison of Parallel- and Series Elastic Elements in an Actuator for Mimicking Human Ankle Joint in Walking and Running*, IEEE ICRA, 2012, pp. 2463-2470.

2011 Mahdy Eslamy, S.Ali.A Moosavian, *Dynamics Modeling of Suspended Mobile Manipulators: An Explicit Approach with Verification*, International Journal of Modeling and Simulation, ACTApress, Vol. 31, No. 2, pp. 112-119, 2011.

2010 Mahdy Eslamy, S.Ali.A Moosavian, *Dynamics and Cooperative Object Manipulation Control of Suspended Mobile Manipulators*, Springer Journal of Intelligent and Robotic Systems, Vol. 60, Issue 2, pp. 181-199, 2010.

✉ m.eslamy@gmail.com

2009 Mahdy Eslamy, S.Ali.A Moosavian, *Control of Suspended Wheeled Mobile Robots with Multiple Arms during Object Manipulation Tasks*, IEEE ICRA, 2009, pp. 3730-3735.

Mahdy Eslamy, S.Ali.A Moosavian, *Cooperative Object Manipulation by Suspended Wheeled Mobile Manipulators*, International Journal of Robotics, NOV. 2009, 1(1), pp. 56-64.

2008 S.Ali.A Moosavian, Mahdy Eslamy, *Object Manipulation by Multiple Arms of a Wheeled Mobile Robotic System*, IEEE International Conference on Robotics, Automation and Mechatronics (RAM), 2008, pp. 1124-1129.

Hobbies

Running, Tennis

Contact

m.eslamy@gmail.com